THE He II FILM IN MOTION

E. VAN SPRONSEN

THE He II FILM IN MOTION

PROEFSCHRIFT

TER VERKRIJGING VAN DE GRAAD VAN DOCTOR IN DE WISKUNDE EN NATUURWETENSCHAPPEN AAN DE RIJKSUNIVERSITEIT TE LEIDEN, OP GEZAG VAN DE RECTOR MAGNIFICUS DR. A.E. COHEN, HOOGLERAAR IN DE FACULTEIT DER LETTEREN, VOLGENS BESLUIT VAN HET COLLEGE VAN DEKANEN TE VERDEDIGEN OP WOENSDAG 4 JUNI 1975 TE KLOKKE 15.15 UUR

door

ENGEL VAN SPRONSEN
geboren te Monster in 1945

PROMOTOREN: PROF. DR. K.W. TACONIS
PROF. DR. R. DE BRUYN OUBOTER

DIT PROEFSCHRIFT IS BEWERKT MEDE ONDER TOEZICHT VAN
DR. H. VAN BEELEN

STELLINGEN

1. De methode die Hensel toepast ter bepaling van de laagste roostertemperatuur in de kerndemagnetisatie-experimenten, is onbetrouwbaar.

   P. Hensel, dissertatie, Oxford, 1972.

2. Bij de interpretatie van Cade's experimentele resultaten ter bepaling van de ontsnappingsfrequentie van positieve ionen uit vortexringen in He II, is het raadzaam rekening te houden met de mogelijkheid dat de focussering van deze vortexringen kan afhangen van de temperatuur en de spanningsverschillen tussen de roosters.

   A.G. Cade, Phys. Rev. Letters 15 (1965) 238.

3. Bij de toetsing van de richtingsafhankelijkheid van de EPR-lijnbreedte bij halve intensiteit aan de theorie, is door Adams e.a. ten onrechte verondersteld dat de verhouding tussen deze lijnbreedte en de zogeheten piek-piek-lijnbreedte konstant is.

   R. Adams, R. Gaura, R. Raczkowski en G. Kokoszka,
   Phys. Letters 49A (1974) 11.

4. Gezien de plannen voor het invoeren van een nieuwe temperatuurschaal gebaseerd op de dampspanningsrelatie van vloeibaar ^{3}He tussen 0,5 K en 3,3 K, is het gewenst het verband tussen de dampspanning en de temperatuur in het gebied van 0,5 K tot 1 K opnieuw te bepalen met behulp van een magnetische thermometer.

   Traveaux du Comité Consultatif de Thermométrie, 10^{e} Session (Sèvres), 1974.

5. De beschrijving die Mooij geeft van de werking van een symmetrisch dubbelkontakt van zwak-gekoppelde supergeleiders in de gelijkstroomtoestand, is onjuist.

   J.E. Mooij, Ned. Tijdschr. Natuurk. 07 (1975) 79.

6. Bij het onderzoek naar de invloed van magnetische velden op de thermodiffusie van gassen, kan men in één toestel zowel de oneven coëfficient D_T^{trans} van de thermodiffusietensor als de even coëfficient $(D_T^{//} - D_T^{\perp})$ meten door een juiste keuze van de oriëntaties van het magnetische veld ten opzichte van het toestel.

G.E.J. Eggermont, P. Oudeman en L.J.F. Hermans,
Phys. Letters 50A (1974) 173.

7. Bij een bombardement van vaste stoffen met zware ionen wordt waargenomen dat de fotonemissie van atomen en ionen een vergelijkbare intensiteit heeft. Dit feit wordt door Jensen en Veje toegeschreven aan het sputteren van molekulen in een predissociatieve toestand. Deze vergelijkbare intensiteiten kunnen echter ook ontstaan door de invloed van stralingsloze deëxcitatie op de gesputterde atomen en ionen.

K. Jensen en E. Veje, Z. Physik 269 (1974) 293.

8. De viscositeit van He II in het temperatuurgebied vlak onder het lambdapunt, kan worden bepaald door de warmtegeleiding van deze heliumfase in een bundel van vele, zeer nauwe capillairen met bekende geometrie te meten.

9. De directe, polarografische bepaling van diazepam in bloed, zoals gedaan is door Fidelus e.a., is te ongevoelig om van enig praktisch nut te zijn.

J. Fidelus, M. Zietek, A. Mikolajek en Z. Grochowska,
Mikrochimika Acta (Wien) 1972, 84.

10. Het is wenselijk de natuurkunde afzonderlijk in het lesrooster van de basisschool te vermelden, teneinde dit vak daar nog enigermate tot zijn recht te laten komen.

11. Uitspraken over bijvoorbeeld het negatieve effect van orale contraceptie zijn zinloos zolang er geen betrouwbare gegevens zijn verzameld over het vóórkomen van lichamelijke en psychische klachten bij de populatie van gezonde Nederlandse vrouwen in de fertiele leeftijd.

P.A.J.M. van Noort, doctoraalscriptie, Leiden, 1973.

12. Het is aan te bevelen dat de instellingen voor wetenschappelijk onderwijs in Nederland grotere aandacht geven aan de geschiedenis der natuurwetenschappen.

E. van Spronsen

Leiden, 4 juni 1975

Aan Gerda en de kinderen

CONTENTS

INTRODUCTION

When liquid ^{4}He is cooled below the lambda temperature of 2.17 K a dramatic change in the properties of the liquid is observed. The most striking property of this liquid phase, which is called He II, is the ability to flow with practically no resistance through very narrow capillaries. A mass of experimental data culminated in a macroscopic phenomenological description of He II known as the two fluid model[1,2]. In this model, He II consists of two components: the normal component, behaving like an ordinary fluid, and the superfluid component, responsible for the extraordinary behaviour of He II. The hydrodynamical behaviour of these two components in the nondissipative velocity region is given by the Landau equations[3].

In this thesis, a remarkable phenomenon of He II is studied, *i.e.* the He II film. Such a film is formed on the walls above the bulk liquid contained in a vessel, as was already discovered in the early days of He II research[4,5]. This film is highly mobile, due to the flow properties of the superfluid component. The thickness of the film not only depends on the height above the bulk liquid, but also on the Van der Waals forces exerted by the solid substrate and on the contamination of this surface. Especially this latter factor can cause spurious results in film experiments. Nevertheless, there are advantages in studying He II by examining the film. Firstly there is the possibility of obtaining in a well determined geometry large superfluid velocities, of the order of 30 cm/s, without noticeable dissipation. Furthermore, the interpretation of the results is simplified by the fact that, due to the viscous force, the normal component is clamped to the wall of the solid substrate in a thin layer a few hundred ångströms thick.

If the Landau equations are adequate to describe the hydrodynamical behaviour of the film, they are still not sufficient to describe the film completely. As the film is in contact with its vapour, equilibrium conditions between liquid and vapour should also be included. For bulk He II, these conditions are derived by Putterman and Uhlenbeck[6]. *A priori*, there seems to be no reason to doubt the validity of the Landau equations, as well as these equilibrium conditions for the description of the film.

However, there are some experimental results which appear to be

contradictory to such a description, in other words it seems that the behaviour of the film is basically different from that of bulk liquid. First, there is the experiment of Keller[7], who found no difference in thickness between a moving film and a static one. According to the Landau equations and the vapour--liquid equilibrium conditions, the moving film should be thinner, as was first shown by Kontorovich[8].

Secondly, there is the experiment of Little and Atkins[9], in which the meniscus of a rotating film was studied and a temperature-dependent meniscus found. This result is consistent with the theory in the case that in the film, unlike the bulk, only the normal component participates in the rotation. It is however not at all obvious why their statement should be fulfilled that a regular array of vortices cannot be formed in the film as is the case in the bulk, where it leads to a classical temperature-independent meniscus. Furthermore, one can raise objections against their experimental arrangement. For instance, they determined the change in film thickness on the rotation axis, where the velocities of both the superfluid- and normal component are zero, so that at first sight no change at all should be expected.

The third group of experiments, pointing towards a deviating behaviour of the film, is concerned with the apparent impossibility to create persistent flow in a saturated film, *i.e.* in a film in contact with bulk liquid[10,11].

In order to explain the different behaviour of the film, additional conditions were conjectured by several authors.

This thesis is concerned with the investigation of this possible difference between bulk- and film behaviour. Mainly the first two types of experiments, namely the Kontorovich effect and the shrunken meniscus, are discussed. For the experiments a new technique was used. In chapter I, measurements on the static film thickness illustrate this new technique. Chapter II describes measurements on the film thinning for different types of flow. The last chapter deals with the rotating He II film in different geometries. Also some attempts to establish persistent flow in a film are described. The recent successful methods to create and detect persistent currents in a saturated He II film by the Leiden group[12,13] will not be treated in this thesis.

References

1. London, F., Nature, Lond. 141 (1938) 643.
2. Tisza, L., C.r. hebd. Séanc.Acad.Sci., Paris 207 (1938) 1035, 1186.

3. Landau, L., Zh. éksp. teor. Fiz. 14 (1944) 112; J. Phys. Moscow 8 (1944) 110.
4. Kamerlingh Onnes, H., Leiden Comm. 159; Trans. Faraday Soc. 18 (1922) No. 53.
5. Rollin, B.V., Proc. 7th. Intl. Cong. Refrig., I.I.R. Paris, 1 (1936) 187. Rollin, B.V. and Simon, F., Physica 6 (1939) 219.
6. Putterman, S.J. and Uhlenbeck, G.E., Phys. of Fluids 12 (1969) 2229.
7. Keller, W.E., Phys. Rev. Letters 24 (1970) 569.
8. Kontorovich, V.M., Sov. Physics-JETP 3 (1956) 770.
9. Little, R.E. and Atkins, K.R., Phys. Rev. Letters 19 (1967) 1224.
10. Wang, T.G. and Rudnick, I., Proc. LT 13, Boulder, U.S.A., 1972.
11. Wagner, F., J. Low Temp. Phys. 13 (1973) 185.
12. Verbeek, H.J., Van Spronsen, E., Mars, H., Van Beelen, H., De Bruyn Ouboter, R. and Taconis, K.W., Physica 73 (1974) 621.
13. Verbeek, H.J., Van Spronsen, E., Van Beelen, H., De Bruyn Ouboter, R. and Taconis, K.W., Physica 77 (1974) 131.

CHAPTER I

THICKNESS OF A STATIC FILM

1. Introduction

Soon after the discovery of the film by Rollin[1], explaining the Kamerlingh Onnes effect[2], and the experiments of Daunt and Mendelssohn[3] and Kikoin and Lasarew[4], the first theoretical treatments were given by Frenkel[5] and Schiff[6]. In these theories, the surface of a static film in equilibrium with bulk liquid is an equipotential surface determined by the gravitational- and Van der Waals forces, yielding the relation for the thickness δ:

$$gz - \frac{\gamma}{\delta^3} = 0 \ , \qquad (1)$$

with z the height above the bulk liquid and γ a constant determining the strength of the Van der Waals forces between solid substrate and helium. Several authors[7-13] refined the theory by including other effects, as for instance the zero point energy, leading to modification of the Van der Waals potential in eq. (1). In order to check the different theories, it is necessary to measure the thickness as a function of the height above the bulk liquid. A range of experimental methods has been used. There is the oscillation technique used by Atkins[14], the adsorption isotherm measurements of Bowers[15], Evenson *et al.*[16] and Herb *et al.*[17], and the optical elliptometry technique of Jackson and co-workers[18-22] and Hemming[23]. Measurements of the change in the resonance frequency of a quartz crystal owing to the mass loading by the helium film have been done by Chester *et al.*[24]. Recently Sabisky and Anderson[25] made very accurate measurements of the thickness on atomically flat regions using high frequency first-sound resonances. They find an exceptionally good agreement with the Lifshitz formula[12]. This relation predicts a $z^{-1/3}$ dependence for small thickness (eq. (1)) and, due to retardation effects, a transition to a $z^{-1/4}$ law for large thickness of the film (see fig. 1).

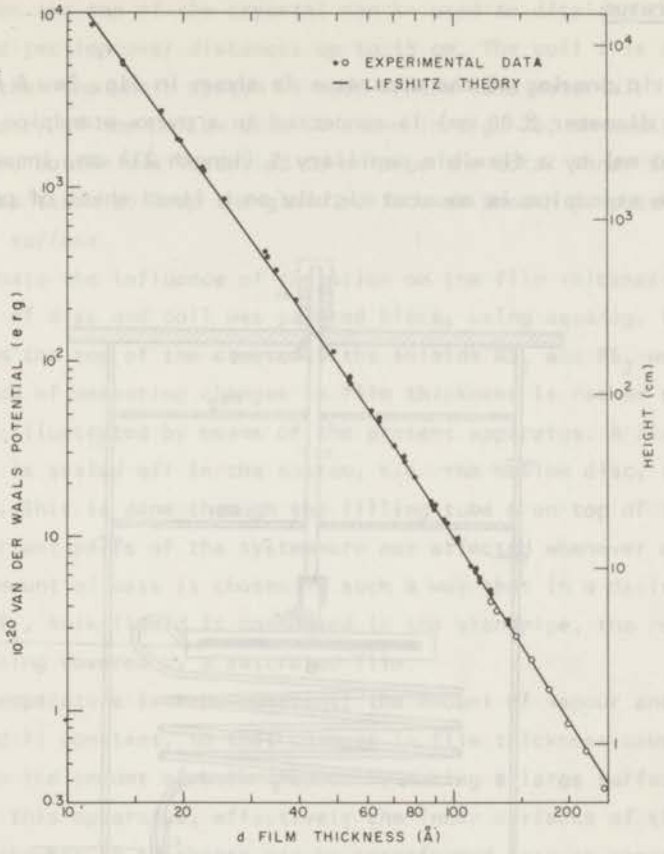

Fig. 1 *The thickness of the film as a function of the height above the bulk, as determined by Sabisky and Anderson. The full line is the theoretical curve corresponding to the Lifshitz formula.*

Comparing the results obtained by different methods and for different substrates, a rather large variation is found, probably due to surface roughness of the solid substrates involved.

The purpose of this chapter is merely to illustrate a new measuring technique for changes in thickness of the saturated He II film used in the further experiments treated in this thesis. The present analysis will therefore be restricted to test the inverse cube law given by eq. (1).

2. The apparatus

A schematic drawing of the apparatus is shown in fig. 2a. A hollow pyrex disc D (inner diameter 8.00 cm) is connected to a pyrex standpipe C (inner diameter 0.020 cm) by a flexible capillary S (length 214 cm, inner diameter 0.035 cm). The standpipe is mounted rigidly on a fixed sheet of perspex. A

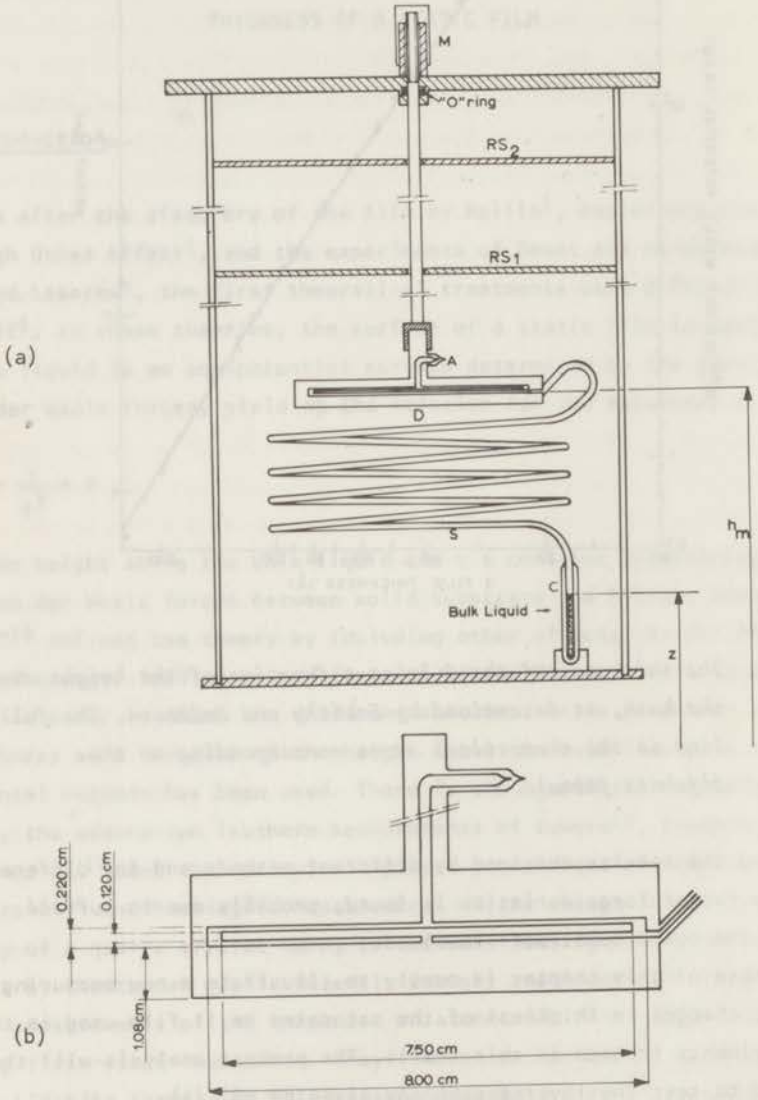

Fig. 2 *Schematic drawing of the apparatus (a) and the hollow disc (b). For symbols, see text.*

micrometer M on the top of the cryostat can be used to displace the disc in the vertical direction over distances up to 15 cm. The coil S is also made of pyrex, so that the whole system is made of the same material.

The geometry of the hollow disc is shown in fig. 2b; an additional disc between top and bottom was installed to enlarge the total inner surface area. Utmost care was taken to keep the glass surface as smooth as possible by flame polishing the surface.

To eliminate the influence of radiation on the film thickness, the entire outer surface of disc and coil was painted black, using aquadag. To reduce the radiation from the top of the cryostat, the shields RS_1 and RS_2 were installed.

The method of measuring changes in film thickness is rather simple, and can be nicely illustrated by means of the present apparatus. A fixed amount of helium gas is sealed off in the system, *i.e.* the hollow disc, the coil, and the standpipe. This is done through the filling tube A on top of the disc, so that the important parts of the system are not affected whenever a refill is needed. The amount of mass is chosen in such a way that in a desired temperature region below T_λ, bulk liquid is condensed in the standpipe, the rest of the system then being covered by a saturated film.

If the temperature is kept constant, the amount of vapour and therefore also of liquid is constant, so that changes in film thickness cause a corresponding change in the amount of bulk liquid. By taking a large surface O_f covered with film (in this apparatus, effectively the inner surfaces of the hollow disc), small changes in thickness can be transformed into an appreciable change in film volume. By taking the cross-sectional area of the standpipe O_s small, this change in film volume causes a change in the height of the bulk level, which can easily be measured, in this case with a cathetometer (accuracy about 10^{-3} cm). The obvious disadvantage which this method shares with most other methods is the fact that it measures an average change in thickness instead of a local change. However, it enables research on the helium film by monitoring bulk liquid levels, which is rather easy compared with other techniques.

The accuracy of the measurements of the change in thickness depends of course on the ratio O_f/O_s, which for this apparatus is about 6×10^5, yielding a change in bulk level of 6×10^{-3} cm if $\overline{\Delta\delta} \simeq 1$ Å.

3. Experimental results

The whole system is immersed in a helium bath the temperature of which is kept constant within $10^{-4} - 10^{-5}$ K. The height of a fixed point on the disc and

the height of the bulk level are measured with respect to an arbitrary reference point. The disc is then lowered over some known distance by the micrometer and the height z of the bulk is measured again. This procedure is repeated as long as possible. An example of such a measuring run is shown in fig. 3. In this figure h_m is the height of the middle of the disc above the reference point.

As the total amount of liquid is constant, the following equation holds:

$$\iint_{O_f} \delta \, dO + O_s z = \text{constant} . \qquad (2)$$

In O_f, one should also include the surface of the coil, the surface of the filling tube, and the connections where the different parts of the glass system are fused together. If, for simplicity, we first neglect all these surfaces contributing to the film volume and assume the same Van der Waals constant γ for all surfaces of the disc, using eq. (1), eq. (2) can be written as:

$$\kappa \iint_{O_f^{disc}} (h - z)^{-1/3} \, dO + O_s z = \text{constant} , \qquad (3)$$

with $\kappa = (\gamma/g)^{1/3}$. By writing the conservation of liquid in this way, the feedback effect on the film thickness due to a change in z is taken into account automatically. The simplest way to check the inverse cube law is to neglect the small differences in height of the surfaces in the hollow disc, and to replace in eq. (3) the variable h by the constant h_m defined earlier. Eq. (3) is then simplified to

$$\kappa \, O_f^{disc} \, (h_m - z)^{-1/3} + O_s z = \text{constant} . \qquad (4)$$

From eq. (4) it follows that the slope of the straight line obtained when $(h_m - z)^{-1/3}$ is plotted against z is given by $-\kappa \, O_f^{disc}/O_s$. Of course, the approximation used to obtain eq. (4) becomes worse, the smaller $h_m - z$. Fig. 4 shows the results for different temperatures, and indeed for not too small values of $h_m - z$ the data fit nicely on a straight line. The large shift in the height of the bulk above the reference point at constant $h_m - z$ can be accounted for by the variation of the saturated vapour pressure with temperature. Note that even if $h_m - z$ is the same for different temperatures, the geometry is not exactly the same, namely the position of the flexible coil is different. Therefore a more accurate method is to use eq. (2) without neglecting any of the surfaces. We have carried this out, using eq. (1) and eq. (2), and assuming

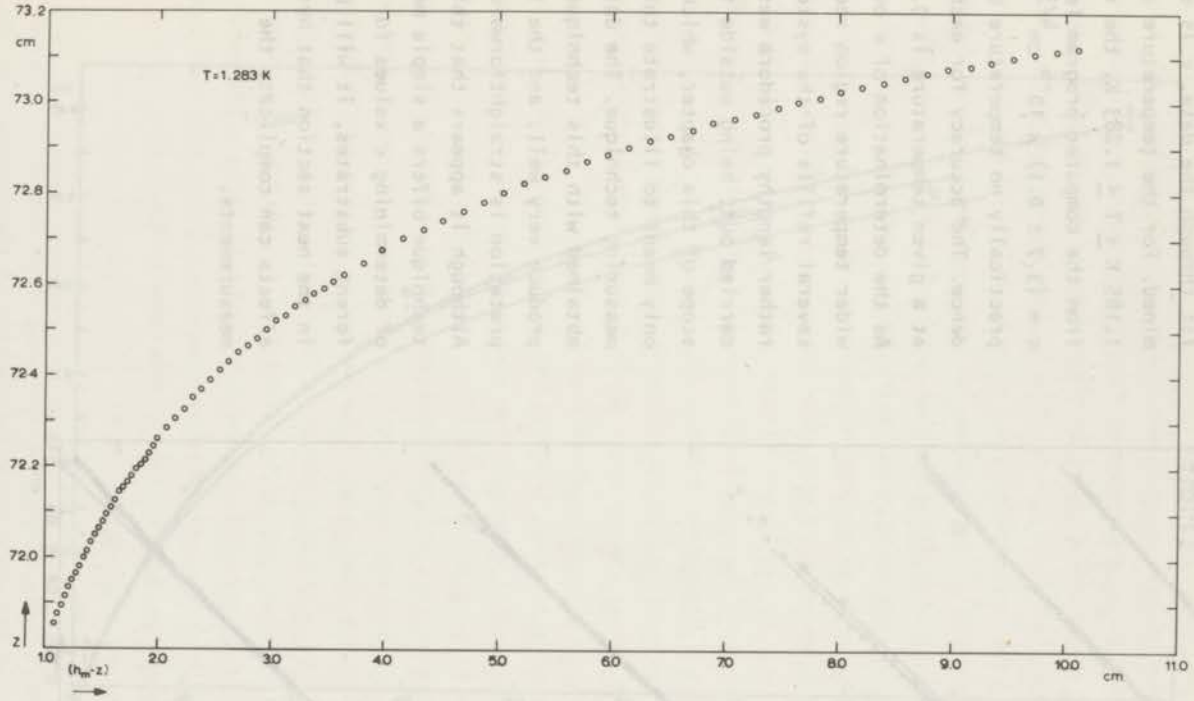

Fig. 3 *The height of the bulk liquid level z in the standpipe as a function of the height $h_m - z$ of the middle of the hollow disc. The absolute values on the ordinate are measured with respect to an arbitrary reference point.*

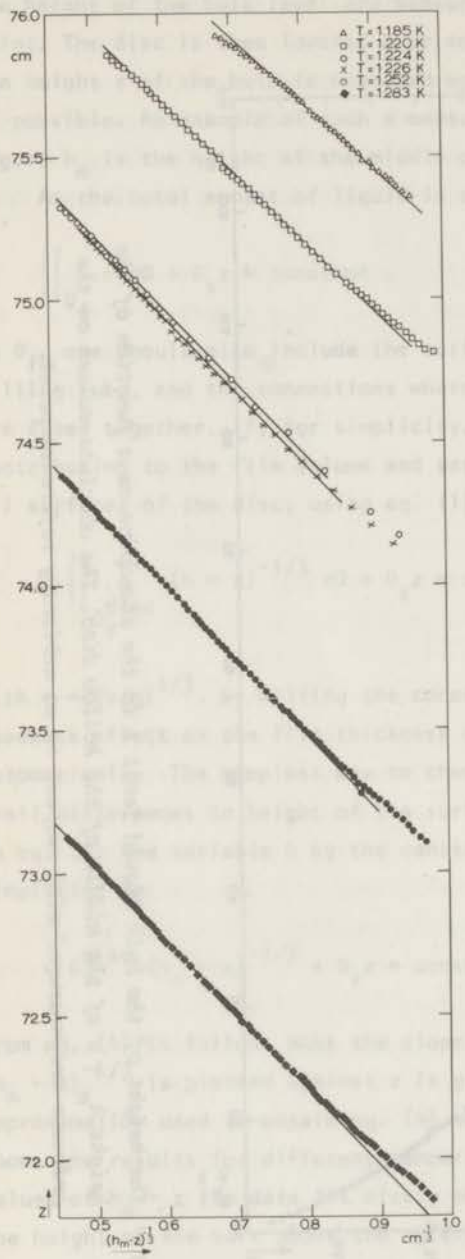

that again κ (or γ) is the same for all surfaces. By a least squares fit through the data, κ is determined. For the temperature range $1.185\ K \leq T \leq 1.283\ K$, the result from the computer program is: $\kappa = (3.7 \pm 0.1) \times 10^{-6}\ cm^{4/3}$, with practically no temperature dependence. The accuracy for each run at a given temperature is 0.5%. As the determination of κ over a wider temperature region requires several refills of the system, this rather lengthy procedure was not carried out, being outside the scope of this chapter, which is only meant to illustrate this new measuring technique. The data obtained with this technique reproduce very well, and the interpretation is straightforward. Although it appears that this technique offers a simple method of determining κ values for different substrates, it will be shown in the next section that hysteretic effects can complicate the measurements.

Fig. 4 *The height of the bulk level (z) as a function of* $(h_m - z)^{-1/3}$ *for different temperatures. The reference point for z is the same for all temperatures.*

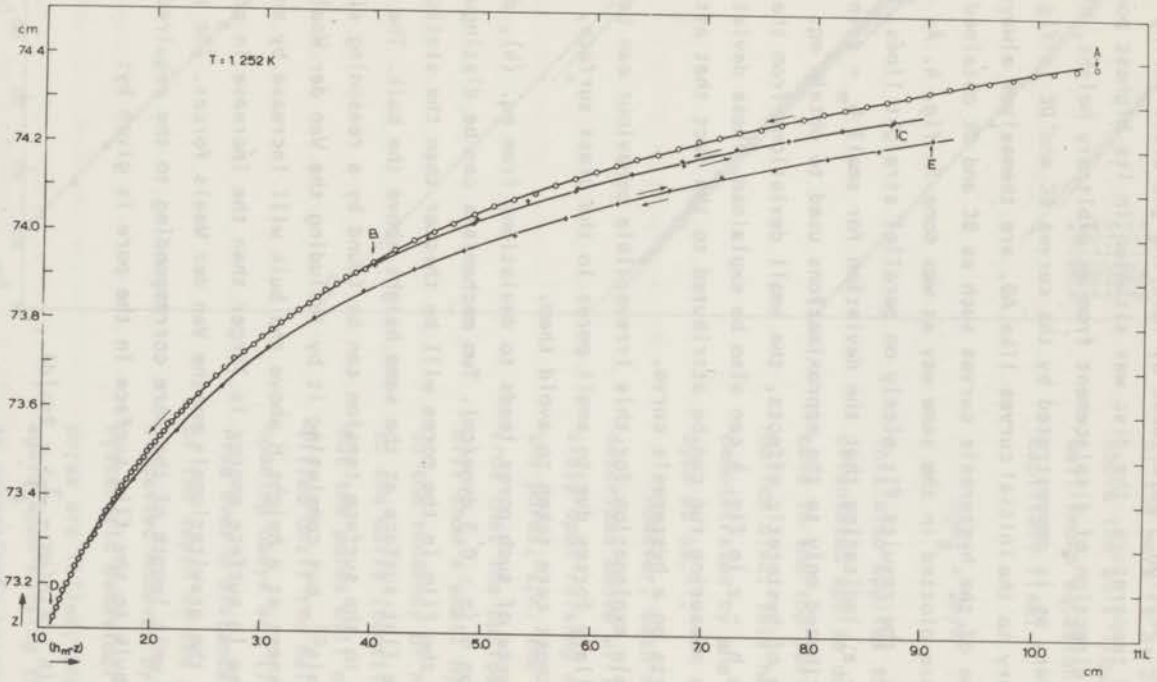

Fig. 5 *Height of the bulk liquid as a function of $h_m - z$, showing hysteretic behaviour. The arrows indicate the direction of the displacement of the disc (raising → , lowering ←).*

4. Hysteretic effects

All data of section 3 were taken by lowering the disc. During the cooldown to the desired temperature, the disc was situated in its highest position. On reversing the direction of displacement from an arbitrary height, hysteretic phenomena appear, as is demonstrated by the curves BC and DE in fig. 5. These curves, contrary to the initial curves like AD, are themselves always reversible. In fig. 6, some of the hysteresis curves such as BC and DE obtained at various temperatures are plotted in the same way as was done in fig. 4. As can be seen from this plot, the results fit nicely on parallel straight lines, even for small values of $h_m - z$, indicating that the deviation for small $h_m - z$ in fig. 4 cannot be attributed only to the approximations used to obtain eq. (4). From the occurrence of hysteretic effects, the small deviations from the straight line for large $h_m - z$ in fig. 4 can also be explained. These deviations at the beginning of a measuring run can be attributed to the fact that after the cooldown, one starts on a hysteresis curve.

A plausible explanation for this irreversible behaviour can be found in terms of capillary forces due to small pores in the glass surface, present despite the utmost care taken to avoid them.

The presence of such pores leads to deviations from eq. (4), due to the surface tension σ ($\sigma \simeq 0.3$ dyne/cm). Two mechanisms can be distinguished.

Firstly, the film in the pores will be thicker than the static film thickness δ_0 on the flat surface at the same height above the bulk. The increase in thickness due to the surface tension can be found by a reasoning similar to that given by Taconis[26], but completing it by including the Van der Waals forces. The film thickness at a height H above the bulk will increase by an amount $d\delta$ if the decrease in surface energy is larger than the increase in potential energy due to the gravitational- and the Van der Waals forces. The total change of energy per unit length of the pore corresponding to the required mass transfer from the bulk to the film surface in the pore is given by:

$$dE = [2\pi(R - \delta)\rho(gH - \frac{\gamma}{\delta^3}) - 2\pi\sigma]d\delta \ , \qquad (5)$$

with R the radius of the pore and ρ the density of the liquid. From eq. (5), it follows that the thickness of the film will increase until an equilibrium value $\delta(\delta \geq \delta_0)$ is reached, obeying the relation:

$$gH - \frac{\gamma}{\delta^3} = \frac{\sigma}{\rho(R - \delta)} \ . \qquad (6)$$

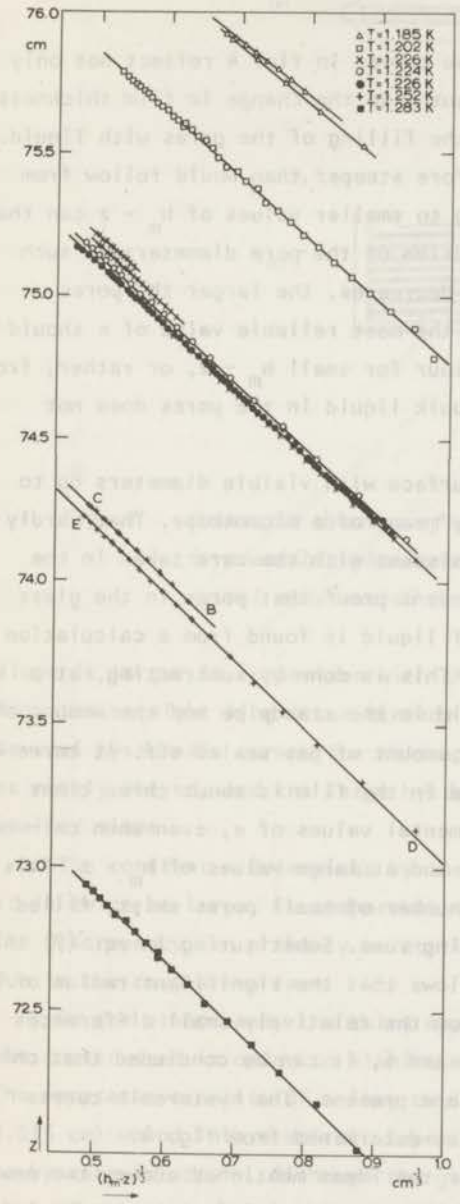

Fig. 6 *Hysteretic curves for different temperatures, showing the inverse cube law. The curves BC and DE correspond to the curves BC and DE in fig. 5.*

Secondly, bulk formation in the pore will occur when the bottom of the pore is at a height H_B above the bulk liquid, obeying the well-known equation for the capillary rise:

$$\rho g H_B = 2\sigma/R \quad . \qquad (7)$$

This also applies to the pores orientated upside down, as is the case in the top surfaces of the hollow disc. This has been nicely demonstrated by the experiments of Dyba *et al.*[27].

However, both mechanisms described above will behave reversibly upon raising or lowering of the pores, *i.e.* the disc. It is true that the upside down pores will show a small hysteresis due to the tendency of helium to stick to the walls (tensile strength[28]). But the pores will only remain filled until the height of its opening obeys eq. (7), implying a rise over a distance of the order of the depth of the pore. It is suggested however by the observed hysteretic behaviour, that once the pores are filled, they do not empty again upon raising the disc over an appreciable height. This situation can be realized if the pores are bottle-shaped, because then they do not empty until the neck is at a height H_N given by eq. (7), replacing R by the smaller

radius of the neck, r, resulting in a height H_N larger than H_B. The occurrence of this type of pore seems reasonable, since the glass surfaces were flame polished.

From these remarks, it follows that the curves in fig. 4 reflect not only the change in thickness given by eq. (1), but also the change in film thickness due to the surface tension (eq. (6)), and the filling of the pores with liquid. The slope of the curves in fig. 4 is therefore steeper than would follow from eq. (1). The decrease of the slope on going to smaller values of $h_m - z$ can then be attributed to the fact that the distribution of the pore diameters is such that the liquid required to fill the pores decreases, the larger the pores. The best check of the inverse cube law and the most reliable value of κ should then be obtained from the asymptotic behaviour for small $h_m - z$, or rather, from the hysteresis curves where the amount of bulk liquid in the pores does not change.

The existence of pores in the glass surface with visible diameters up to a few microns has been directly verified by means of a microscope. That hardly any larger pores have been observed is consistent with the care taken in the construction of the hollow disc. An independent proof that pores in the glass surface do contain a considerable amount of liquid is found from a calculation of the total amount of helium in the film. This is done by subtracting, at a given temperature, the amount of bulk liquid in the standpipe and the amount of vapour in the known volume, from the total amount of gas sealed off. It turns out that the so-calculated amount of liquid in the film is about three times as large as would correspond to the experimental values of κ, even when calculated from the steepest slopes in fig. 4 and at large values of $h_m - z$. This indicates that in this apparatus, a large number of small pores exist, filled with liquid at all times during the measuring runs. Substituting in eq. (7) the largest values of $h_m - z$ ($\simeq$ 10 cm), it follows that the significant radius of these pores should be smaller than 5 μ. From the relatively small differences in κ values as determined from the figs. 4 and 6, it can be concluded that only small number of larger pores (up to 50 μ) are present. The hysteresis curves in fig. 6 yield a κ value about 10% lower as determined from fig. 4.

In order to obtain further support for the ideas mentioned above, two new pieces of apparatus were constructed from the same material (schematic drawings are shown in fig. 7). To obtain a sizeable number of large pores, rough glass surfaces, fused together with sharp rims, were used (7a). Furthermore, little care was taken to avoid contamination. In fig. 8a, some examples of measurements of the initial curves for different temperatures are shown. As expected, the

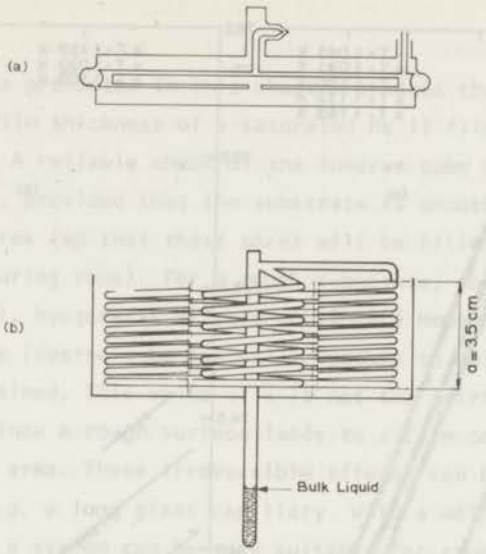

Fig. 7 *Schematic drawing of the hollow disc made to enlarge the irreversible phenomena (a), schematic drawing of the long spiral constructed to eliminate hysteretic effects (b).*

slope is larger in comparison with the previous results, and obvious deviations from the straight line occur already at a rather large $h_m - z$. Fig. 8b shows several hysteresis curves for this apparatus. The inverse cube law appears to be nicely obeyed, and the large hysteresis is clearly shown by their much smaller slope.

The constant κ determined by the slope of the lines in fig. 8b, although it is twice as large, is comparable to that determined in the first apparatus. The discrepancy can probably be attributed to an increase of the effective area due to the rougher surface.

On the other hand, the third apparatus, schematically drawn in fig. 7b, was constructed in order to eliminate irreversible phenomena as much as possible. The apparatus consists of a long capillary (length 166 m, inner diameter 0.035 cm) wound into a spiral. Experimentally it is found that indeed practically no hysteresis occurs. Although the general behaviour is again very similar to that of the other apparatus, detailed results will not be given as an exact calculation of the thickness dependence cannot be carried out. This is due to the fact that in order to obtain a close packing (the height a of the coil is kept as small as possible), the distribution of the windings over the height a is not precisely known.

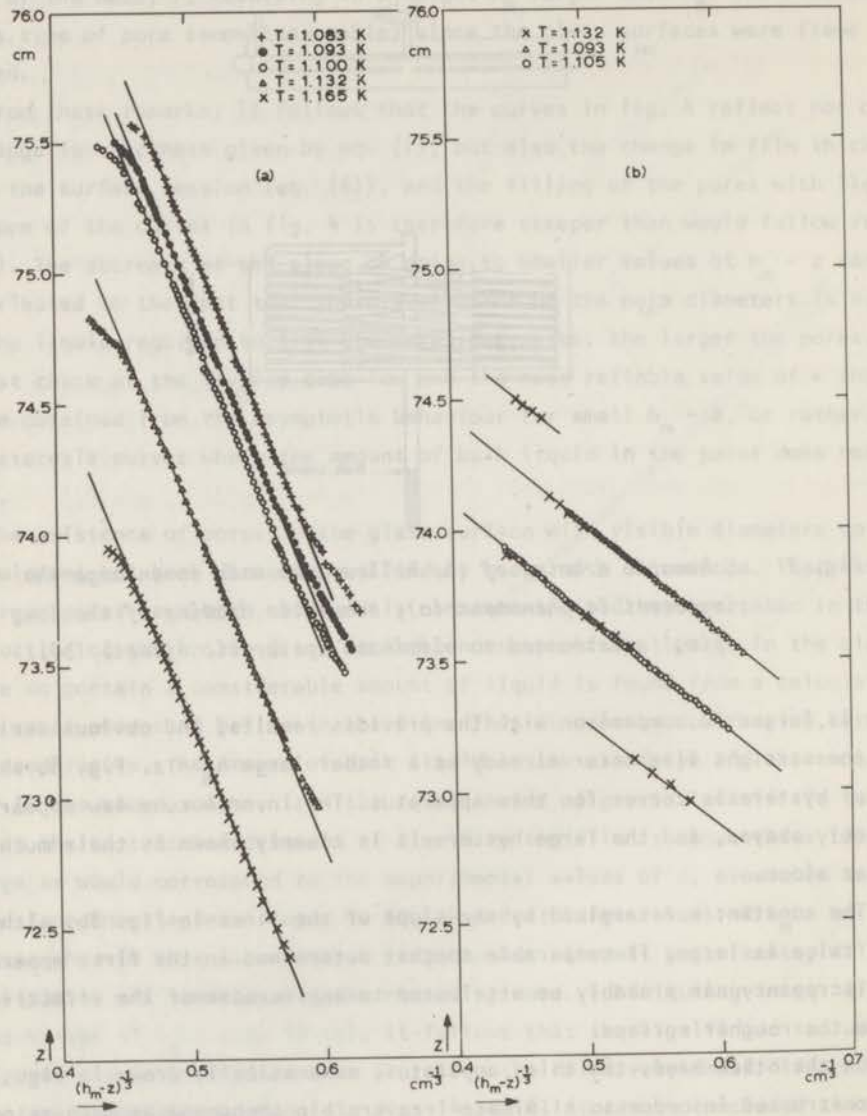

Fig. 8 *Dependence of z on $(h_m - z)^{-1/3}$ for some initial curves obtained for the disc shown in fig. 7a (a), and some hysteretic curves for the same disc (b).*

5. Conclusion

The new technique presented in this chapter creates the possibility of studying changes in film thickness of a saturated He II film by monitoring bulk liquid level(s). A reliable check of the inverse cube law for the film thickness is obtained, provided that the substrate is smooth, containing none or only very small pores (so that these pores will be filled by liquid at all times during the measuring runs). For a rough substrate, containing pores of relatively large radii, hysteretic effects do appear. However, for the hysteretic curves, the inverse cube law still appears to hold, and an effective value of κ can be obtained. This value of κ is not the intrinsic value for the substrate material, since a rough surface leads to a film covering a not exactly known surface area. These irreversible effects can be practically eliminated by using *e.g.* a long glass capillary. With a well-known distribution of the windings, such a system can be very suitable for studying changes in film thickness in He II or in ^{3}He-^{4}He mixtures below their lambda temperature.

References

1. Rollin, B.V., Proc. 7th Intl. Cong. Refrig., I.I.R. Paris, 1 (1936) 187; Rollin, B.V. and Simon, F., Physica 6 (1939) 219.
2. Kamerlingh Onnes, H., Leiden Comm. 159, Trans. Faraday Soc. 18, (1922) No. 53.
3. Daunt, J.G. and Mendelssohn, K., Proc. Roy. Soc. A170 (1939) 423, 439.
4. Kikoin, A.K. and Lasarew, B.G., Nature 141 (1938) 912; 142 (1938) 289.
5. Frenkel, J., J. Phys. Moscow 2 (1940) 345.
6. Schiff, L., Phys. Rev. 59 (1941) 839.
7. Bijl, A., De Boer, A. and Michels, J., Physica 8 (1941) 655.
8. Mott, N.F., Phil. Mag. 40 (1949) 61.
9. Atkins, K.R., Canad. J. Phys. 32 (1954) 347.
10. Franchetti, S., Nuovo Cimento 4 (1956) 1504; 5 (1957) 183.
11. Casimir, H.B.G. and Polder, D., Phys. Rev. 73 (1948) 360.
12. Lifshitz, E.M., Zh. Eksperim. i. Teor. Fiz. 29 (1955) 94 [Sov. Phys.-JETP 2 (1956) 73]; Dzyaloshinskii, I.E., Lifshitz, E.M. and Pitaevskii, L.P., Advan. Phys. 10 (1961) 165.
13. Matsuda, H. and Van den Meijdenberg, C.J.N., Physica 26 (1960) 939.
14. Atkins, K.R., Proc. Roy. Soc. A203 (1950) 119.

15. Bowers, R., Phil. Mag. 44 (1953) 465, 485.
16. Evenson, A., Brewer, D.F., Symonds, A.J. and Thomas, A.L., Phys. Letters 33 (1970) 35.
17. Herb, J.A. and Dash, J.G., Phys. Rev. Letters 29 (1972) 846.
18. Burge, E.J. and Jackson, L.C., Proc. Roy. Soc. A205 (1951) 270.
19. Jackson, L.C. and Henshaw, D.G., Phil. Mag. 44 (1953) 14.
20. Ham, A.C. and Jackson, L.C., Phil. Mag. 44 (1953) 214; 45 (1954) 1084; Proc. Roy. Soc. A240 (1957) 243.
21. Jackson, L.C. and Grimes, L.G., Phil. Mag. Suppl. 7 (1958) 435.
22. Grimes, L.G. and Jackson, L.C., Phil. Mag. 4 (1959) 1346.
23. Hemming, D., Canad. J. Phys. 49 (1971) 2621.
24. Chester, M., Yang, L.C. and Stephens, J.B., Phys. Rev. Letters 29 (1972) 211.
25. Sabisky, E.S. and Anderson, C.H., Phys. Rev. Letters 24 (1970) 1049; Phys. Rev. A7 (1973) 790.
26. Taconis, K.W., Phys. Rev. 97 (1955) 1176.
27. Dyba, R.V., Lane, C.T. and Blakewood, C.H., Phys. Rev. 95 (1954) 1365.
28. Beams, J.W., Phys. Rev. 104 (1956) 880.

CHAPTER II

THE THICKNESS OF A MOVING He II FILM, THE KONTOROVICH EFFECT

1. Introduction

Kontorovich[1] derived from the Landau equations that a moving film is thinner than a static one by an amount

$$\Delta\delta/\delta_0 = -\tfrac{1}{2}\rho_s v_s^2/3\rho g H \quad . \tag{1}$$

In this expression δ_0 is the static film thickness, v_s the superfluid velocity, and H the height of the film above the bulk liquid. Measurements of this thickness reduction by Keller[2] gave negative results: no change of film thickness was observed.

In this chapter, experiments are presented to study the change in film thickness caused by a superfluid velocity. The same technique is used as described in chapter I. The system consists of a long glass capillary closed at both ends by standpipes (see fig. 1). The film is brought into oscillatory motion by creating a level difference between the bulk levels in the standpipes[3]. This oscillation will be called an "Atkins oscillation", as Atkins was the first to study this type of film motion[4]. The Atkins oscillation is studied by monitoring the bulk levels in the standpipes. The Kontorovich effect can be deduced directly from the amount of excess liquid in the standpipes caused by the thinner film when the film is moving at its maximum velocity during the oscillation, since the total amount of liquid in film and bulk is constant if the temperature is constant.

In this chapter, a full discussion will be given of the results obtained in glass capillaries of different lengths, ranging up to 200 m. Also measurements on the Kontorovich effect are reported for which the flow is stationary, which is, strictly speaking, not the case during an oscillation.

In section 2 the apparatus is described, in section 3 the various

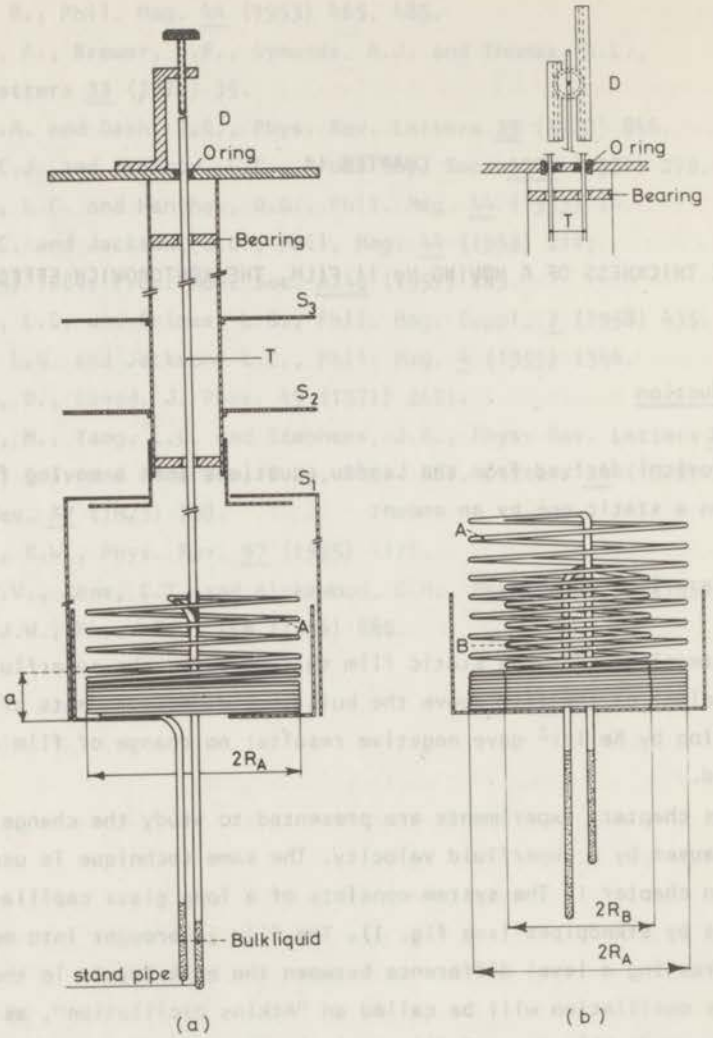

Fig. 1 *Schematic drawing of the apparatus of type a and b (see text).*

experimental methods will be discussed. The Atkins oscillation itself, ignoring changes in film thickness, is discussed in section 4. Changes in film thickness, such as the Kontorovich effect, but also the third-sound waves which accompany the Atkins oscillation, are treated in section 5. Finally, in section 6, a survey of the experimental results is given, and it is shown how the Kontorovich effect is deduced from these results.

2. The apparatus

In all the experiments, a long and narrow glass capillary wound into a spiral is used. The capillary is closed at both ends by vertical standpipes (see fig. 1). In table 1, the characteristics of the different coils are given.

TABLE 1

CHARACTERISTICS OF THE APPARATUS

Type of apparatus		Length of the capillary (m)		Inner diameter of the capillary (cm)		Inner diameter standpipes (cm)	Winding radius of the coils (cm)		Height of the coils a (cm)
		spiral A	spiral B	d_A	d_B		R_A	R_B	
a	1	21	-	.036	-	.036	3.0	-	5
	2	166	-	.035	-	.034	6.0	-	5
b	1	120	2	.033	.04	.033	5.0	3.0	4
	2	100	100	.027	.027	.025	7.0	6.0	1.8

The capillaries are filled with a certain amount of pure He gas, which is sealed off at liquid-nitrogen temperature. The amount of helium is chosen in such a way that when the spirals are cooled down to a temperature below the lambda point of He, bulk liquid is formed at the lowest parts of the spiral, partially filling the standpipes, while the inner wall of the capillary is covered over its whole length by a saturated He film. Loss of He due to diffusion through the thin glass wall of the capillary (pyrex of 0.025 cm wall) can be prevented by storing the spirals at low temperature.

Although the measurements are carried out with the whole system immersed in the He bath, complications due to unwanted temperature differences can still arise due to radiation. For this reason the brass shield S_1, painted black on the inside, surrounds the coil. To reduce the radiation from the top of the cryostat, the extra shields S_2 and S_3 are installed.

The film is brought into motion by a vertical displacement of the standpipes, which is accomplished by means of a mechanical device D outside the cryostat, connected to the standpipes by stainless steel tubes (T). The liquid levels in the standpipes are monitored using a cathetometer.

In the earlier experiments (fig. 1a), only one of the standpipes could be displaced by the mechanical system. This has the obvious disadvantage that, upon each displacement, the averaged height of the film above the liquid levels in the standpipes undergoes a corresponding change. In the later experiments (fig. 1b), this disadvantage has been removed, both standpipes are displaced

simultaneously by the same amount, but in opposite directions. Moreover, in the final arrangement, two spirals A and B, of the same length and inner diameter were used in series, and at the same height above the bulk liquid. In this way complications due to the inherent asymmetry of a single spiral are eliminated. This asymmetry results in a difference between the amplitude in both standpipes (see fig. 3b), due to the difference in height of the outer windings at both ends of the coil above the nearest bulk liquid.

3. Experimental methods

The whole system is immersed in the He bath. The temperature of the bath is adjusted to the desired value, which is kept constant to within 10^{-4} K. The first experiment, using a capillary of only 21 m length, was carried out in order to investigate whether superfluidity would extend in a thin film over distances of this order of magnitude. This proved to be the case and the expected Atkins oscillation could indeed be generated. Due to the comparatively short length of the capillary, the amount of excess liquid in the standpipes provided by the Kontorovich thinning is too small to be measured with sufficient accuracy. In order to increase the sensitivity, the measurements were extended to a capillary of 166 m length. The aim was to generate an Atkins oscillation, and to deduce the Kontorovich effect from a comparison of the amount of liquid in the standpipes at the moment during the oscillation when the film is at rest, with the amount when the film moves at maximum velocity. However, it will be shown in section 5 that, due to the nonstationary character of the Atkins oscillation, this method is incorrect. The Kontorovich effect should be deduced from a comparison of the thickness at maximum velocity with the thickness before the Atkins oscillation is started, *i.e.* when the film is completely at rest. In practice, it proved to be difficult to carry out this latter procedure in the present apparatus. In this long capillary, almost undamped additional level oscillations always appear to be present. These oscillations will be identified as standing third-sound waves in section 5.

One of the methods to reduce the amplitude of these additional oscillations is to use a shorter capillary. The loss of sensitivity can be compensated by allowing for a smaller H (eq. (1)). This could not be accomplished with the capillary of 166 m, due to the fact that one of the standpipes was connected to the capillary some distance below the lowest winding of the coil. As at such a connection the diameter is nonuniform, measurements for small H are prohibited. The 120 m capillary was therefore constructed, on which the earlier reported

results on the Kontorovich effect are obtained[3]. Both standpipes are connected to the top of the spiral, thus allowing for a smaller possible H, while furthermore the construction is such that both standpipes are simultaneously movable (see section 2). From these experiments, a better understanding of the additional effects, such as the standing third-sound waves, is obtained. It became clear how the influence of these effects could be largely eliminated from the data in order to deduce the thinning effect separately from the overall results (see section 6). The sensitivity of the measurements could therefore be increased again, by using a capillary with a length of 200 m. By taking two coils of the same length and inner diameter, the additional advantage of a symmetric apparatus is incorporated.

The Kontorovich effect is measured for the following types of film flow:

1. nonstationary flow
   - during the Atkins oscillation (3.1.1)
   - during film flow with constant acceleration (3.1.2)
2. stationary flow *i.e.* the film flows at constant velocity
   - at or just above the critical velocity (3.2.1)
   - at subcritical velocities (3.2.2)
   - in persistent film flow (3.2.3)

In the following subsections, the methods used to obtain these different types of flow are discussed in some detail.

3.1 Nonstationary flow

3.1.1 The Atkins oscillation. Suppose the film is originally at rest. By giving the standpipe(s) a vertical displacement, a level difference is created starting an Atkins oscillation, from which the Kontorovich effect can be determined. A possible error could be introduced in this way by a slight variation of the inner diameter along the standpipes. Therefore, after half a period of oscillation, the standpipe(s) are moved back to their original position, thereby increasing the amplitude of the oscillation. In this way any desired maximum velocity below the critical velocity can in principle be generated.

However, it should be remarked that in order to obtain a high velocity, a large displacement of the standpipes would be required, introducing

simultaneously pronounced third-sound effects in the system. Figure 2 shows a clear example of an Atkins oscillation on which a third-sound wave is superimposed. To avoid the generation of third sound as much as possible, a series

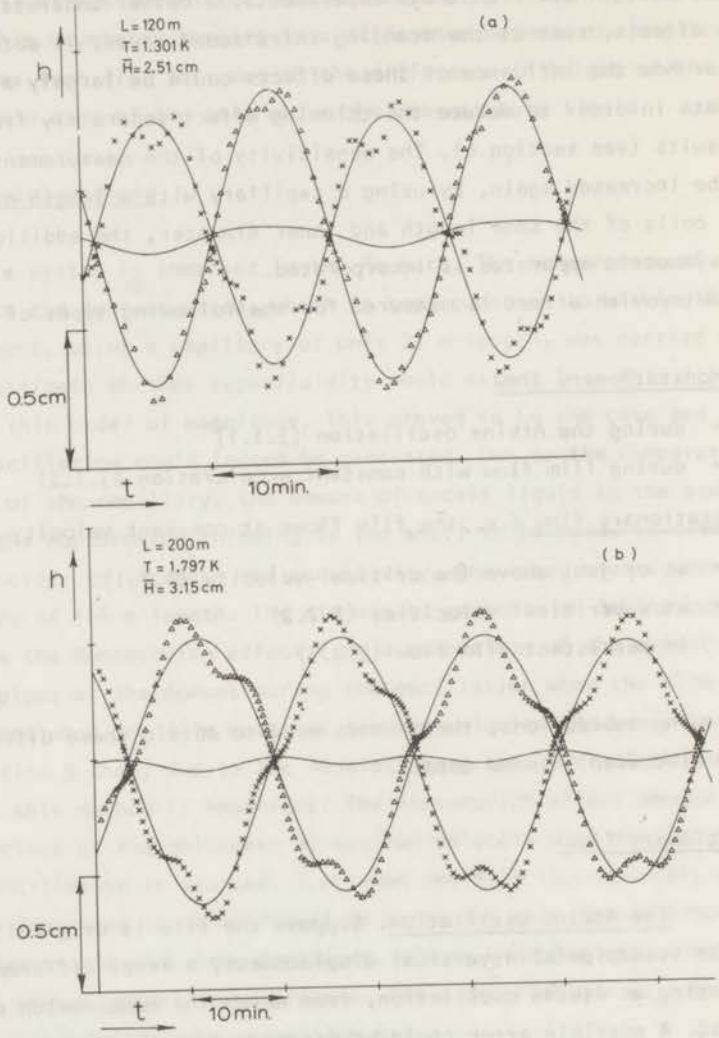

Fig. 2 *Observed level oscillations clearly showing standing third-sound waves superimposed on the Atkins oscillation.* Δ: h_r; ×: h_l.

of small displacements should be used instead of a large one.

In view of the oscillation time, this procedure is rather tedious. Another method to obtain high velocities without introducing large third-sound

effects is to first accelerate the film to its critical velocity and maintain it at this velocity during a time interval long enough to damp out the third--sound waves. Some examples of an Atkins oscillation generated in this way are shown in fig. 3, the maximum velocity being about the critical velocity. In practice, this procedure is carried out in the following way: first the standpipes are displaced over a large distance, by which the film is accelerated to its critical velocity (of course at the same time also generating a third-sound wave). The flow at the critical velocity is prolonged by creating a small level difference every time the levels in the standpipes are again equal. This

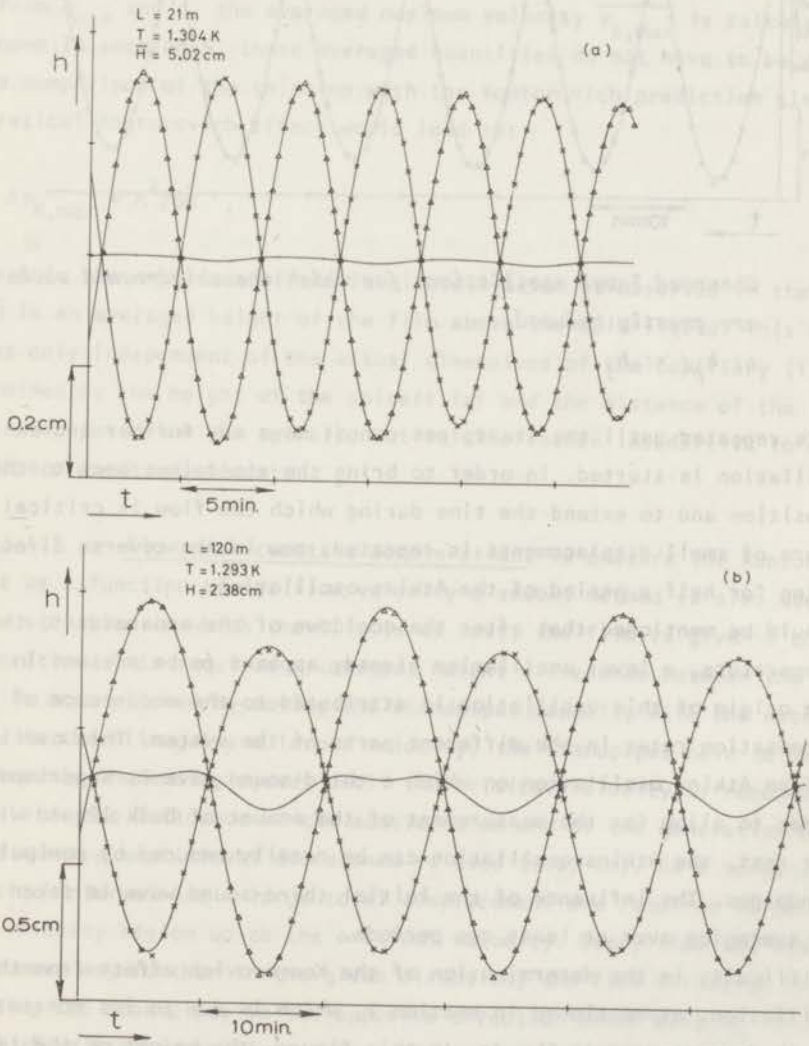

Fig. 3a, 3b.

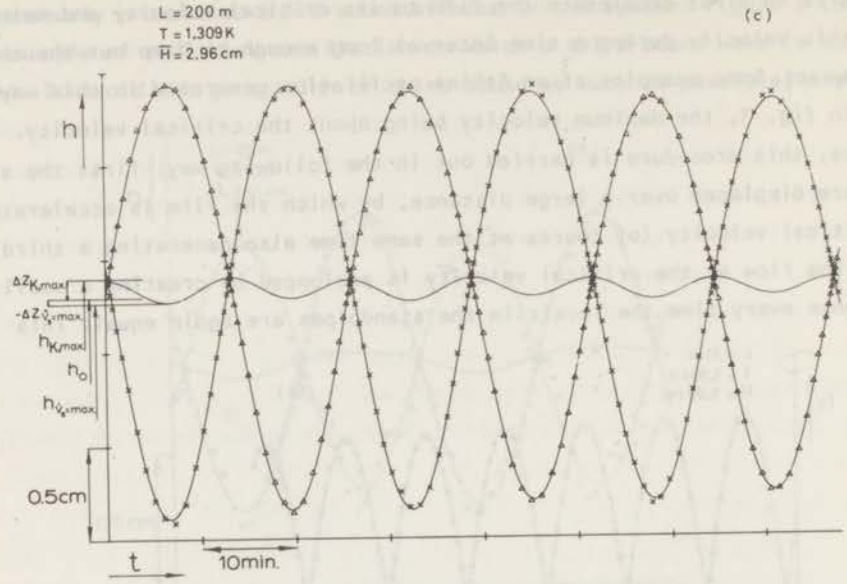

Fig. 3 *Observed level oscillations for which the third-sound waves are greatly reduced.*
Δ: h_r; ×: h_l.

procedure is repeated until the standpipes cannot move any further and an Atkins oscillation is started. In order to bring the standpipes back to their original position and to extend the time during which the flow is critical, the procedure of small displacements is repeated, now in the reverse direction, after waiting for half a period of the Atkins oscillation.

It should be mentioned that after the cooldown of the apparatus to the desired temperature, a level oscillation already appears to be present in the system. The origin of this oscillation is attributed to the occurrence of different condensation rates in the different parts of the system. This oscillation consists of an Atkins oscillation on which a third-sound wave is superimposed.

In order to allow for the measurement of the amount of bulk liquid with the film at rest, the Atkins oscillation can be readily reduced by manipulation of the standpipes. The influence of the initial third-sound wave is taken into account by averaging over at least two periods.

The difficulty in the determination of the Kontorovich effect from the Atkins oscillation, as mentioned in section 2, which is due to its nonstationary character, is demonstrated in fig. 3c. In this figure, the height of the levels is indicated for the case that the film is at rest before the Atkins oscillation

is started (h_0), as well as the averaged height for the case that the film is at rest during the oscillation. The full line, obtained by averaging the levels in both standpipes, represents the amount of bulk liquid at every moment during the oscillation. The experimental Kontorovich effect is determined only when the film moves at maximum velocity, *i.e.* the mean acceleration being zero, from the level difference $\Delta z_{K,max}$, as indicated in the figure. From the period of the Atkins oscillation and the temperature, one obtains the averaged thickness, d, of the film. The maximum of the rate of transport $\dot{M}$ through the film is derived from the maximum velocity of the levels in the standpipes (see section 4). From $\dot{M}_{max}$ and d, the averaged maximum velocity $\overline{v_{s,max}}$ is calculated. As will be shown in section 5, these averaged quantities do not have to be determined for a comparison of the thinning with the Kontorovich prediction since the theoretical Kontorovich effect would lead to:

$$\Delta z_{K,max} = A^2/6\bar{H} \quad , \tag{2}$$

where A is the amplitude of the level oscillation as observed in the standpipes and $\bar{H}$ is an averaged height of the film above the bulk liquid. This mean height is not only independent of the actual dimensions of the capillary (it is largely determined by the height of the spirals (a) and the distance of the levels in the standpipes below the spiral), but is also rather insensitive to $\overline{v_{s,max}}$ and d in the present experiments.

3.1.2 Flow with constant acceleration. To measure the Kontorovich effect as a function of the flow velocity a second method is also used. Starting from a situation in which the film is at rest, the film is given a constant acceleration. This requires a constant height difference between the levels, which is accomplished by moving the standpipes manually with the necessary speed. As the film gains a larger velocity, the standpipes have to be moved with continuously increasing speed, until the critical velocity is reached. In order to minimize the influence of the acceleration and of the generation of third-sound waves, a small level difference is used (0.07 cm). As a consequence, a long time interval and a large total displacement are required to cover the whole velocity region up to the critical velocity. Every time the standpipes cannot move any further in the given direction, the flow direction is reversed by moving the standpipes in the opposite direction after waiting for half a period of an Atkins oscillation (see also section 3.1.1).

The rate of mass transfer is deduced from the velocity of the standpipes.

The thickness of the film is deduced from the period of a separately measured Atkins oscillation. Naturally, using this method, a small error may be introduced by a slight variation of the inner diameter along the standpipes.

The results with this method appeared to be in fair agreement with the Kontorovich prediction. Only one series of measurements is carried out in this way, because it appears rather difficult to maintain a constant level difference by hand.

3.2 Stationary flow

In order to avoid complications in the interpretation due to acceleration of the film, the Kontorovich effect is also measured with the film at constant velocity. The following methods were used.

3.2.1 Flow at constant, critical velocity. During the time interval in which the film is kept at its critical velocity, in order to damp out the third-sound waves using the method of 3.1.1, the flow is practically stationary. By measuring the height of the bulk levels every time the difference between them is zero, and comparing this value with the height with the film at rest, one obtains the amount of excess liquid due to the Kontorovich effect. From the rate at which the level difference disappears, $v_s d$ can be calculated. The averaged thickness d is calculated from the period of the Atkins oscillation, which is measured after this procedure.

Also with this method, a slight variation of the inner diameter of the standpipes may cause a small error in the results. The expected thinning is indeed observed.

3.2.2 Flow at constant, subcritical velocity. A possible objection to the method of 3.2.1 is the fact that the film moves at critical velocity. Complications might arise from vorticity and dissipative effects. In spite of the fact that it is not expected that in the long capillaries this dissipation will lead to serious consequences - probably only a small portion of the film will form the bottleneck for the flow - also a subcritical method is used. After the film is accelerated to the desired subcritical velocity, the level difference is kept zero by manipulating the mechanical device. The relevant quantities are obtained in the same way as described in 3.1.2. For the same reasons as mentioned before in section 3.1.2, only a few measurements were done in this way, showing again a thinning in the right order of magnitude.

3.2.3 Persistent flow. This type of flow cannot be realized in the present apparatus. However the Leiden group was the first to create a persistent current in a saturated He II film with a length of about 130 m, see Verbeek *et al.*[5]. The apparatus used is very similar to the ones described in this chapter, the difference being an additional short connection between both standpipes containing a superleak which serves as a valve. The result is perhaps the nicest demonstration of the existence of the Kontorovich effect during stationary flow in a saturated moving He II film. The Kontorovich effect is again deduced from a comparison of the amount of bulk liquid during persistent flow with the amount when the film is at rest. The kinetic energy of the persistent flow is measured from the Atkins oscillation, which arises when the superleak is closed, giving $v_s d$ and d at the same time.

4. The Atkins oscillation

Basically, the Atkins oscillations follows immediately from the conservation of mechanical energy and the continuity equation:

$$E = E^{kin}_{film} + E^{pot}_{bulk} = \int_{x=0}^{x=L} \tfrac{1}{2}\rho_s v_s^2 O_f dx + \rho g O_s z^2 \qquad (3)$$

and

$$\dot{M} = \rho_s O_f v_s = \rho O_s \dot{z}_l = - \rho O_s \dot{z}_r \quad . \qquad (4)$$

In these equations, $O_f = 2\pi r\delta$, the cross-sectional area of the film, O_s the cross-sectional area of each standpipe, L the length of the film and $z_l = - z_r = z$ the displacement of the levels from the equilibrium position. (The subscripts l and r stand for left- and right hand standpipe, see fig. 4.) Differentiation of eq. (3) and using eq. (4) gives:

$$\frac{dE}{dt} = \dot{M} [\ddot{z} L_{eff} + 2gz] = 0 \quad , \qquad (5)$$

where

$$L_{eff} = \int_0^L \frac{\rho O_s}{\rho_s O_f} dx \ .$$

The solution is an undamped harmonic oscillation with

$$\omega_0^2 = \frac{2g}{L_{eff}} \quad . \qquad (6)$$

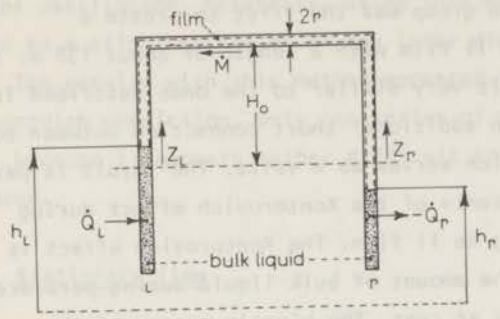

Fig. 4 *Geometry used for the calculations.*

If the film thickness were constant, ω_0^2 should be proportional to ρ_s/ρ according to eq. (6). As an example of the observed ω^2 as a function of ρ_s/ρ, fig. 5 shows the results for the 21 m capillary. Three sets of data can be

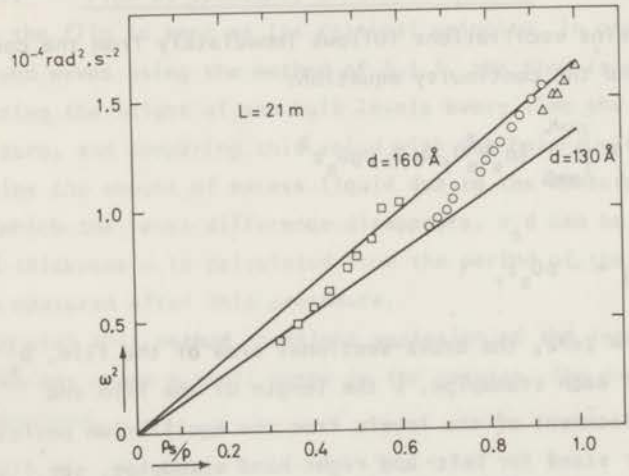

Fig. 5 *The square of the angular frequency as a function of ρ_s/ρ for the 21 m coil. Different symbols correspond to different fillings of the coil.*

clearly distinguished, corresponding to three different fillings of the capillary. The deviations of a straight line correspond to a changing thickness, which is due to the evaporation of liquid with increasing temperature, leading to an increase in height of the film above the bulk and consequently to a decrease in d. As the static film thickness δ_0 is governed by the relation[6]

$$\delta_0^3 = \frac{\gamma}{gH_0} \quad , \tag{7}$$

with H_0 the height of the film above the bulk and γ the constant in the Van der Waals forces between substrate and film, an additional decrease of ω_0^2 occurs when the temperature is raised. In fact, an average value of the film thickness can be obtained from eq. (6) and the observed ω^2. These values for the different capillaries are listed in the tables and range from about 80 to 160 Å, indicating a very clean glass surface owing to the way in which the the capillaries are fabricated.

In the above derivation, a possible change of the potential energy of the film, due to a changing thickness, has been neglected. Furthermore, changes in the internal energy U^{int} of vapour and liquid and possible damping effects have not been taken into account. The total energy of the system should be written as:

$$E_{syst} = E^{pot}_{bulk} + E^{kin}_{film} + E^{pot}_{film} + E^{kin}_{vapour} + E^{pot}_{vapour} + U^{int} \quad . \tag{8}$$

A discussion of the effects leading to changes in the potential energy of the film will be postponed to section 5. In this section, it will be assumed that E^{pot}_{film} is constant and $E^{kin}_{vapour} = 0$. The latter assumption is justified by the fact that transport of vapour is effectively blocked by the long and narrow capillary.

Damping of the Atkins oscillation will be caused by the flow of heat from the liquid in the standpipes to the bath over the Kapitza resistance. A second contribution to the damping may arise from a possible dissipation in the film, due to such mechanisms as proposed *e.g.* by Allen *et al.*[7], by Calvani *et al.*[8] and by Langer and Fisher[9].

First the damping due to the Kapitza resistance only will be considered, using thermodynamic considerations.

The rate of change of the mechanical energy is given by

$$\frac{dE}{dt} = \dot{Q}_l + \dot{Q}_r - \frac{dU^{int}}{dt} \quad , \tag{9}$$

where $\dot{Q} = \kappa\,(T_{bath} - T)$ is the heat flow into a standpipe, κ being the effective heat conductance coefficient to the bath. In view of the length of the thin-walled glass capillaries used, all heat conduction along the capillary can be neglected. It will therefore be assumed that the only source of entropy production is the heat flow from the bath, so that

$$T_l \frac{dS_l}{dt} = \dot{Q}_l \qquad \text{and} \tag{10a}$$

$$T_r \frac{dS_r}{dt} = \dot{Q}_r \quad . \tag{10b}$$

Combining eqs. (9) and (10) shows that the rate of change of mechanical energy is given by:

$$\frac{dE}{dt} = T_l \frac{dS_l}{dt} - \frac{dU_l^{int}}{dt} + T_r \frac{dS_r}{dt} - \frac{dU_r^{int}}{dt} \quad . \tag{11}$$

As the volume of each standpipe is constant, this can be written as:

$$\frac{dE}{dt} = -\dot{M}(\mu_l - \mu_r) \quad , \tag{12}$$

where μ is the chemical potential per gram of the helium in the standpipes, liquid and vapour being in local equilibrium.

The equation of motion which follows from eq. (12), neglecting higher order terms in the temperature difference $\Delta T = T_l - T_r$ is:

$$\int_{x=0}^{x=L} \dot{v}_s dx = 2gz - (s - \frac{1}{\rho} \frac{dP^{sat}}{dT})\Delta T = 0 \quad . \tag{13}$$

The differential equation for the temperature difference ΔT can be obtained by subtracting eqs. (10a) and (10b):

$$2\dot{M}T(s - \frac{1}{\rho} \frac{dP^{sat}}{dT}) + C\dot{\Delta T} = -\kappa \Delta T \quad , \tag{14}$$

where κ is the mean heat conduction coefficient of both standpipes and one can take $C = \overline{M}c$ with c the specific heat of the liquid and $\overline{M}$ the average of the mass of helium in both standpipes.

Eliminating ΔT from eqs. (13) and (14), using $\frac{\rho_{vap}}{\rho} \ll 1$, leads to

$$\dddot{z} + \frac{\kappa}{C} \ddot{z} + \omega_0^2 f \dot{z} + \frac{\kappa}{C} \omega_0^2 z = 0 \quad , \tag{15}$$

where

$$f = 1 + \frac{\rho 0_s \beta^2 s^2 T}{gC}$$

and

$$\beta = (1 - \frac{1}{\rho s} \frac{dP^{sat}}{dT}) \approx 1 \quad .$$

The solution for the case that $\omega_0^2 f C^2/\kappa^2 \ll 1$, which is realized in the present

experiments, is:

$$z = ae^{-\frac{\kappa(1 - 2\alpha C/\kappa)t}{C}} + be^{-\alpha t}\sin(\omega t + \phi) \quad , \tag{17}$$

with

$$\alpha = \frac{\omega_0^2 C}{2\kappa}(f - 1) = \omega_0^2 \rho 0_s \beta^2 s^2 T/2\kappa g \tag{18}$$

and

$$\omega^2 = \omega_0^2\left(1 - \frac{3\omega_0^2 f C^2}{\kappa^2}\right) \quad . \tag{19}$$

The constants a, b, and ϕ are determined by the intial conditions. For the narrow standpipes, the time constant C/κ can be estimated to be smaller than 0.1 s, while the time constant $\alpha^{-1} > 10^3$ s.

Therefore the presence of the exponential term in eq. (17) can be ignored in the analysis of the experimental data, and we will simply use

$$z = be^{-\alpha t}\sin(\omega t + \phi) \quad . \tag{20}$$

Fig. 6 shows the experimental values of α as a function of temperature for the 21 m and 200 m capillary. The most striking feature of this plot is that α appears to be roughly inversely proportional to the length of the capillary, as can be expected from eqs. (6) and (18). A complete check of eq. (18) cannot be made, since κ is not directly measured. Nevertheless, a rather good fit is obtained for the 21 m as well as for the 200 m capillary, using $\kappa_{21} = 3.2 \times 10^4 T^{5.8}$ erg/s K and $\kappa_{200} = 2\kappa_{21}$. The factor two is taken because the length of the standpipes of the 200 m capillary is twice as large. This fit is shown by the drawn curves in fig. 6. In view of the variety of the measured Kapitza resistances by various authors, this κ does not seem unacceptable for pyrex, although the power of the temperature dependence is rather high. Nevertheless, one can conclude therefore that the heat flow over the Kapitza resistance is responsible for the observed damping, as is recently found by Hallock and Flint[10], although a contribution due to dissipation in the film is not completely excluded. However, such a contribution should be relatively small, as it cannot be expected to be inversely proportional to L. It should be remarked that above a critical velocity of the order of 25 cm/s, damping in the film does occur, and rapidly becomes dominant, to such an extent that the film can hardly be accelerated above this critical velocity[11,12]. There is a possibility that this damping mechanism still has some influence on the

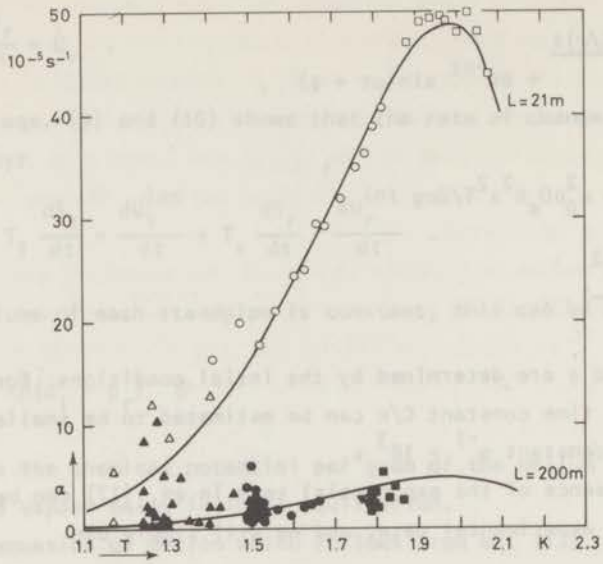

Fig. 6 *The damping constant as a function of the temperature for the 21 m coil (open symbols) and the 200 m coil (closed symbols). Different symbols correspond to different fillings. In the calculations of the drawn curves, we have taken a fixed value of* $\beta^2 = 0.90$ *(see text) and of the the thickness* δ_0 *(150 Å for the 21 m capillary and 100 Å for the 200 m capillary), the temperature dependence of* β^2 *and* δ_0 *has not been taken into account.*

observed Atkins oscillations at the highest velocities obtained. An indication of this effect can be found from the values of α for different amplitudes of the Atkins oscillation, the other conditions being left unchanged (see table 4 and 5 series a, b, c).

Since the aim of the present investigations is the measurement of the Kontorovich effect, a further analysis of the damping will be omitted.

5. Changes in film thickness

In order to investigate the variations in the film thickness, the Landau equations of motion for the superfluid in the nondissipative region are taken as a starting point (see appendix):

$$\frac{d_s \vec{v}_s}{dt} = -\vec{\nabla}(\mu_{Liq} + \Omega) \quad , \tag{21}$$

where Ω is the potential energy per gram of the external forces

$$\Omega = gH - \frac{\gamma}{Y^3} \quad . \tag{22}$$

$-\frac{\gamma}{Y^3}$ is the potential from the Van der Waals forces, with Y the distance to the wall. With $\vec{\nabla} \times \vec{v}_s = 0$ and $\vec{v}_n = 0$, equation (21) can be rewritten as:

$$\frac{\partial \vec{v}_s}{\partial t} = -\frac{\vec{\nabla} P_{Liq}}{\rho} + s\vec{\nabla}T - \frac{\rho_s}{\rho}\vec{\nabla}\frac{v_s^2}{2} - \vec{\nabla}\Omega \quad . \tag{23}$$

Note that by integration of eq. (23) from bulk to bulk in both standpipes, eq. (13) is regained. Therefore, the damping (see section 4) can also be calculated starting from the Landau equations, as in fact is done by Robinson[13]. In principle, the thickness as a function of the distance x along the film could be calculated from eq. (23) if the x dependence of the other quantities in eq. (23) were known along the surface of the film. The measured quantity in these experiments, the amount of excess liquid in the standpipes, is proportional to $\overline{\delta}_0 - \overline{\delta}$, where $\overline{\delta}_0$ is the mean thickness when the film is in equilibrium, *i.e.* when both the velocity and acceleration in the film are zero. This static thickness can be easily calculated from eq. (23), since for this case $\vec{v}_s = 0$, $\vec{\nabla}T = 0$, and the pressure along the surface equals the saturated vapour pressure, $P^{(s)}_{Liq}(x) = P^{sat}$ so that:

$$\vec{\nabla}^{(s)}\left(gH(x) - \frac{\gamma}{\delta_0^3(x)}\right) = 0 \quad . \tag{24}$$

From the geometry of the apparatus, the mean thickness $\overline{\delta}_0$ can be calculated. However, the calculation of $\overline{\delta}$ from eq. (23) is obviously much more complicated and therefore the influence of the different terms in eq. (23) will be separately investigated, looking at simplified experimental arrangements.

First the isothermal case of stationary flow will be considered. In this case, integration of eq. (23) along the surface from the bulk level in the standpipes to a point on the film, yields

$$\frac{\gamma}{\delta^3} = \frac{P^{(s)} - P^{sat}}{\rho} + \frac{\rho_s}{\rho}\frac{v_s^2}{2} + gH \quad . \tag{25}$$

If one simply takes $P^{(s)}_{Liq} = P^{sat}$ at the surface of the film, one obtains the

Kontorovich formula (1).

However, this *ad hoc* assumption may be too simple. As the value of $P_{Liq}^{(s)}$ at the surface of the moving film directly determines the thickness δ according to eq. (25), this crucial problem is now considered in somewhat more detail.

In the first place, in order to satisfy the momentum balance, the surface of a plane interface cannot sustain a pressure jump, so that

$$P_{Liq}^{(s)} = P_{vap}^{(s)} \quad . \tag{26}$$

Secondly, from the well-established experimental fact that below some critical velocity steady film flow is nondissipative, it follows that the value of $P_{Liq}^{(s)}$ is determined by some vapour-liquid equilibrium condition. *A priori* there is no reason to assume this condition to be different from that of bulk helium, since the only difference between film and bulk is the large Van der Waals forces in the film. For instance, the equilibrium condition as derived for the bulk[14] (see appendix)

$$\mu_{Liq}^{(s)} + \tfrac{1}{2}\vec{v}_s^{\,2} - \vec{v}_n \cdot \vec{v}_s = \mu_{vap}^{(s)} - \tfrac{1}{2}\vec{v}_{vap}^{\,2}$$

should also apply to the film*.

Since at the surface of the film $\vec{v}_n = \vec{v}_{vap} = 0$, this condition reduces to

$$\mu_{Liq}^{(s)} + \tfrac{1}{2}\vec{v}_s^{\,2} + \Omega^{(s)} = \mu_{vap}^{(s)} + \Omega^{(s)} \quad , \tag{27}$$

where the external potential $\Omega^{(s)}$ is added to both sides for convenience[15]. As for steady flow, according to eq. (21), the left-hand side of eq. (27) is uniform throughout the liquid, it follows that also $\mu_{vap}^{(s)} + \Omega^{(s)}$ is constant along the interface and equal to its value at the bulk level in the standpipe. For the isothermal case, neglecting the extremely small variations in the vapour density ρ_{vap}, this yields directly:

$$P_{vap}^{(s)}(x) - P^{sat} = -\rho_{vap}\Omega^{(s)}(x) \quad .$$

Combining this result with eqs. (26) and (25) leads to a thickness of the stationary moving film given by:

---

* Note that by taking $P_{Liq}^{(s)} = P^{sat}$ this relation is violated.

$$\frac{\gamma}{\delta^3} = \frac{\rho_s}{\rho - \rho_{vap}} \frac{v_s^2}{2} + gH \quad . \tag{28}$$

For the saturated vapour pressure above the moving film one finds:

$$p^{(s)}(v_s) = p^{sat} + \frac{\rho_{vap}}{\rho - \rho_{vap}} \tfrac{1}{2}\rho_s v_s^2 \quad . \tag{29}$$

These results, given by eqs. (28) and (29) are, owing to the smallness of ρ_{vap}/ρ, almost identical to the Kontorovich prediction, and we therefore expect the Kontorovich effect to occur for steady film flow. Note that for the case of He II in a rotating bucket with $\omega < \omega_{c1}$[14], one finds for the pressure at the interface:

$$p^{(s)}(v_n) = p^{sat} + \frac{\rho_{vap}}{\rho - \rho_{vap}} \tfrac{1}{2}\rho_s v_n^2 \quad ,$$

which is identical to eq. (29) when considered from the rotating system, in which the normal component is at rest. Note that, as has been pointed out before[16,17], both the moving film and the rotating bulk liquid are in equilibrium with a vapour pressure slightly higher than p^{sat}. Condensation of vapour into liquid at rest is however very unlikely to occur in the present experiments, in view of for instance the small dimensions of the relevant supersaturated vapour regions involved.

It should be remarked that in the actual experiment, a very small temperature difference arises between the liquid in both standpipes, due to the Kapitza resistance to the bath (see section 4). However, as the thin-walled capillary is in direct contact with the bath, the film will be at the bath temperature for almost its entire length, a small temperature gradient being located at the extreme ends. Though this effect may contribute to the observed damping, it does not affect the results given in eqs. (28) and (29), which are strictly given only for the isothermal case.

Let us now turn our attention to nonstationary flow, as is encountered for instance during the Atkins oscillation. Also in this case eq. (26) should apply. The experimental observation that the damping of the oscillation can be fully attributed to the irreversible heat exchange between the standpipes and the bath (see section 4) indicates that local equilibrium still prevails, *i.e.* eq. (27) should still apply locally. The influence of the simultaneously occurring vapour oscillations can certainly be neglected. Again taking the isothermal case, integration of eq. (23) from *e.g.* the level in the standpipe

on the right (see fig. 4) to a point at the surface of the film, using the conditions (26) and (27), yields for the film thickness:

$$\frac{\gamma}{\delta^3} = \frac{\rho_s}{\rho - \rho_{vap}} \frac{v_s^2}{2} + g(H_0(x) - z_r) + \int_0^x \dot{v}_s dx \quad , \tag{30}$$

instead of eq. (28). The pressure at the surface is still given by eq. (29). $H_0(x)$ is the height of the film above the levels in both standpipes when the film is completely at rest, *i.e.* $v_s = 0$ and $\dot{v}_s = 0$. According to eq. (30), one can now calculate $\delta(x)$, and from this, the excess liquid appearing in the standpipes, if one assumes for simplicity that $\dot{M}$ is constant throughout the film, *i.e.* the film moves as a whole. Let us first calculate the maximum increase in the liquid levels, $\Delta z_{K,max}$, at the moment during the Atkins oscillation when the levels are at equal height (*i.e.* $z_r = 0$ and $\dot{v}_s = 0$). In this case, eq. (30) becomes identical with eq. (28) with $v_s = v_{s,max}$, and the Kontorovich effect is again obtained. From the conservation of the total amount of liquid follows:

$$2 O_s \Delta z_K = - \int_0^L 2\pi r \Delta\delta dx \quad . \tag{31}$$

By using eq. (28) and neglecting ρ_{vap} compared to ρ, eq. (31) can be written to first order in $\Delta\delta/\delta$ as:

$$\Delta z_{K,max} = \int_0^L \frac{2\pi r \delta \frac{1}{2} \rho_s v_{s,max}^2}{6\rho g O_s H} dx = \frac{E_{film}^{kin,max}}{6\rho g O_s} \frac{\int_0^L \frac{dx}{Hr\delta}}{\int_0^L \frac{dx}{r\delta}} \equiv \frac{E_{film}^{kin,max}}{6\rho g O_s \overline{H}} =$$

$$= \frac{E_{film}^{kin,max}}{E_{bulk}^{pot,max}} \cdot \frac{A^2}{6\overline{H}} = \frac{A^2}{6\overline{H}} \quad , \tag{32}$$

where the condition is used that $\dot{M}$ or $r\delta v_s$ is constant along the film. It should be remarked that the excess liquid, due to the thinning film, causes H in the eqs. (32) and (28) to be somewhat smaller than the corresponding H_0 in the static case. Especially for small values of $H_0(x)$, $H(x)$ can be considerably different from $H_0(x)$. In section 6 in the analysis of the results this point will be considered again. The advantage of writing $\Delta z_{K,max}$ in this form is that it shows that the observed increase of the level heights can be directly

related to the observed amplitude A of the Atkins oscillation, and it is rather insensitive to the exact geometrical shape of the film. Furthermore, the dependence on temperature is also incorporated. The geometry enters through the averaging of H. How $\overline{H}$ is calculated for the coils will be shown in section 6.

Now consider the case that $\dot{v}_s \neq 0$. Integration of eq. (30) over the entire film to the bulk level in the standpipe on the left yields

$$\int_0^L \dot{v}_s dx = - g(z_l - z_r) \quad . \tag{33}$$

In order to simplify the calculations, the following simple geometry will be considered: a film with a constriction in its width at a constant height $H_0(x) = H_0$. The constriction of length L is supposed to be so narrow that the velocity in the film outside the constriction can be taken zero. If it is assumed again that $\frac{\partial v_s}{\partial t}$ is constant throughout the film constriction, it follows from eqs. (30) and (33) that:

$$\delta = \frac{\gamma^{1/3}}{[\frac{\rho_s}{\rho}\frac{v_s^2}{2} + g(H_0 - z_r) - \frac{x}{L} g(z_l - z_r)]^{1/3}} \quad . \tag{34}$$

The averaged thickness of the film $\overline{\delta}$ will only be calculated for the case that the acceleration is at its maximum during the Atkins oscillation, *i.e.* $v_s = 0$ and $z_l = - z_r = A$. Note that if $v_s = 0$, the acceleration of the film is due to a gradient in its thickness, *i.e.* $\dot{\vec{v}}_s = \vec{\nabla} \frac{\gamma}{\delta^3}$ (eq. (30)). For this le simple case, eq. (34) yields

$$\overline{\delta}_{max} = \frac{1}{L} \int_0^L \frac{(\gamma/g)^{1/3} dx}{[\frac{x}{L}(H_0 - z_l) + (1 - \frac{x}{L})(H_0 - z_r)]^{1/3}} =$$

$$= \frac{1}{L} \int_0^L (\frac{\gamma}{g H_{eff}(x)})^{1/3} dx \quad . \tag{35}$$

Expression (35) is written in this specific form in order to answer the following question: "What is the effective height that determines the thickness of a horizontal film when it is in contact with two bulk reservoirs with different levels?" The effective height appears to be simply a linear average of both heights with respect to the distance along the film. Integration of

eq. (35) gives:

$$\overline{\delta}_{max} = \delta_0 \frac{3H_0}{4A} \left[\left(1 + \frac{A}{H_0}\right)^{2/3} - \left(1 - \frac{A}{H_0}\right)^{2/3} \right] \quad . \tag{36}$$

For $A/H_0 \ll 1$, eq. (36) can be approximated by

$$\overline{\delta}_{max} = \delta_0 \left(1 + \frac{2}{27} \frac{A^2}{H_0^2}\right) \quad , \tag{37}$$

showing that $\overline{\delta}_{max} > \delta_0$, resulting in a decrease $- \Delta z_{\dot{V}_s=max}$ of the mean height of the levels in the standpipes compared to the heights when the film is completely at rest. This is the reason why the Kontorovich effect is determined by comparison with the amount of bulk liquid before the Atkins oscillation is started and not with the amount when the film is at rest during the Atkins oscillation (see section 3).

In order to show that the effect mentioned above does indeed occur, in fig. 7 $- \Delta z_{\dot{V}_s=max}$ is plotted *versus* $\left(\frac{A\omega}{\overline{H}}\right)^2 \frac{\rho}{\rho_s}$ for a series of measurements

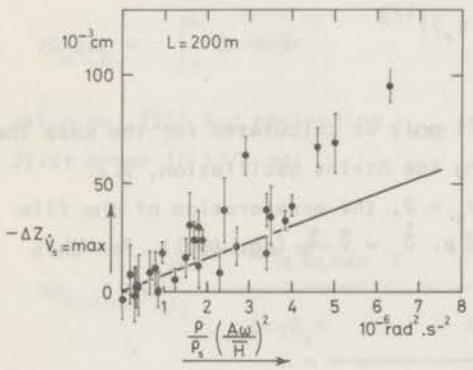

Fig. 7 *The maximum effect due to the acceleration for one filling of the 200 m capillary. The drawn line corresponds to the approximation given by eq. (38).*

carried out with one fixed amount of helium in the 200 m capillary. The drawn curve is calculated from eq. (37), and obeys the relation

$$- \Delta z_{\dot{V}_s=max} = \frac{2}{27} \frac{L\delta_0}{r} \frac{A^2}{\overline{H}^2} = \frac{L^2}{54g} \frac{\rho}{\rho_s} \left(\frac{A\omega}{\overline{H}}\right)^2 \quad . \tag{38}$$

In this expression, of course, an averaged value $\overline{H}$ is used instead of H_0, which for simplicity is taken to be the $\overline{H}$ used in the calculation of the Kontorovich effect. As one can see, the experimental results are of the right order of magnitude.

There is also a third cause for a change in film thickness as is demonstrated in fig. 2. Let us consider the additional, almost undamped, oscillation in somewhat more

detail. It is already present before the Atkins oscillation is started. Some of the nicest examples are given in fig. 8. This oscillation of the two levels

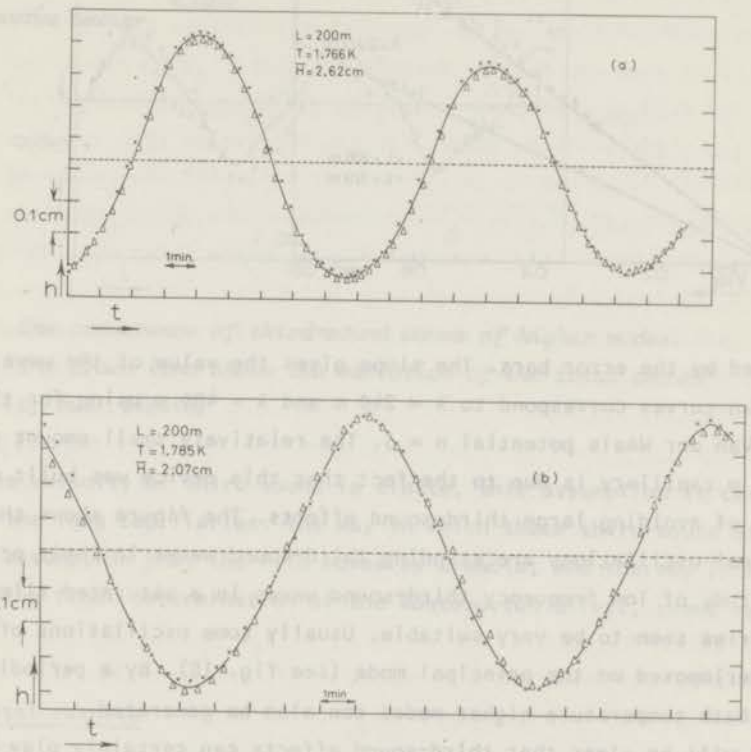

Fig. 8 *Examples of the level oscillations due to a standing third-sound wave. Δ: h_r; ×: h_l. The drawn line corresponds to the variation of the amount of bulk liquid, $(h_l + h_r)/2$.*

in phase represents a periodic exchange of liquid between film and bulk, and it will be shown now that it can be interpreted as a standing third-sound wave of low frequency ($\nu_3 \simeq 2 \times 10^{-3}$ Hz). According to Atkins' formula[18], the velocity v_3 of third sound is given by:

$$v_3^2 = \frac{\rho_s}{\rho}\,\delta\,\frac{d\Omega^{(s)}}{d\delta} = \frac{\rho_s}{\rho}\,ngH \quad . \tag{39}$$

In fig. 9, $\frac{1}{\nu_3}\sqrt{\frac{\rho_s}{\rho}}$ is plotted *versus* $\sqrt{\frac{1}{H}}$ for the 120 m and 200 m spirals for different temperatures and fillings, where again $\overline{H}$ is given the same value as is used for the calculation of the Kontorovich effect. The period $1/\nu_3$ is measured before as well as after the Atkins oscillation, the difference is

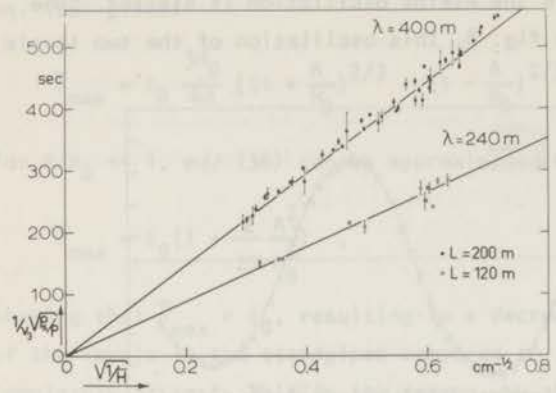

Fig. 9 *Overall results on the standing third-sound waves.*

indicated by the error bars. The slope gives the value of the wave length λ. The drawn curves correspond to λ = 240 m and λ = 400 m using for the exponent in the Van der Waals potential n = 3. The relatively small amount of data for the 120 m capillary is due to the fact that this device was built with the purpose of avoiding large third-sound effects. The figure shows that these additional oscillations are standing third-sound waves in their principal mode. For a study of low frequency third-sound waves in a saturated film, these long capillaries seem to be very suitable. Usually some oscillations of higher modes are superimposed on the principal mode (see fig. 10). By a periodic variation of the bath temperature higher modes can also be generated.

It will be clear that third-sound effects can certainly play an important role in these experiments. In the derivation of the changes in film thickness due to transport velocity and acceleration, it is assumed that after elimination of the standing third-sound waves, $\partial v_s/\partial t$ is constant throughout the film.

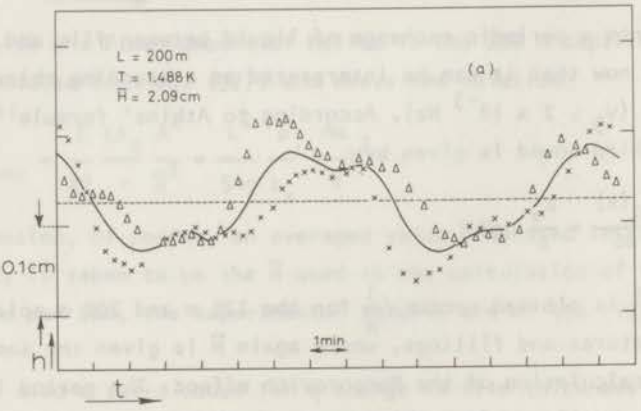

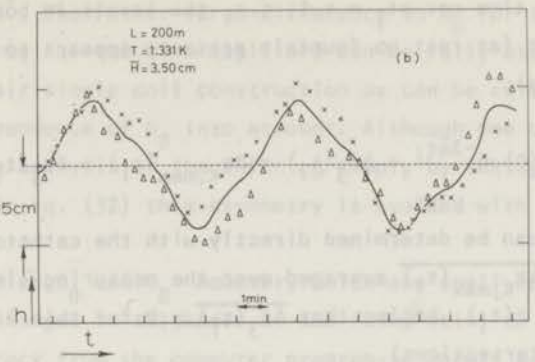

Fig. 10 *The occurrence of third-sound waves of higher modes. The drawn line shows the variation of the total amount of bulk liquid.*

However, as the velocity of third sound is finite, this assumption is certainly incorrect for the long capillaries. The way in which these third-sound effects do affect the assumption that the film moves as a whole, and thereby introduce an error into the final determination of the Kontorovich effect, seems rather complicated.

6. Experimental results

6.1 Nonstationary methods

6.1.1 The Atkins oscillation. Most of the data are obtained from the Atkins oscillations. As stated before, not only the Kontorovich effect, but also the damping, the effect due to acceleration, and the standing third-sound waves as well as their possible cross-effects, contribute to the observed level oscillations. These latter cross-effects are expected to be small under the experimental conditions prevailing and will be neglected in the analysis. Up to first order in $\Delta\delta/\delta$, using $z_1 = -z_r = Ae^{-\alpha t}\sin\omega t$, it follows from eq. (34) that the change in the sum of the level heights of both standpipes should obey:

$$\Delta z(t) = [\Delta z_{K,max}(0) - \Delta z^{\cdot}_{v_s=max}(0)]e^{-2\alpha t}\cos^2\omega t + \Delta z^{\cdot}_{v_s=max}(0)e^{-2\alpha t} + \Delta z_3(t)\ , \tag{40}$$

where $\Delta z_{K,max} = (A^2/6\bar{H})_{t=0}$ eq. (32), $\Delta z^{\cdot}_{v_s=max} = -\frac{L^2}{54g}\frac{\rho}{\rho_s}(\frac{A\omega}{\bar{H}})^2$ eq. (38), and

$\Delta z_3(t)$ is the periodic variation due to the third-sound waves. From eq. (40) it follows that every time $\cos \omega t_i = \pm 1$, *i.e.* the levels in both standpipes are at the same height (at rest no fountain pressure appears to be present in the actual experiments):

$$\Delta z(t_i) = \Delta z_{K,max}(0)\ e^{-2\alpha t_i} + \Delta z_3(t_i) = \Delta z_{K,max}(t_i) + \Delta z_3(t_i) \quad .$$

The values of $z(t_i)$ can be determined directly with the cathetometer. In order to obtain a value of $\overline{\Delta z_{K,max}(t_i)}$ averaged over the measuring time, one can average the measured $z(t_i)$, hoping that $\overline{\Delta z_3(t_i)} = 0$ for this limited number of points (5, 6, or 7 intersections).

One can improve on this visual method, which only makes use of the data close to the intersection points, by making a least squares fit through all the data of each standpipe separately. In order to eliminate the standing third-sound waves at the same time in accordance with eq. (40), the following equation is tried:

$$h = A_0 e^{-\alpha t} \sin(\omega t + \phi) + B_0 e^{-2\alpha t} \cos^2(\omega t + \phi) + C_0 e^{-2\alpha t} + h_0 \quad , \qquad (41)$$

with the adjustable parameters A_0, α, ω, ϕ, B_0, C_0, and h_0, and with h being the height of the level above an arbitrary reference point (see fig. 4). In principle, all the relevant quantities follow directly from the so-determined parameters; in particular, h_0 should be the observed level height in the static case. However, it appears by comparison of the computed results with the observed values that the accuracy obtained for h_0 in this way is insufficient to resolve the small thinning of the film accurately from the data. In view of the above, the results are analyzed by fixing h_0 in eq. (41) at the observed value, *i.e.* fitting the data for each leg to:

$$z = A_0 e^{-\alpha t} \sin(\omega t + \phi) + B_0 e^{-2\alpha t} \cos^2(\omega t + \phi) + C_0 e^{-2\alpha t} \quad , \qquad (42)$$

containing six adjustable parameters. Some examples of this fit are shown by the curves drawn through the data in the figs. 2 and 3. As can be seen from *e.g.* fig. 2, the standing third-sound waves seem to be eliminated adequately.

For the initial amplitude of the Atkins oscillation A_0, the angular frequency ω, and the damping constant α, the agreement between the values found for both standpipes individually is generally rather good. The values averaged for both standpipes are used in the figs. 5, 6 and 7. A survey of the results

is given in the tables, the difference between the values for both standpipes is also compiled†. The rather large difference in A_0 for the 120 m, 166 m, and to a lesser degree for the 21 m capillary can be fully ascribed to the inherent asymmetry of their single coil construction as can be calculated from eq. (34), taking the x dependence of H_0 into account. Although one can account for this asymmetry in the analysis of the thinning simply by taking the mean value of the amplitudes in eq. (32) this asymmetry is avoided with the 200 m capillary (see section 2).

The quantities B_0 and C_0 however, which are small compared to A_0 and are related to the changes in thickness of the film, still do not follow with sufficient accuracy from the computer program to permit a direct identification with the changes in thickness. A somewhat more accurate method is instead to determine the changes in film thickness from the smoothed curves computed according to eq. (42). The maximum effect of the acceleration follows from $-\Delta z_{v_s=max} = \frac{1}{2}(z_{l,max} + z_{r,min})$. An example of the results has been shown in fig. 7 (see section 5). The Kontorovich effect is determined from the intersections of the calculated curves for both standpipes with each other, where $\Delta z_{K,max}(t_i) = z_l(t_i) = z_r(t_i)$. In analogy with the visual method, $\overline{\Delta z_{K,max}(t_i)}$ is plotted in the figs. 11 and 12. In order to compare this result with the

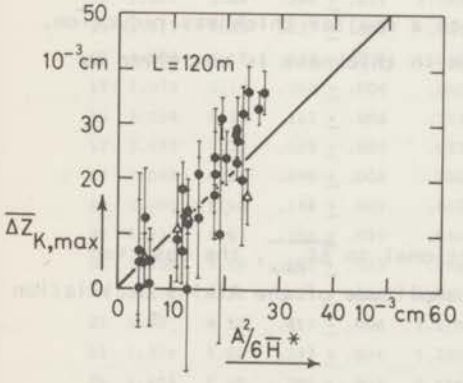

Fig. 11 *The averaged observed Kontorovich effect versus the expected value $A^2/6\bar{H}^*$ for the 120 m capillary (for the symbols Δ see text).*

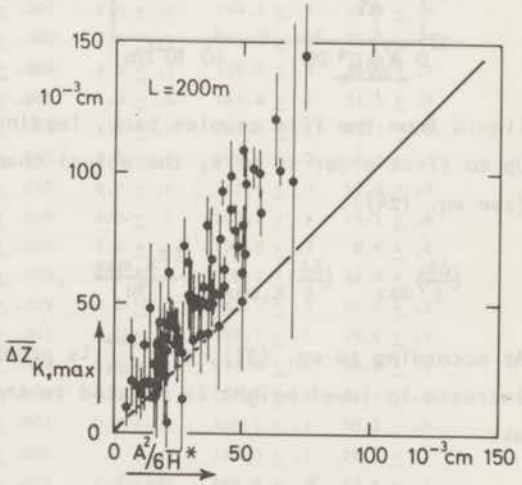

Fig. 12 *The averaged observed Kontorovich effect versus the expected value $A^2/6\bar{H}^*$ for the 200 m capillary.*

† For the tables see pages 53, 54, 55, 56 and 57.

Kontorovich prediction $A^2/6\overline{H}$, the damping $e^{-\alpha t}$ of the Atkins oscillation is taken into account. The value $\overline{H}$ is calculated from the definition given in eq. (32) under the simplifying assumptions: r = constant, $\delta \propto H^{-1/3}$ (thereby neglecting the influence of the velocity dependence of δ on $\overline{H}$), and $H - H(0) \propto x$ over the height a of the coils. For the lowest value H(0), the distance between the lowest winding(s) of the coil and the bulk in the standpipes in the presence of the excess liquid is taken. In practice it turns out that $\overline{H} \simeq H(0) + \frac{a}{2}$, except for the smallest values of H(0).

In figs. 11, 12 and 13, the observed thinning $(\overline{\Delta z_{K,max}(t_i)})$ is plotted *versus* $A^2/6\overline{H}^*$, $\overline{H}^*$ being the value of $\overline{H}$ corrected for the fact that the excess

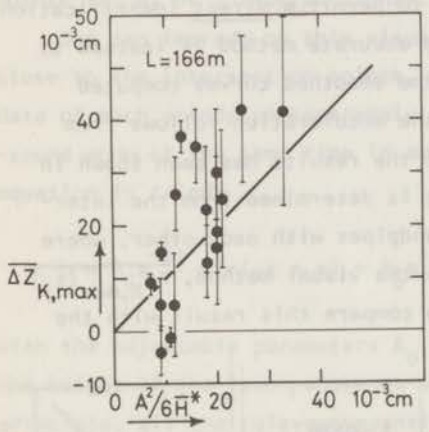

Fig. 13 *The Kontorovich effect versus the expected value for the 166 m capillary, determined from the total change in thickness during the Atkins oscillation, subtracting the calculated effect due to the acceleration.*

liquid from the film couples back, leading to a smaller thickness reduction. Up to first order in $\Delta\delta/\delta$, the actual change in thickness is now given by (see eq. (24)):

$$\left(\frac{\Delta\delta}{\delta}\right)_{max} = \left(\frac{\Delta\delta}{\delta}\right)_{K,max} + \frac{\Delta z_{K,max}}{3H} \quad .$$

As according to eq. (31), $\overline{\Delta z_{K,max}}$ is proportional to $\overline{\Delta\delta_{max}}$, the observed increase in level height is related to the amplitude of the Atkins oscillation as:

$$\overline{\Delta z}_{K,max} = \frac{A^2}{6\overline{H}} \left(1 + \int_0^L \frac{2\pi r \delta_0}{60_s H(x)}\, dx\right)^{-1} \equiv A^2/6\overline{H}^* \quad .$$

In the present geometry, using the narrow standpipes, the correction due to this feedback effect can be considerable, reducing the expected thinning as much as $\simeq$ 25% for the smallest values of $\overline{H}$ [†].

† The analysis of the data of the 120 m coil is somewhat different from the one presented earlier[3], the main difference being concerned with the calculation of $\overline{H}$. A few data incorporated in fig. 11 (Δ) are obtained by the visual method only, and are not incorporated in the table. For these runs, only the amplitudes and the intersection points were measured.

TABLE 2

RESULTS FOR THE 21 m COIL

no	T (K)	$\overline{H}$ (cm)	A_o (cm)	ω (10^{-2} rad.s^{-1})	α ($10^{-4}s^{-1}$)	d (Å)	$\overline{v_{s,max}}$ (cm s^{-1})
1	1.473	4.05	.273 ± .006	1.219 ± .000	2.0 ± .0	159.4 ± .1	20.9 ± .4
2	1.795	7.06	.282 ± .002	.981 ± .001	3.9 ± .1	135.3 ± .0	24.8 ± .2
3	1.606	5.02	.342 ± .005	1.137 ± .001	2.4 ± .1	149.9 ± .1	28.1 ± .4
4	1.523	4.37	.333 ± .005	1.190 ± .000	1.8 ± .0	156.0 ± .1	26.1 ± .4
5	1.719	6.14	.316 ± .006	1.050 ± .000	3.2 ± .0	141.6 ± .1	28.1 ± .5
6	1.561	4.66	.357 ± .006	1.165 ± .000	2.1 ± .0	153.o ± .1	28.6 ± .4
7	1.755	6.54	.282 ± .000	1.021 ± .000	3.5 ± .1	139.2 ± .1	25.8 ± .0
8	1.658	5.51	.347 ± .002	1.099 ± .000	3.0 ± .1	146.0 ± .1	29.5 ± .2
9	1.631	5.24	.346 ± .005	1.119 ± .001	2.5 ± .0	148.1 ± .1	28.9 ± .4
10	1.678	5.77	.337 ± .006	1.076 ± .000	2.9 ± .1	143.8 ± .0	29.3 ± .5
11	1.775	6.75	.282 ± .007	.996 ± .004	3.6 ± .1	135.5 ± .1	26.5 ± .7
12	1.407	3.68	.286 ± .011	1.243 ± .000	1.6 ± .0	161.4 ± .1	21.5 ± .8
13	1.817	7.33	.237 ± .005	.958 ± .002	4.1 ± .2	133.0 ± .1	23.1 ± .5
14	1.909	4.17	.213 ± .005	1.016 ± .001	4.9 ± .0	176.6 ± .2	19.6 ± .5
15	1.972	5.34	.164 ± .004	.860 ± .010	4.9 ± .1	148.4 ± .3	17.8 ± .4
16	2.024	6.33	.113 ± .004	.753 ± .006	5.0 ± .0	168.3 ± .3	14.1 ± .4
17	2.073	7.39	.058 ± .004	.643 ± .005	4.4 ± .1	122.5 ± .3	8.4 ± .4
18	2.048	6.84	.089 ± .004	.700 ± .005	4.8 ± .1	129.2 ± .2	11.8 ± .5
19	2.000	5.90	.134 ± .001	.803 ± .009	4.8 ± .2	141.3 ± .3	15.6 ± .1
20	1.933	4.62	.196 ± .005	.934 ± .001	5.0 ± .1	157.7 ± .1	19.6 ± .5
21	1.959	5.09	.178 ± .003	.890 ± .003	5.0 ± .1	152.4 ± .1	18.7 ± .3
22	1.878	4.23	.223 ± .005	1.022 ± .001	4.7 ± .1	167.5 ± .2	20.4 ± .5
23	1.00	4.52	.413 ± .006	1.279 ± .001	2.4 ± .1	159.1 ± .1	30.2 ± .5
24	1.304	5.02	.333 ± .004	1.229 ± .000	.9 ± .0	153.0 ± .1	25.3 ± .3
25	1.403	5.49	.289 ± .003	1.198 ± .001	1.3 ± .0	149.6 ± .2	22.6 ± .2
26	1.17	4.78	.268 ± .004	1.256 ± .000	.6 ± .0	155.8 ± .1	19.9 ± .3
27	1.265	4.83	.409 ± .009	1.279 ± .000	1.2 ± .0	164.4 ± .1	29.9 ± .6

TABLE 3

RESULTS FOR THE 166 m COIL

no	T (K)	$\bar{H}$ (cm)	A_0 (cm)	ω (10^{-3} rad.s^{-1})	α ($10^{-5}s^{-1}$)	d (Å)	$\overline{v_{s,max}}$ (cm s^{-1})
1	1.421	12.87	.850 ± .008	3.579 ± .002	2.3 ± .1	103.4 ± .1	28.0 ± .2
2	1.295	10.00	.771 ± .020	3.775 ± .002	1.2 ± .2	114.6 ± .2	23.6 ± .6
3	1.192	5.43	.648 ± .010	4.413 ± .004	.2 ± .1	142.2 ± .2	17.4 ± .3
4	1.195	5.43	.795 ± .004	4.409 ± .001	2.3 ± .0	142.1 ± .0	21.3 ± .1
5	1.195	5.40	.842 ± .007	4.404 ± .002	3.2 ± .0	141.8 ± .1	22.6 ± .2
6	1.250	6.03	.790 ± .001	4.292 ± .003	3.3 ± .0	136.1 ± .2	21.8 ± .0
7a	1.192	5.40	.863 ± .011	4.405 ± .001	1.2 ± .1	141.8 ± .1	23.2 ± .3
b		5.40	.829 ± .010	4.403 ± .000	.6 ± .1	141.6 ± .0	22.3 ± .3
8	1.327	7.13	.785 ± .003	4.129 ± .004	2.9 ± .1	128.1 ± .3	22.5 ± .1
9	1.305	3.86	.793 ± .034	4.355 ± .002	1.4 ± .1	141.9 ± .1	22 ± 1
10	1.497	8.78	.695 ± .003	3.722 ± .001	2.7 ± .0	110.9 ± .1	22.1 ± .1
11	1.362	5.02	.780 ± .008	4.206 ± .001	1.3 ± .0	133.9 ± .1	21.9 ± .2
12	1.414	6.24	.704 ± .007	4.047 ± .001	1.7 ± .3	126.4 ± .1	20.6 ± .2
13	1.548	10.70	.719 ± .009	3.629 ± .002	2.5 ± .0	108.6 ± .1	23.4 ± .3
14	1,466	7.76	.756 ± .005	3.885 ± .003	2.4 ± .2	118.9 ± .2	23.0 ± .2
15	1.389	5.55	.870 ± .000	4.126 ± .001	1.5 ± .0	130.3 ± .1	24.9 ± .0
16	1.281	3.48	.956 ± .052	4.398 ± .000	4.3 ± .1	143.8 ± .0	24 ± 1

The error bars in fig. 11 and fig. 12 account for the uncertainty in h_0; in the first place for the effectiveness with which the standing third-sound waves are eliminated, which is done by averaging h_0 over at least two periods of the third-sound waves. In the second place, because of the fact that h_0 is sometimes found to be different before and after the measuring run, a linear average over these two values is taken in the computer program. Note that this small hysteretic effect in the coils, contributing considerably to the error bars, is due to the mechanisms mentioned in chapter I, where it turned out to be of practically no importance in the determination of the static film thickness.

The results for the 166 m capillary are also given (fig. 13), although the static height of the levels was not determined. The data were analyzed by means of eq. (41). The Kontorovich effect is obtained by subtracting the acceleration effect, calculated from the approximation in eq. (38) from the total change in thickness according to:

$$\overline{\Delta z_{K,max}} = \overline{[h_{K,max} - \tfrac{1}{2}(h_{l,max} + h_{r,min})]} + \Delta z^{approx}_{v_s=max} \quad .$$

TABLE 4

RESULTS FOR THE 120 m COIL

no	T (K)	$\bar{H}$ (cm)	A_o (cm)	ω (10^{-3} rad.s^{-1})	α ($10^{-5}s^{-1}$)	d (Å)	$\overline{v_{s,max}}$ (cm s^{-1})
1	1.635	9.63	.518 ± .015	4.233 ± .001	5.2 ± .9	111.5 ± .0	20.0 ± .6
2	1.587	7.76	.500 ± .007	4.464 ± .004	3.2 ± .3	119.8 ± .2	18.3 ± .3
3	1.153	2.49	.601 ± .050	5.584 ± .000	1.9 ± .1	164.3 ± .0	17. ± 1
4	1.301	2.51	.489 ± .043	5.537 ± .015	1.1 ± .0	165 ± 1	14 ± 1
5	1.297	2.48	.585 ± .048	5.514 ± .004	.7 ± .1	164.8 ± .2	17 ± 1
6	1.293	2.38	.626 ± .058	5.488 ± .002	1.7 ± .0	163.0 ± .0	18 ± 2
7a	1.290	2.29	.625 ± .053	5.499 ± .001	1.0 ± .7	163.8 ± .0	18 ± 2
b		2.32	.501 ± .048	5.507 ± .002	.9 ± .0	164.4 ± .1	14 ± 1
c		2.34	.287 ± .033	5.525 ± .009	.4 ± .7	165.6 ± .6	8 ± 1
8	1.283	2.11	.656 ± .073	5.507 ± .001	1.7 ± .1	165.0 ± .1	19 ± 2
9a	1.283	2.14	.697 ± .080	5.507 ± .005	6.0 ± .4	164.9 ± .3	20 ± 2
b		2.17	.468 ± .050	5.532 ± .003	.5 ± .3	166.6 ± .2	13 ± 1
10	1.289	2.24	.557 ± .057	5.514 ± .003	1.0 ± .0	165.2 ± .1	16 ± 2
11a	1.286	2.24	.461 ± .048	5.528 ± .003	.9 ± .4	166.2 ± .2	13 ± 1
b		2.26	.305 ± .037	5.545 ± .005	1 ± 1	167.3 ± .3	9 ± 1
12a	1.293	2.30	.623 ± .060	5.500 ± .005	1.6 ± .0	164.5 ± .4	18 ± 2
b		2.34	.448 ± .045	5.525 ± .001	.6 ± .5	166.1 ± .0	13 ± 1
c		2.34	.323 ± .033	5.540 ± .001	3 ± 1	167.0 ± .0	9 ± 1
13	1.370	3.56	.702 ± .029	5.268 ± .004	3.9 ± .1	151.6 ± .2	22 ± 1
14a	1.292	2.35	.695 ± .066	5.503 ± .000	6.8 ± .4	164.2 ± .0	20 ± 2
b		2.38	.454 ± .044	5.519 ± .002	.9 ± .3	165.3 ± .1	13 ± 1
c		2.39	.298 ± .031	5.540 ± .002	.7 ± .0	166.6 ± .1	9 ± 1
15	1.422	4.56	.691 ± .023	5.061 ± .000	2.8 ± .0	141.8 ± .1	22.2 ± .7
16	1.207	2.26	.636 ± .070	5.559 ± .002	3.5 ± .2	165.1 ± .1	18 ± 2
17	1.214	2.33	.636 ± .063	5.548 ± .001	1.4 ± .1	164.4 ± .0	18 ± 2
18	1.199	2.17	.581 ± .068	5.572 ± .001	.9 ± .2	166.1 ± .1	17 ± 2
19a	1.206	2.23	.619 ± .066	5.562 ± .003	3.5 ± .3	165.5 ± .1	18 ± 2
b		2.26	.416 ± .040	5.582 ± .004	.5 ± .5	166.8 ± .2	12 ± 1
c		2.27	.268 ± .034	5.606 ± .006	.1 ± .2	168.3 ± .4	8 ± 1
20	1.252	2.70	.603 ± .049	5.497 ± .004	1.5 ± .0	161.5 ± .1	18 ± 2

The accuracy of this analysis of the data of the 166 m capillary is of course rather poor. The error bars are now obtained from the difference in the value for B_0 for each standpipe, this being an indication of the accuracy.

We will return to the experimental results in the discussion at the end of section 6. An independent indication of the occurrence of the thinning can also be found from a comparison of runs with different amplitudes, all other external parameters remaining unchanged (see the tables). A decrease in ω

TABLE 5

RESULTS FOR THE 200 m COIL

no	T (K)	$\bar{H}$ (cm)	A_o (cm)	ω (10^{-3} rad.s^{-1})	α ($10^{-5}s^{-1}$)	d (Å)	$\overline{v_{s,max}}$ (cm s^{-1})
1	1.272	2.23	.971 ± .002	4.216 ± .003	1.1 ± .3	110.1 ± .2	22.5 ± .0
2	1.239	1.74	.885 ± .020	4.322 ± .001	4.0 ± .2	115.4 ± .1	19.9 ± .4
3	1.251	1.90	.853 ± .012	4.289 ± .002	2.3 ± .0	113.7 ± .1	19.4 ± .3
4	1.264	2.12	.901 ± .001	4.241 ± .003	1.6 ± .5	111.2 ± .1	20.7 ± .1
5	1.291	2.59	.925 ± .010	4.156 ± .004	1.3 ± .1	107.2 ± .2	21.7 ± .3
6	1.331	3.50	1.144 ± .011	3.990 ± .001	5.0 ± .0	99.6 ± .0	28.1 ± .3
7	1.309	2.96	1.169 ± .010	4.073 ± .003	2.5 ± .0	103.4 ± .2	28.1 ± .3
8	1.375	4.62	1.070 ± .014	3.835 ± .001	.6 ± .0	93.1 ± .0	27.3 ± .4
9	1.426	6.35	1.072 ± .011	3.656 ± .002	2.2 ± .0	86.0 ± .1	28.8 ± .3
10	1.457	7.48	1.062 ± .005	3.564 ± .001	3.5 ± .0	82.8 ± .0	29.2 ± .1
11a	1.291	2.54	1.199 ± .002	4.143 ± .012	5.6 ± .5	106.6 ± .7	28.3 ± .1
b		2.59	.838 ± .012	4.170 ± .006	.9 ± .2	108.0 ± .3	19.6 ± .3
c		2.62	.603 ± .003	4.187 ± .001	.5 ± .0	108.9 ± .1	14.1 ± .1
12	1.352	4.01	1.109 ± .011	3.907 ± .001	.9 ± .0	96.1 ± .0	27.8 ± .3
13a	1.246	1.87	1.078 ± .021	4.274 ± .006	9.5 ± .2	113.0 ± .3	25.0 ± .0
b		1.92	.577 ± .054	4.377 ± .007	.6 ± .2	116.4 ± .4	12.9 ± .1
c		1.97	.277 ± .014	4.367 ± .010	.6 ± .3	118.0 ± .6	6.2 ± .0
14a	1.300	2.81	1.039 ± .010	4.105 ± .000	.7 ± .2	104.8 ± .0	24.7 ± .2
b		2.86	.854 ± .008	4.121 ± .002	.4 ± .2	105.6 ± .1	20.3 ± .2
c		2.86	.621 ± .008	4.138 ± .005	.5 ± .4	106.5 ± .5	14.7 ± .2
15a	1.398	5.40	1.104 ± .011	3.747 ± .000	2.2 ± .1	89.5 ± .0	28.9 ± .3
b		5.41	.820 ± .011	3.757 ± .001	.7 ± .1	90.0 ± .0	21.4 ± .3
16a	1.258	1.97	.974 ± .015	4.259 ± .005	1.8 ± .4	112.1 ± .2	22.3 ± .3
b		2.04	.797 ± .008	4.275 ± .002	.2 ± .0	112.9 ± .1	18.2 ± .2
c		2.05	.606 ± .009	4.302 ± .002	.3 ± .2	114.4 ± .1	13.7 ± .2
17a	1.277	2.36	1.011 ± .005	4.211 ± .019	10.7 ± .3	110 ± 1	23.4 ± .0
b		2.38	.670 ± .003	4.229 ± .015	.1 ± .2	110.8 ± .8	15.5 ± .0
c		2.40	.502 ± .004	4.243 ± .021	.1 ± .0	112 ± 1	11.6 ± .2
18	1.492	9.00	1.109 ± .001	3.431 ± .001	2.9 ± .1	78.0 ± .0	31.7 ± .0
19	1.532	11.04	.944 ± .009	3.292 ± .001	1.6 ± .0	73.4 ± .0	28.1 ± .3
20a	1.785	2.07	1.211 ± .003	3.529 ± .005	3.6 ± .3	106.1 ± .3	33.4 ± .0
b		2.16	.848 ± .009	3.558 ± .006	2.9 ± .3	107.8 ± .3	23.2 ± .2
c		2.25	.566 ± .017	3.566 ± .018	1.5 ± .4	108 ± 1	15.5 ± .4
21	1.865	10.27	.755 ± .008	2.755 ± .003	2.8 ± .0	72.8 ± .1	26.9 ± .3
22	1.845	7.92	.893 ± .015	2.915 ± .001	4.1 ± .1	78.7 ± .0	30.0 ± .5
23a	1.797	3.12	1.126 ± .007	3.392 ± .002	3.6 ± .5	99.4 ± .1	32.5 ± .2
b		3.20	.825 ± .004	3.405 ± .011	2.3 ± .0	100.1 ± .6	23.7 ± .1
c		3.15	.573 ± .018	3.426 ± .006	2 ± 1	101.4 ± .4	16.4 ± .5

TABLE 5 (continued)

no	T (K)	$\bar{H}$ (cm)	A_o (cm)	ω (10^{-3} rad.s^{-1})	α ($10^{-5}s^{-1}$)	d (Å)	$\overline{v_{s,max}}$ (cm s^{-1})
24	1.830	6.26	.877 ± .006	3.072 ± .003	3.0 ± .0	85.5 ± .2	28.0 ± .2
25	1.814	4.80	.957 ± .007	3.230 ± .001	5.5 ± .2	92.1 ± .0	29.0 ± .2
26	1.766	2.62	1.248 ± .004	3.523 ± .005	2.8 ± .2	103.1 ± .3	34.6 ± .2
27	1.779	3.77	1.226 ± .002	3.381 ± .001	2.6 ± .1	96.2 ± .0	35.5 ± .1
28	1.787	4.49	1.145 ± .001	3.302 ± .001	3.0 ± .2	92.6 .1	34.0 ± .0
29a	1.500	1.96	.915 ± .010	4.043 ± .005	1.3 ± .7	109.6 ± .3	22.1 ± .2
b		2.02	.717 ± .020	4.053 ± .015	1 ± 3	110.2 ± .8	17.2 ± .4
c		2.05	.535 ± .008	4.071 ± .028	.5 ± .7	111 ± 2	12.8 ± .3
30a	1.510	2.38	1.127 ± .001	3.954 ± .003	2.4 ± .2	105.1 ± .2	27.8 ± .0
b		2.44	.774 ± .013	3.977 ± .003	1.2 ± .6	106.3 ± .2	19.0 ± .3
c		2.46	.619 ± .001	3.993 ± .015	1.1 ± .3	107.1 ± .8	15.1 ± .1
31	1.520	2.83	.975 ± .003	3.904 ± .001	2.0 ± .1	102.9 ± .0	24.4 ± .1
32	1.662	11.45	1.164 ± .009	3.110 ± .002	2.6 ± .0	71.9 ± .1	36.7 ± .3
33	1.642	9.93	1.171 ± .004	3.191 ± .001	2.3 ± .2	74.4 ± .0	36.0 ± .1
34	1.626	8.79	1.140 ± .017	3.265 ± .001	1.9 ± .1	76.9 ± .0	34.2 ± .5
35a	1.515	2.70	.965 ± .003	3.926 ± .005	2.6 ± .0	103.9 ± .3	24.0 ± .0
b		2.72	.730 ± .007	3.935 ± .002	1.3 ± .5	104.3 ± .1	18.1 ± .2
c		2.75	.540 ± .004	3.942 ± .020	.9 ± .3	105 ± 1	13.4 ± .2
36	1.597	6.95	1.071 ± .011	3.429 ± .005	1.5 ± .4	83.1 ± .2	30.6 ± .3
37	1.563	4.94	1.018 ± .002	3.627 ± .001	1.8 ± .0	91.0 ± .0	27.5 ± .0
38	1.534	3.58	1.166 ± .005	3.783 ± .002	1.6 ± .2	97.3 ± .1	30.2 ± .1
39a	1.528	3.21	.961 ± .012	3.851 ± .004	2.5 ± .5	100.5 ± .2	24.4 ± .3
b		3.25	.703 ± .004	3.866 ± .001	.8 ± .5	101.3 ± .1	17.8 ± .1
c		3.27	.518 ± .010	3.864 ± .013	1 ± 1	101.1 ± .7	13.1 ± .3
40a	1.501	2.19	.421 ± .045	4.055 ± .071	5 ± 2	110 ± 4	10 ± 1
b		2.14	.690 ± .017	4.040 ± .012	2 ± 2	109.4 ± .7	16.7 ± .4
41a	1.511	2.62	.769 ± .023	3.944 ± .006	4 ± 2	104.6 ± .3	19.1 ± .6
b		2.62	.813 ± .015	3.949 ± .027	3.0 ± .6	105 ± 1	20.1 ± .2
42a	1.523	3.22	.450 ± .006	3.883 ± .018	1.5 ± .3	102 ± 1	11.3 ± .1
b		3.20	.758 ± .012	3.871 ± .003	1.5 ± .8	101.3 ± .2	19.2 ± .3
c		3.18	.954 ± .007	3.862 ± .007	2.3 ± .2	100.8 ± .3	24.2 ± .2
43a	1.526	3.99	.672 ± .003	3.768 ± .003	1.1 ± .4	96.0 ± .1	17.5 ± .1
b		3.99	.967 ± .001	3.755 ± .001	1.3 ± .0	95.3 ± .1	25.2 ± .0
44a	1.488	2.78	.697 ± .017	3.948 ± .003	1 ± 1	103.5 ± .2	17.3 ± .5
b		2.75	1.008 ± .004	3.926 ± .007	1.3 ± .4	102.2 ± .4	25.1 ± .2
45a	1.488	2.15	.566 ± .015	4.075 ± .008	1 ± 1	111.0 ± .4	13.5 ± .4
b		2.09	.934 ± .001	4.051 ± .003	4.0 ± .0	109.1 ± .1	22.5 ± .0

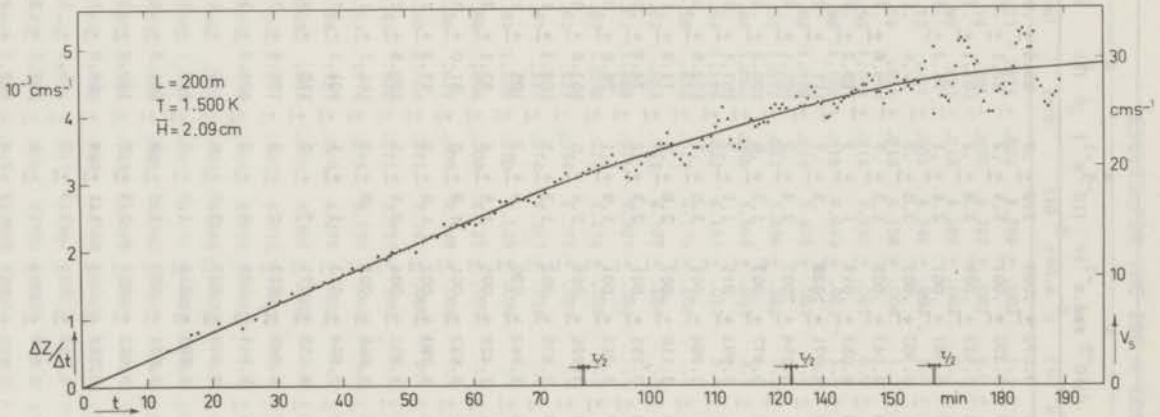

Fig. 14 *The velocity of the standpipes $\Delta z/\Delta t$ versus time; $\tau/2$ corresponds to the half period of the Atkins oscillation which is necessary to reverse the flow direction. The drawn line is used as $\dot{z}(t)$ in fig. 15. The observed third-sound oscillations, which are enhanced during the reversal of the flow direction, are reduced by taking the average of five subsequent measuring points.*

corresponding to an averaged thinning of the film can be noticed when the velocity increases. A calculation shows that the shift is the right order of magnitude as predicted by eq. (1). However, these long capillaries are not too well suited to allow for an accurate determination of the Kontorovich effect in this way[24].

6.1.2 Flow with constant acceleration. In section 3.1.2 the measuring procedure is already described. In fig. 14, the averaged velocity of the standpipes, $\Delta z/\Delta t$, necessary to maintain a constant level difference of about 0.07 cm between the liquid in both standpipes is plotted *versus* time. At the thin vertical lines, the flow direction is reversed, as is described in section 3.1.2. The curve drawn through the data, $\dot{z}(t)$, is taken to represent the rate of liquid transport, thereby eliminating the superimposed third-sound oscillations. In fig. 15, the observed increase in height due to the thinning film as

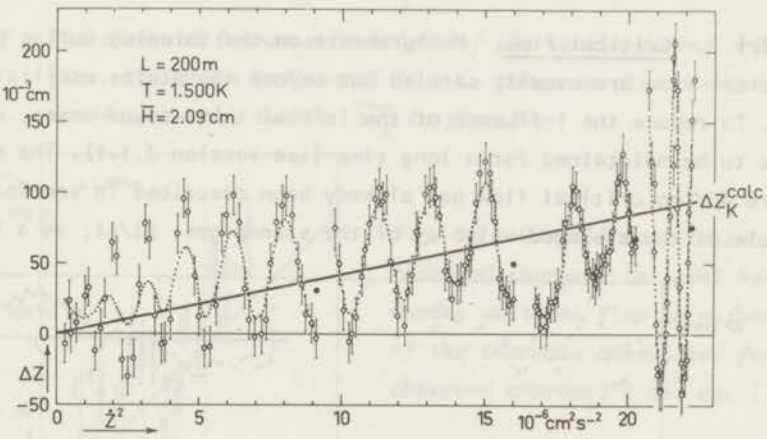

Fig. 15 *The increase in the levels due to the thinning of the film as a function of* $\dot{z}^2$. *The dotted curve is obtained by the same averaging procedure as used in fig. 14. The drawn line corresponds to the expected thinning deduced from eq. (1). The black circles are calculated using* $A^2/6\overline{H}^*$, *A being the amplitude of the Atkins oscillation during the flow reversal.*

a function of $\dot{z}^2$ is plotted. The error bars represent the uncertainty in h_0. The curve drawn in fig. 15 corresponds to the calculated Kontorovich effect. For the calculation of this effect, the thickness of the film is taken to be constant throughout the whole run and equal to the averaged value determined

from the period of the Atkins oscillation, which follows after the run is completed. The feedback correction has also been applied. The results seem to be in fair agreement with the Kontorovich prediction, in spite of the limited accuracy obtained with this method. The agreement seems better than is obtained from the Atkins oscillations (fig. 12). In this respect, it should be mentioned that the amplitudes of the Atkins oscillations, observed during the reversal of the flow direction, are always lower than expected from the initial value of $\dot{z}(\omega A < \dot{z})$. This is shown in fig. 15 by the black circles, which represent $A^2/6\overline{H}^*$. This indicates that even for velocities well below the critical value, not all the kinetic energy of the film shows up as potential energy in the standpipes during the Atkins oscillation. We will come back to this point in the discussion at the end of this section.

6.2 Flow at constant velocity

6.2.1 Critical flow. Measurements on the thinning during stationary but critical flow are usually carried out before the Atkins oscillations are started. To reduce the influence of the initial third-sound waves, critical flow has to be maintained for a long time (see section 3.1.1). The measuring procedure during critical flow has already been described in section 3.2.1. An example of the averaged velocity of the standpipes, $\Delta z/\Delta t$, as a function of

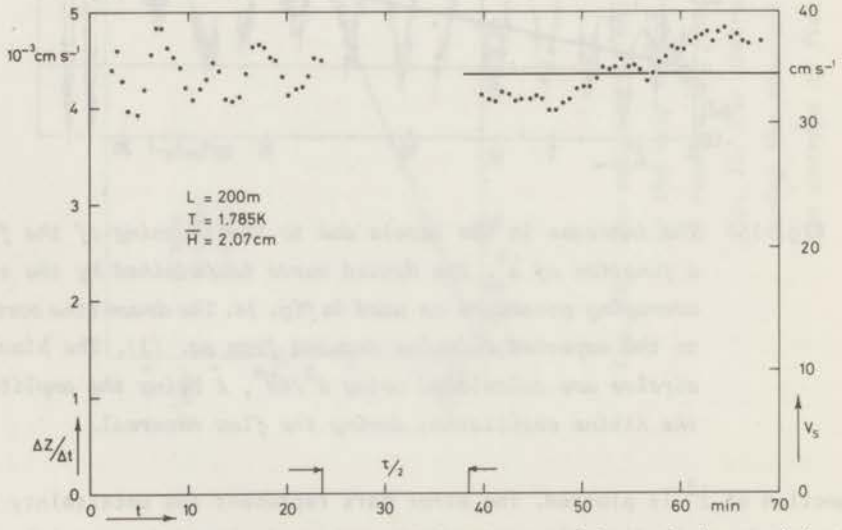

Fig. 16 *The velocity of the liquid in the standpipes during critical flow, the third-sound amplitude is reduced in the same way as in fig. 14. The drawn horizontal line is taken as the velocity of the levels.*

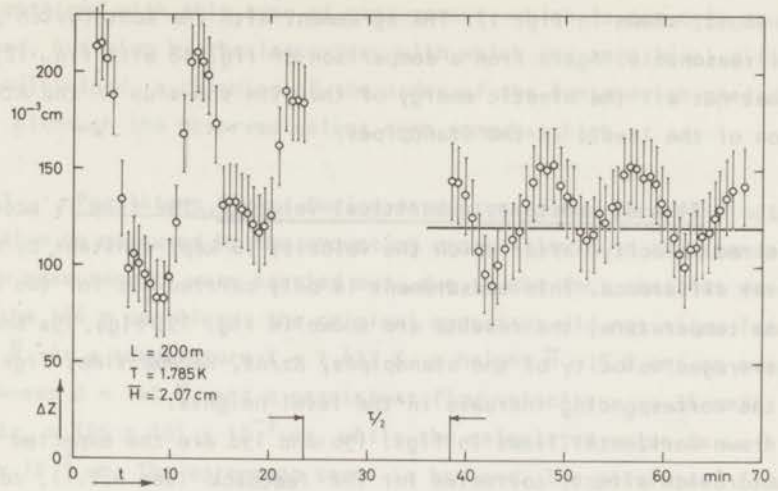

Fig. 17 *The observed increase in height of the levels during critical flow. The drawn horizontal line is taken as the observed increase in the levels.* $\overline{\Delta z_K}$ *in fig. 18.*

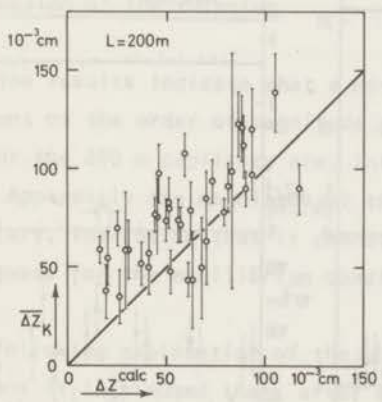

Fig. 18 *Overall results on the observed increase in level height during critical flow as a function of the increase calculated from the observed averaged* $\dot{z}$ *and eq. (1).*

time is plotted in fig. 16. Figure 17 shows the corresponding increase in height of the levels, Δz, due to the reduction in the thickness of the film. Only the data taken after the flow is reversed are analyzed, since the effect of third sound should be less important in this region. The value of $\dot{z}$ and $\overline{\Delta z_K}$ are obtained by averaging both $\Delta z/\Delta t$ and Δz over this entire region. (see horizontal lines in figs. 16 and 17). In fig. 17, the error bars correspond to the uncertainty in h_0. The overall results are shown in fig. 18, where the observed $\overline{\Delta z_K}$ are plotted *versus* their expected values, calculated from $\dot{z}$ and using the thickness as determined from the subsequent Atkins oscillation. The error bars

in fig. 18 account for both the uncertainty in h_0 and the uncertainty due to the third sound, shown in fig. 17. The agreement with the Kontorovich prediction seems reasonable. Again from a comparison of fig. 18 with fig. 12, it appears that not all the kinetic energy of the film shows up in the Atkins oscillation of the levels in the standpipes.

6.2.2 Flow at constant, subcritical velocity. The film is accelerated to the desired velocity, after which the velocity is kept constant by maintaining a zero level difference. This measurement is only carried out for two velocities at the same temperature, the results are shown in fig. 19. Figs. 19a and 19c show the averaged velocity of the standpipes, $\Delta z/\Delta t$, *versus* time, figs. 19b and 19d show the corresponding increase in the level heights.

The drawn horizontal lines in figs. 19b and 19d are the expected values of the Kontorovich effect, corrected for the feedback (see 6.1.1), corresponding to $\dot{z}$ given by the drawn lines in the figs. 19a and 19c. The error bars

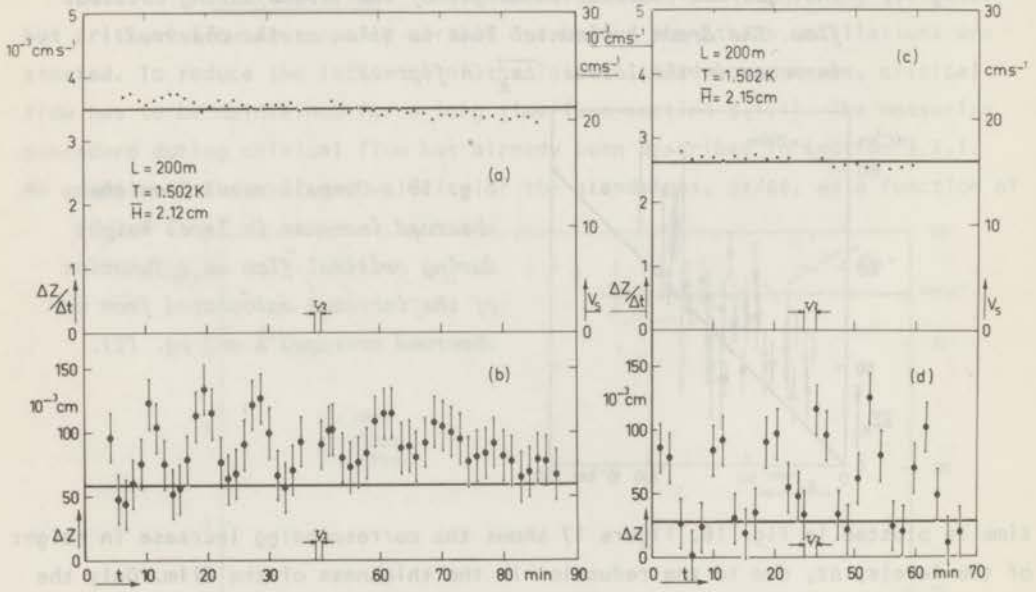

Fig. 19 *The velocity of the standpipes (a,c) and the observed increase in the height of the levels during subcritical flow (b,d), with zero level difference. The drawn lines in the figs. 19b and 19d correspond to the calculated increase in the levels using eq. (1) and the averaged velocity of the standpipes (horizontal line in the figs. 19a and 19c).*

give an indication of the measuring accuracy. In spite of the poor measuring accuracy obtained with this type of measurement, which is not only caused by third sound, but also by the inaccuracy with which the zero level difference could be maintained, a thinning of the order of the Kontorovich prediction is observed, although the observed values seem somewhat high.

6.2.3 Persistent flow. During persistent flow, the thinning of the film can also be measured by the amount of excess liquid in the standpipes. Only a few measurements were carried out, due to the fact that, as was the case for the 166 m capillary, the original apparatus did not allow for small values of $\overline{H}$. At a temperature T = 1.427 K, a height $\overline{H}$ = 5.6 cm, an averaged film thickness d = 140 Å, and a persistent flow velocity $v_s \simeq 36$ cm/s, we observed $\Delta z_K = (25 \pm 10) \times 10^{-3}$ cm, while the calculated value is: $\Delta z_K = 29 \times 10^{-3}$ cm. The agreement seems to be good. The persistent flow apparatus has now been modified to allow for smaller $\overline{H}$, making more accurate measurements possible. The results in persistent flow will be published separately.

6.3 Discussion of the thinning

All the results indicate that a moving film is thinner than a static one by an amount of the order of magnitude predicted by Kontorovich. The quantitative results for the 200 m capillary are, inlike the results for 120 m, substantially too high. Apparently the magnitude of the discrepancy depends on the length of the capillary, indicating that it cannot be due to the fact that wrong assumptions are made for the equilibrium conditions between the moving film and its vapour.

The following explanation of the observed discrepancy is suggested. In the calculations it is assumed that, after elimination of the standing third-sound waves, the mass transfer rate $\dot{M}$ is constant throughout the entire film. The influence of cross-effects and retardation effects, due to the finite speed of third sound (with which information travels along the film), has been totally neglected. These effects become more important the longer the capillary. For instance, it is most likely that at the moment that the potential energy of the levels during the Atkins oscillation is at its maximum, the entire film is not at rest. That not all the kinetic energy shows up in the amplitude is supported by the observations in sections 6.1.2 and 6.2.1. According to eq. (32) with $(E^{kin,max}_{film}/E^{pot,max}_{bulk}) > 1$, this would lead to a higher expected value of the

thinning.

This is also the case with the applied correction for the feedback, which is taken too large, as retardation has been neglected. In order to check this explanation of the observed discrepancy for the longest capillary, the 200 m device is now being modified into a persistatron, in which retardation effects should not play an important role.

The present experimental results provide strong evidence that the thinning of the film as predicted by Kontorovich does indeed occur. That the thinning of the film does not only occur owing to the obstruction of the vapour in these narrow capillaries[3] has recently been shown by others, who confirm our findings on the thinning[19,20,24,25]. The accuracy of the experimental results on the thinning does not allow one to detect corrections of the order of $(1 - \rho_{vap}/\rho)$. Nevertheless in view of the present results there seems to be no reason to doubt the validity of the assumption that the vapour-film equilibrium condition is identical to that of the bulk. No phenomena, additional to those occurring in the bulk, have to be introduced to explain the behaviour of the film.

However, there remain the negative findings of Keller (and recently by Telschow *et al.*[21]). No convincing explanation of these negative results has been proposed[16,23]. Attempts to reconcile the contradictory results are so far unsatisfactory[3,22].

Appendix

The equations describing the behaviour of He II in the nondissipative region are the Landau equations.

1. Continuity equation:

$$\frac{\partial \rho}{\partial t} + \vec{\nabla}\cdot\vec{j} = 0, \text{ with } \vec{j} = \rho\vec{v} = \rho_s\vec{v}_s + \rho_n\vec{v}_n \text{ and } \rho = \rho_s + \rho_n \ .$$

2. Euler equation for the superfluid:

$$\frac{d_s\vec{v}_s}{dt} = -\vec{\nabla}(\mu + \Omega) = -\frac{1}{\rho}\vec{\nabla}P + s\vec{\nabla}T + \frac{\rho_n}{2\rho}\vec{\nabla}(\vec{v}_n - \vec{v}_s)^2 - \vec{\nabla}\Omega \ ,$$

with Ω the potential of the external forces.

3. Entropy conservation:

$$\frac{\partial \rho s}{\partial t} + \vec{\nabla}\cdot(\rho s\vec{v}_n) = 0 \ .$$

4. The momentum balance:

$$\frac{\partial j_i}{\partial t} + \sum_\alpha \frac{\partial \Pi_{\alpha i}}{\partial x_\alpha} = - \rho \frac{\partial \Omega}{\partial x_i} \quad ,$$

with $\Pi_{\alpha i} = P\delta_{\alpha i} + \rho_n v_{n\alpha} v_{ni} + \rho_s v_{s\alpha} v_{si}$.

The equilibrium conditions between liquid and vapour as given by Putterman and Uhlenbeck[14]:

1. $\vec{v}_n = \vec{v}_{vap}$
2. $P_{Liq} = P_{vap}$
3. $T_{Liq} = T_{vap}$
4. $\mu_{Liq} + \frac{1}{2}\vec{v}_s^{\,2} - \vec{v}_n \cdot \vec{v}_s = \mu_{vap} - \frac{1}{2}\vec{v}_{vap}^{\,2}$.

References

1. Kontorovich, V.M., Soviet Physics-JETP 3 (1956) 770.
2. Keller, W.E., Phys. Rev. Letters 24 (1970) 569.
3. Van Spronsen, E., Verbeek, H.J., De Bruyn Ouboter, R., Taconis, K.W. and Van Beelen, H., Phys. Letters 45A (1973) 49.
4. Atkins, K.R., Proc. Roy. Soc. A203 (1950) 119.
5. Verbeek, H.J., Van Spronsen, E., Mars, H., Van Beelen, H., De Bruyn Ouboter, R. and Taconis, K.W., Physica 73 (1974) 621.
6. Sabisky, E.S. and Anderson, C.H., Phys. Rev. Letters 24 (1970) 1049; Phys. Rev. A7 (1973) 790.
7. Allen, J.F., Proc. Int. School of Physics, Course XII - Liquid Helium G. Careri, ed. (1963) p. 305.
8. Calvani, P., Gruelich, R. and Maraviglia, B., Lettere Al Nuovo Cimento 6 (1973) 536.
9. Langer, J.S. and Fisher, M.E., Phys. Rev. Letters 19 (1969) 560.
10. Hallock, R.B. and Flint, E.B., Phys. Rev. A10 (1974) 1285. See also: Allen, J.F., Armitage, J.G.M. and Saunders, B.L., *ibid*, ref. 11.
11. Hoffer, J.K., Fraser, J.C., Hammel, E.F., Campbell, L.J., Keller, W.E. and Sherman, R.H., Proc. 13th Int. Conf. on Low Temp. Physics (Boulder, 1972).
12. Liebenberg, D.H., Phys. Rev. Letters 26 (1971) 744.
13. Robinson, J.F., Phys. Rev. 82 (1951) 440.

14. Putterman, S.J. and Uhlenbeck, G.E., Phys. Fluids 12 (1969) 2229. See also Putterman, S.J., Superfluid Hydrodynamics, North-Holland Publ. Comp. (Amsterdam, 1974) p. 37, 38.
15. See for instance Guggenheim, E.A., Thermodynamics, North-Holland Publ. Comp. (Amsterdam, 1957) p. 404.
16. Goodstein, D.L. and Saffman, P.G., *ibid*, ref. 11.
17. De Bruyn Ouboter, R., J. Low Temp. Phys. 12 (1973) Nos 1/2.
18. Atkins, K.R. and Rudnick, I., Progr. in low Temp. Phys. Vol. 6, North-Holland Publ. Comp. (Amsterdam, 1970), C.J. Gorter, ed., p. 37.
19. Williams, G.A. and Packard, R., Phys. Rev. Letters 32 (1974) 587.
20. Banton, M.E., Hoffer, J.K. and Keller, W.E., Bull. Am. Phys. Soc. 19 (1974) 436.
21. Telschow, K., Wang, T. and Rudnick, I., J. Low Temp. Phys. 18 (1975) 43. See also Telschow, K., dissertation, UCLA (1973).
22. Goodstein, D.L. and Saffman, P.G., J. Low Temp. Phys. 18 (1975) 435.
23. Putterman, S.J. and Rudnick, I., Physics Today, August 1971.
24. Flint, E.B. and Hallock, R.B., Phys. Rev. B11 (1975) 2062.
25. Graham, G.M. and Vittoratos, E., Phys. Rev. Letters 33 (1974) 1136.

CHAPTER III

THE ROTATING He II FILM, THE SHRUNKEN MENISCUS

1. Introduction

The meniscus of rotating helium II has been the object of many investigations. According to the Landau equations one expects a shrunken temperature-dependent parabolic meniscus if the angular velocity of the bucket does not exceed a critical value ω_{c1} below which the superfluid is at rest, as was predicted by London[1] in 1946 for the first time. For $\omega = \omega_{c1}$ the first quantized vortex line appears in order to minimize the free energy of the rotating helium. When $\omega >> \omega_{c1}$ many quantized vortices are created rotating with the fluid, effectively resulting in a nondissipative solid-body rotation of the whole fluid leading to a classical meniscus. This classical meniscus was experimentally found by Osborne[2] and others[3] and explained on these lines by Onsager[4] and Feynman[5].

In the first experiments done on the meniscus of rotating He II, the angular velocities were far too large to observe a shrunken parabolic interface or to measure a state with the superfluid at rest: $v_s = 0$[6]. (In analogy with superconductivity, this zero quantum state is called the Meissner state.) The more recent measurements of the angular momentum by Hess and Fairbank[7] and Packard and Sanders[8], with rotating buckets of small diameter, have shown that a state with $v_s = 0$ does exist for $\omega < \omega_{c1}$. Even for $\omega > \omega_{c1}$, a metastable state with $v_s = 0$ was observed by Reppy *et al.*[9]. Unfortunately, one has not been able to observe the meniscus in these experiments, so the question as to whether or not a state with $v_s = 0$ implies a shrunken meniscus has still not been answered experimentally. A review on the experimental and theoretical situation until 1966 is given by Andronikashvili and Mamaladze[10], and the present state of affairs in bulk He II is discussed by Putterman and Uhlenbeck[11].

Until now no experiments have been done on the meniscus of bulk for $\omega < \omega_{c1}$, mainly because of the difficulty of determining the meniscus in a

bucket with a small diameter, where capillarity dominates. However, Little and Atkins[12] carried out an experiment on a He II film covering a rotating cylinder. They measured the change of film thickness in the centre of the cylinder and claimed to have found a shrunken temperature-dependent meniscus. They interpreted the failure to induce rotation in the superfluid component as evidence that it is either very difficult to form vortices with their axes perpendicular to the plane of the film or that the vortex lines could not attain their equilibrium array due to a large pinning force.

Since these arguments were not completely convincing, a similar experiment was begun in which the thickness of a rotating film in a hollow spinning top was studied.

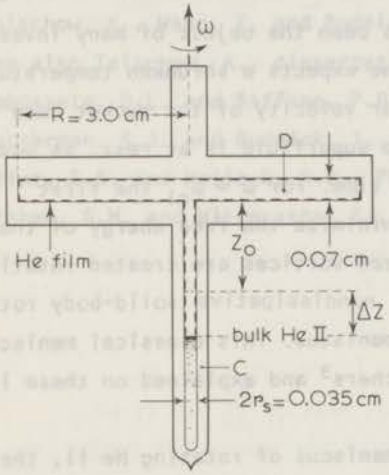

Fig. 1 *Schematic drawing of the top.*

2. Change in film thickness by using a spinning top

2.1 The apparatus: the hollow spinning top

The apparatus is shown in fig. 1 and is made completely out of glass. It consists of a hollow circular flat disc (D) onto which a very narrow standpipe (C) is fused. The axis of rotation ($\vec{\omega}$) is chosen vertically and coincides with the axis of the standpipe, providing cylindrical symmetry. At liquid-nitrogen temperature a fixed amount of helium gas was sealed off in the hollow top, in such a way that at temperatures below the lambda point the standpipe is partially filled with He II. The walls of the hollow disc and the standpipe will be covered on the inside by a helium film. The rest of the volume will be filled with saturated helium vapour. The inner diameter of the standpipe is chosen such that

ω_{c1} of the standpipe is relatively large, about 8 rad/s, so that the effects of vortex lines in the standpipe are negligible. When rotating the top, helium is centrifuged to the outside of the disc, deforming the film. The fluid necessary to deform the film is drawn from the standpipe giving rise to a lowering of the level by an amount Δz. The measurements are straightforward. Δz is measured as a function of the angular velocity ω with the help of a cathetometer. To keep the temperature in the top constant, the whole apparatus is immersed in a helium bath which is regulated within 0.1 mK; this means that a warming up or cooling down of the helium vapour gives a correction in Δz of about 10^{-3} cm, depending on the temperature dependence of the saturated vapour pressure at the working temperature.

2.2 Theory

The equations describing the behaviour of He II in the nondissipative region are the Landau equations.

1) Continuity equation:

$$\frac{\partial \rho}{\partial t} + \vec{\nabla}\cdot\vec{j} = 0, \text{ with } \rho\vec{v} = \vec{j} = \rho_s\vec{v}_s + \rho_n\vec{v}_n \text{ and } \rho = \rho_s + \rho_n \ .$$

2) Euler equation for the superfluid:

$$\frac{d_s\vec{v}_s}{dt} = -\vec{\nabla}(\mu + \Omega) = -\frac{1}{\rho}\vec{\nabla}P + s\vec{\nabla}T + \frac{\rho_n}{2\rho}\vec{\nabla}(\vec{v}_n - \vec{v}_s)^2 - \vec{\nabla}\Omega \ ,$$

with Ω the potential of the external forces.

3) Entropy conservation:

$$\frac{\partial \rho s}{\partial t} + \vec{\nabla}\cdot(\rho s\vec{v}_n) = 0 \ .$$

4) The momentum balance:

$$\frac{\partial j_i}{\partial t} + \sum_\alpha \frac{\partial}{\partial x_\alpha}\Pi_{\alpha i} = -\rho\frac{\partial}{\partial x_i}\Omega \ .$$

At the free surface the equilibrium conditions between liquid and vapour are derived by Putterman[13] as:

1. $\vec{v}_n = \vec{v}_{vap}$; 3. $T_{Liq} = T_{vap}$;

2. $P_{Liq} = P_{vap}$; 4. $\mu_{Liq} + \frac{1}{2}\vec{v}_s^2 - \vec{v}_n \cdot \vec{v}_s = \mu_{vap} - \frac{1}{2}\vec{v}_{vap}^2$.

In this section, rotating bulk He II (section 2.2.1) and a rotating helium film (section 2.2.2) are considered on the basis of the above set of equations. One can show that in the case of a stationary rotating system in thermal equilibrium a solution with $\vec{v}_s = 0$ and $\vec{v}_n = \vec{\omega} \times \vec{r}$ (Meissner state) fulfils all Landau equations if:

$$\frac{1}{\rho} \vec{\nabla} P + \vec{\nabla} \Omega - \frac{\rho_n}{\rho} \omega^2 \vec{r} = 0 \quad . \tag{1}$$

The free surface is determined by the equilibrium conditions 1 and 2, the equilibrium conditions 3 and 4 are identically fulfilled. For the vortex state of rotating He II, the averaged hydrodynamics are derived by Bekarevich and Khalatnikov[14]. Considering a stationary nondissipative state in thermal equilibrium with a uniform distribution of vortex lines their equations reduce to the Euler equation for the superfluid, in which one must take for the averaged superfluid velocity

$$\vec{v}_s = \vec{\omega} \times \vec{r} = \vec{v}_n \quad .$$

In this way one obtains

$$\frac{1}{\rho} \vec{\nabla} P + \vec{\nabla} \Omega - \omega^2 \vec{r} = 0 \quad .$$

The equilibrium conditions in this case are

$$\vec{v}_n = \vec{v}_{vap} = \vec{\omega} \times \vec{r} \qquad \text{and} \qquad P_{Liq} = P_{vap} \quad .$$

The other conditions are again identically fulfilled. The independent equations for the vortex state only differ from those derived for the Meissner state in that the ratio ρ_n/ρ is replaced by 1; therefore all results from the Meissner state can be used for the vortex state by replacing ρ_n/ρ by 1.

2.2.1 Rotating bulk He II. Let us consider a rotating stationary system of bulk He II in the Meissner state. Eq. (1), describing the behaviour of the fluid, now reads for regions not too close to the vessel wall

$$-\frac{1}{\rho}\vec{\nabla}P + \frac{\rho_n}{2\rho}\vec{\nabla}(\vec{\omega}\times\vec{r})^2 - \vec{\nabla}gz = 0 \quad ,$$

or if considering regions in which ρ and ρ_n are constant,

$$-\frac{P}{\rho} + \tfrac{1}{2}\frac{\rho_n}{\rho}\omega^2 r^2 - gz = \text{const.} = -\frac{P^{sat}}{\rho} \quad . \tag{2}$$

Eq. (2) shows that the isobars in these regions are shrunken temperature--dependent paraboloïds. In the vapour the following equation holds

$$\frac{d\vec{v}_{vap}}{dt} = -\frac{1}{\rho_{vap}}\vec{\nabla}P - \vec{\nabla}gz \quad ,$$

or since we have a stationary state with $\vec{v}_{vap} = \vec{\omega}\times\vec{r}$,

$$-\vec{\nabla}\tfrac{1}{2}\omega^2 r^2 = -\frac{1}{\rho_{vap}}\vec{\nabla}P - \vec{\nabla}gz \quad ,$$

which for constant ρ_{vap} is equivalent to

$$-\frac{P}{\rho_{vap}} + \tfrac{1}{2}\omega^2 r^2 - gz = \text{const.} = -\frac{P^{sat}}{\rho_{vap}} \quad . \tag{3}$$

This shows that the isobars in the vapour are not shrunken temperature--independent paraboloïds. The shape of the interface between liquid and vapour is determined by the equilibrium condition $P_{Liq} = P_{vap}$ along the meniscus. If one considers the free surface of the liquid as a region of constant densities ρ and $\rho_n^{(s)}$, where $\rho_n^{(s)}$ is the density of the normal component at the free surface, this equilibrium condition combined with eqs. (2) and (3) immediately leads to the relation:

$$\tfrac{1}{2}\rho_{vap}\omega^2 r^2 - \rho_{vap}gz = \tfrac{1}{2}\rho_n^{(s)}\omega^2 r^2 - \rho gz \quad ,$$

or

$$z = \frac{\rho_n^{(s)} - \rho_{vap}}{\rho - \rho_{vap}}\frac{\omega^2 r^2}{2g} \quad .$$

Substituting this expression for z in eq. (2) or eq. (3), one finds for the pressure above the meniscus

$$P^{(s)} = P^{sat} + \frac{\rho_{vap}}{\rho - \rho_{vap}}\tfrac{1}{2}\rho_s\omega^2 r^2 \qquad \text{(see chapter II).}$$

If $\rho_n^{(s)} = \rho_n^{bulk}$, this result represents an even more shrunken temperature--dependent parabolic profile than the generally used expression for the shrunken meniscus, in which the density of the vapour is neglected. If, on the other hand, one follows the tentative suggestion made by Putterman and Rudnick[15], by taking $\rho_n^{(s)} = \rho$, the equation for the meniscus reduces to $z = \omega^2 r^2/2g$, just as in a classical fluid. With this additional boundary condition at the free surface of the liquid, a state with $v_s = 0$ does not imply a shrunken parabolic interface.

For the vortex state one can use the above results from the Meissner state by substituting $\rho_n^{(s)}/\rho = 1$, giving $z = \omega^2 r^2/2g$ (a temperature-independent non-shrunken meniscus).

2.2.2 The rotating helium film. In the rotating helium film the Van der Waals forces are not negligible. Let us again consider the Meissner state. The schematic geometry of the spinning top is shown in fig. 2.
Eq. (1) in this case reads

$$-\frac{1}{\rho}\vec{\nabla}P + \frac{\rho_n}{2\rho}\vec{\nabla}\omega^2 r^2 - \vec{\nabla}gz + \vec{\nabla}\gamma/x^3 = 0$$

or

$$-\frac{P}{\rho} + \tfrac{1}{2}\frac{\rho_n}{\rho}\omega^2 r^2 - gz + \frac{\gamma}{x^3} = \text{const.}$$

in regions with constant ρ and ρ_n. The equilibrium condition $P_{Liq} = P_{vap}$ along the interface of liquid and vapour leads to a film thickness δ on the flat disc, determined by:

$$-g(z_\omega + \delta) + \frac{\gamma}{\delta^3} + \tfrac{1}{2}\left(\frac{\rho_n^{(s)} - \rho_{vap}}{\rho - \rho_{vap}}\right)\omega^2 r^2 = \frac{\gamma}{r_s^3} \approx 0 \quad ,$$

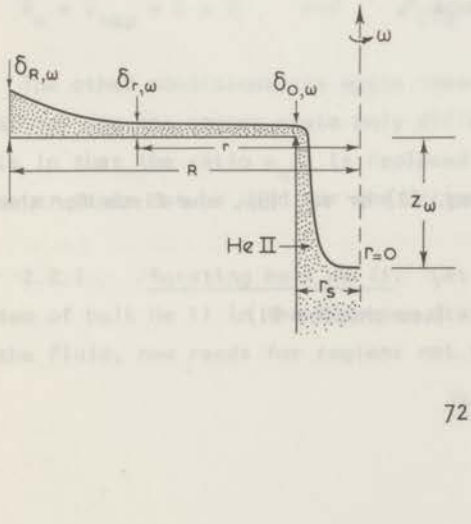

Fig. 2 *The schematic geometry used in the calculations for the top.*

in which r_s is the radius of the standpipe. If one neglects ρ_{vap} with respect to $\rho_n^{(s)}$ in this case, one obtains:

$$-g(z_\omega + \delta) + \frac{\gamma}{\delta^3} + \frac{\rho_n^{(s)}}{2\rho}\omega^2 r^2 = 0 \quad . \tag{4}$$

The equation results in a shrunken meniscus modified by the Van der Waals forces. If the film is full of vortex lines, the results of the Meissner state can be used again by setting the parameter $\rho_n^{(s)}/\rho$ equal to 1. Another way to obtain a modified nonshrunken meniscus is by assuming the speculative boundary condition $\rho_n^{(s)} = \rho$ of Putterman and Rudnick[15].

In order to check eq. (4) experimentally, the change in the level in the standpipe Δz as a function of ω is calculated, by making some reasonable simplifications:

1) $z_{\omega=0} \equiv z_0$ is rather large, so the film thickness on upper and lower surface of the hollow disc is nearly equal; and therefore, both sides are taken to be equivalent.

2) The amount of film on the vertical wall on the hollow disc and in the standpipe and effects such as due to *e.g.* surface tension in the corners are neglected.

With these assumptions, the volume of the film at a certain angular velocity is:

$$V_{f,\omega} = 2\int_{r_s}^{R} 2\pi r\delta(r)dr \simeq 4\pi\int_0^R r\delta(r)dr \quad .$$

By solving for r as a function of δ from eq. (4) and integrating over δ, one finds:

$$V_{f,\omega} = \frac{2\pi g}{(\rho_n^{(s)}/\rho)\omega^2}(\delta_{R,\omega}^2 - \delta_{0,\omega}^2) - \frac{6\pi\gamma}{(\rho_n^{(s)}/\rho)\omega^2}\left(\frac{1}{\delta_{R,\omega}^2} - \frac{1}{\delta_{0,\omega}^2}\right)$$

and

$$V_{f,0} = 2\pi R^2\delta_{0,0} = 2\pi R^2\delta_{R,0}$$

($\delta_{r,\omega}$ stands for the thickness of the film at radius r and angular velocity ω). The conservation of mass for the fluid gives:

$$\Delta z = \frac{V_{f,\omega} - V_{f,0}}{\pi r_s^2} = \frac{1}{(\rho_n^{(s)}/\rho)\omega^2 r_s^2}\left[g(\delta_{R,\omega}^2 - \delta_{0,\omega}^2) - 3\gamma\left(\frac{1}{\delta_{R,\omega}^2} - \frac{1}{\delta_{0,\omega}^2}\right)\right.$$

$$\left. - \frac{\rho_n^{(s)}}{\rho}\omega^2 R^2\delta_{0,0}\right] \quad . \tag{5}$$

From eq. (4) the following two formulae are derived:

$$\Delta z = \frac{\gamma}{g}\left(\frac{1}{\delta^3_{0,\omega}} - \frac{1}{\delta^3_{0,0}}\right) - \left(\delta_{0,\omega} - \delta_{0,0}\right) \quad , \tag{6}$$

$$\Delta z = \frac{\gamma}{g}\left(\frac{1}{\delta^3_{R,\omega}} - \frac{1}{\delta^3_{0,0}}\right) - \left(\delta_{R,\omega} - \delta_{0,0}\right) + \tfrac{1}{2}\frac{\rho_n^{(s)}}{\rho}\omega^2 R^2 \quad . \tag{7}$$

By eliminating Δz and $(\rho_n^{(s)}/\rho)\omega^2$ from the eqs. (5), (6) and (7) one finds:

$$\delta^4_{R,\omega} + \delta^3_{R,\omega}(\delta_{0,\omega} - \alpha) + \delta^2_{R,\omega}\left(\frac{3\kappa^3}{\delta^2_{0,\omega}} - \frac{\alpha\kappa^3}{\delta^3_{0,\omega}}\right)$$

$$+ \delta_{R,\omega}\left(\frac{3\kappa^3}{\delta_{0,\omega}} - \frac{\alpha\kappa^3}{\delta^2_{0,\omega}}\right) - \frac{\alpha\kappa^3}{\delta_{0,\omega}} = 0 \quad , \tag{8}$$

in which

$$\kappa = (\gamma/g)^{1/3}, \qquad \alpha = 2\delta_{0,0} + \frac{r_s}{R^2}\Delta z \quad \text{and} \quad \delta_{0,0} = \frac{\kappa}{z_0^{1/3}} \quad .$$

Using $\delta_{0,\omega}$ as a variable parameter, one can first calculate Δz from eq. (6), if κ is known. Together with the measured value of z_0, from which one finds the value of α, one can now calculate the root $\delta_{R,\omega}$ from eq. (8). The proper value of $(\rho_n^{(s)}/\rho)\omega^2$ follows then from eq. (7).

Since the formulae given above do not give very much direct information, it is sensible to work out some approximations. One can easily find from eqs. (4), (5) and (6):

$$1) \quad \Delta z = \frac{1}{3}\frac{\kappa}{z_0^{4/3}}\frac{R^2}{r_s^2}\frac{\rho_n^{(s)}}{\rho}\frac{\omega^2 R^2}{2g} \quad , \text{ for small } \omega^2, \text{ and} \tag{9a}$$

$$2) \quad \Delta z = \frac{\rho_n^{(s)}}{\rho}\frac{\omega^2 R^2}{2g} - z_0 \quad , \text{ for high } \omega^2 \quad . \tag{9b}$$

For high angular velocities, one must expect a vortex state, so in the approximation for high angular velocities $\rho_n^{(s)}/\rho$ should be taken equal to 1. Thus eq. (9b) gives

$$z_\omega = \Delta z + z_0 = \frac{\omega^2 R^2}{2g} \quad . \tag{10}$$

The range where these approximations fit the calculations considered above very strongly depends on the initial value of $z, (z_0)$, but generally as one finds from the experimental data, formula (9a) fits very well if $\omega^2 < 100$ rad^2/s^2 and formula (10) if $\omega^2 > 700$ rad^2/s^2.

2.3 Results and discussion

The experimental results for top 1 are shown in fig. 3, where for different temperatures Δz is plotted as a function of ω^2 on a logarithmic scale. The theoretical curves are determined by the three parameters z_0, $\rho_n^{(s)}/\rho$ and κ, from which only z_0 is known from direct measurement, while $\rho_n^{(s)}/\rho$ may even vary along the curves. In the low angular-velocity region the experimental values of Δz show, within the experimental accuracy, the dependence on ω^2 as given by eq. (9a), so that in matching eq. (9a) to the experimental points one finds a value for the quantity $\kappa(\rho_n^{(s)}/\rho)$.

This is found to be $\kappa(\rho_n^{(s)}/\rho) = (7.8 \pm 0.5) \times 10^{-6}cm^{4/3}$ *for all temperatures.* This means that the temperature dependence of the experimental curves is fully determined by the value of z_0, which is a function of temperature, since the total mass in the top is constant.

For further experimental evidence that the only temperature dependence of the curves arises from z_0, top 2 was made (radius 2.74 cm) in which a variable amount of helium gas could be sealed off. In this way about the same z_0 for different temperatures could be obtained. The results are shown in figs. 5a, 5b and 5c. The lower ω^2 region can be fitted quite well with $\kappa(\rho_n^{(s)}/\rho) = (6.0 \pm 0.5) \times 10^{-6}cm^{4/3}$.

These results for $\kappa(\rho_n^{(s)}/\rho)$ imply, that if one assumes $\rho_n^{(s)}/\rho = (\rho_n/\rho)^{\text{bulk}}(T)$, one finds κ to be strongly temperature dependent, in order to counter the temperature dependence of ρ_n. This is in contradiction with the nature of the Van der Waals forces and with the experimental results of Grimes and Jackson[16] on metals. Besides, one finds 34×10^{-6}cm$^{4/3} < \kappa < 56 \times 10^{-6}cm^{4/3}$ for top 1 and 24×10^{-6}cm$^{4/3} < \kappa < 42 \times 10^{-5}cm^{4/3}$ for top 2, in the temperature regions used. These are orders of magnitude which disagree with a crude estimate one can make from the total amount of helium in the top from which one finds $\delta_{0,0} = (1 \pm 0.5) \times 10^{-5}$cm, corresponding to a κ value of about 10^{-5}cm$^{4/3}$. This latter value of κ is in good agreement with the calculation of Schiff[17] who finds a theoretical value for glass: $\kappa_{th} = 4 \times 10^{-6}cm^{4/3}$. It should be remarked that such a calculation can only be considered as an indication for the order of magnitude of κ, since κ is strongly dependent on the roughness and the

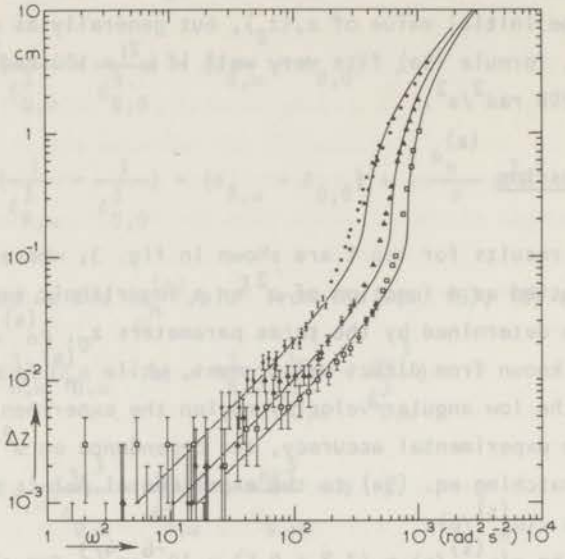

Fig. 3 *Experimental results of top 1.* (•) z_0 = 1.50 cm, T = 1.552 K; (Δ) z_0 = 2.56 cm, T = 1.624 K; (□) z_0 = 3.53 cm, T = 1.692 K. *The drawn curves are calculated with* $\kappa = 7.8 \times 10^{-6}$ cm$^{4/3}$ *and* $\rho_n^{(s)}/\rho = 1$.

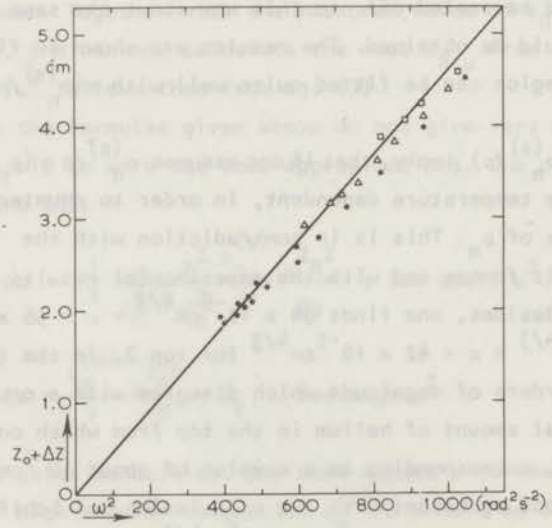

Fig. 4 *The high angular-velocity data from fig. 3 compared with the relation* $\Delta z + z_0 = \omega^2 R^2/2g$.

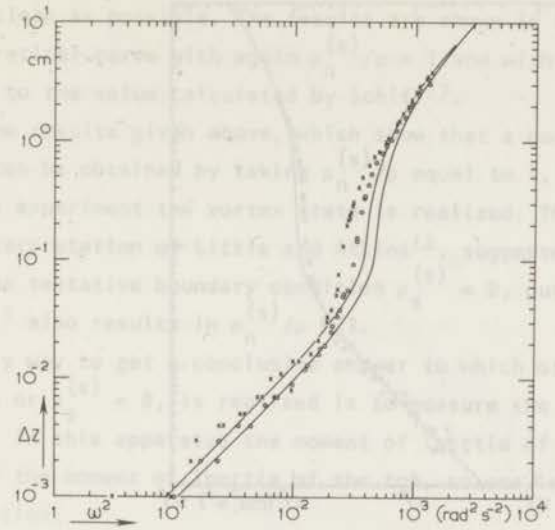

Fig. 5a *Experimental and calculated* ($\kappa = 6.0 \times 10^{-6}$ cm$^{4/3}$, $\rho_n^{(s)}/\rho = 1$) *results of top 2.* (×) $z_0 = 1.37$ cm, $T = 1.49$ K; (o) $z_0 = 1.68$ cm, $T = 1.09$ K. *For clarity the error bars are omitted.*

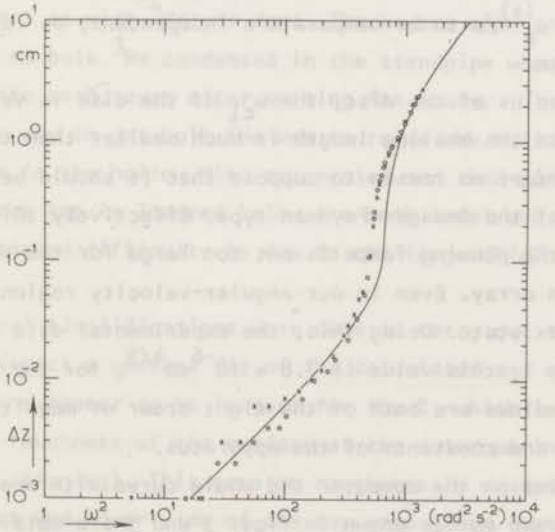

Fig. 5b *Experimental and calculated* ($\kappa = 6.0 \times 10^{-6}$ cm$^{4/3}$, $\rho_n^{(s)}/\rho = 1$) *results of top 2.* (×) $z_0 = 2.33$ cm, $T = 1.60$ K; (o) $z_0 = 2.34$ cm, $T = 1.31$ K. *For clarity the error bars are omitted.*

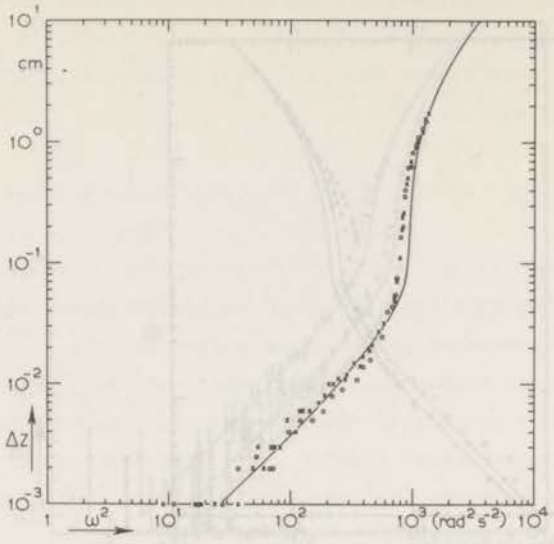

Fig. 5c *Experimental and calculated* ($\kappa = 6.0 \times 10^{-6}$ cm$^{4/3}$, $\rho_n^{(s)}/\rho = 1$) *results of top 2.* (×) $z_0 = 3.41$ *cm,* $T = 1.72$ *K;* (o) $z_0 = 3.41$ *cm,* $T = 1.49$ *K. For clarity the error bars are omitted.*

contamination of the material. To eliminate the large temperature dependence of κ, one has to assume $\rho_n^{(s)}/\rho$ to be temperature independent, as is *e.g.* the case for the vortex state.

Due to the large radius of the disc, the ω_{c1} of the disc is very small ($\omega_{c1} \approx 10^{-4}$ rad/s). Since the healing length is much smaller than the film thickness, there is *a priori* no reason to suppose that it should be difficult to create vortex lines of the Onsager-Feynman type. Effectively this results in ρ_n/ρ equal to 1, if the pinning force is not too large for the vortices to attain an equilibrium array. Even in our angular-velocity region, $\omega >> \omega_{c1}$, one may expect the vortex state. Using this, the experimental data can be fitted with only one κ. For top 1, this value is 7.8×10^{-6} cm$^{4/3}$, for top 2, 6.0×10^{-6} cm$^{4/3}$. These values are both of the right order of magnitude, temperature independent and constants of the apparatus.

If one now calculates on the computer the whole curve with one constant κ and $\rho_n^{(s)}/\rho = 1$, the drawn curves shown in figs. 3 and 5 are obtained. As can be seen from these figures, the fit is rather good*. The high angular-velocity measurements of top 1 are shown in fig. 4 on a linear scale. The drawn curve is approximation (10): $z_0 + \Delta z = \omega^2 R^2/2g$. To study the dependence of κ on the

---

* For note see page 79.

roughness of the glass, top 3 was made with utmost care to keep the glass as smooth and clean as possible. The results are shown in fig. 6. The drawn curve is the theoretical curve with again $\rho_n^{(s)}/\rho = 1$ and with $\kappa = 4.6 \times 10^{-6} cm^{4/3}$, a value close to the value calculated by Schiff[17].

From the results given above, which show that a good fit between experiment and theory can be obtained by taking $\rho_n^{(s)}/\rho$ equal to 1, it is strongly suggested that in this experiment the vortex state is realized. This result is in contrast with the interpretation of Little and Atkins[12], suggested by their experimental results†. The tentative boundary condition $\rho_s^{(s)} = 0$, put forward by Putterman and Rudnick[15] also results in $\rho_n^{(s)}/\rho = 1$.

The only way to get a conclusive answer to which of the two possibilities, vortex state or $\rho_s^{(s)} = 0$, is realized is to measure the angular momentum of the helium film. In this apparatus the moment of inertia of the film is very much smaller than the moment of inertia of the top, so one is unable to extract this information.

The behaviour of He II suggested that an ordinary rotating fluid with a film could show the same dependence of Δz as a function of the angular velocity. The equilibrium state can be reached by evaporation of the liquid in the standpipe and condensation on the flat discs if the mobility in the film should be too small due to viscosity. In top 3, an amount of ^3He was sealed off, and the same experiment as with ^4He was done. There were some problems with the experiment. First, no bulk ^3He condensed in the standpipe when the whole top was immersed in the bath, even after waiting for hours.

The only way to get bulk ^3He was to raise the hollow disc of the top above the bath; ^3He in the hollow disc evaporated and then condensed in the standpipe. After this, the top is lowered below the bath level and the measuring procedure starts. The second difficulty is due to the large dP/dT of ^3He at the working

---

* As several simplifications were made to carry out the calculations, one cannot expect a perfect fit of the calculated and experimental data. The deviations appear to be largest for top 2, which is probably due to a greater roughness of the surface at the outer perimeter (cracks, temperature effects, pinning). This greater roughness is caused by the epoxy by which the upper and lower side of the top were glued together.

† It should be remarked that due to pinning of the vortices, there exists the possibility that effectively $\rho_n^{(s)}/\rho$ could be somewhat smaller than 1. The accuracy of the experimental data is not sufficient to exclude such a possibility.

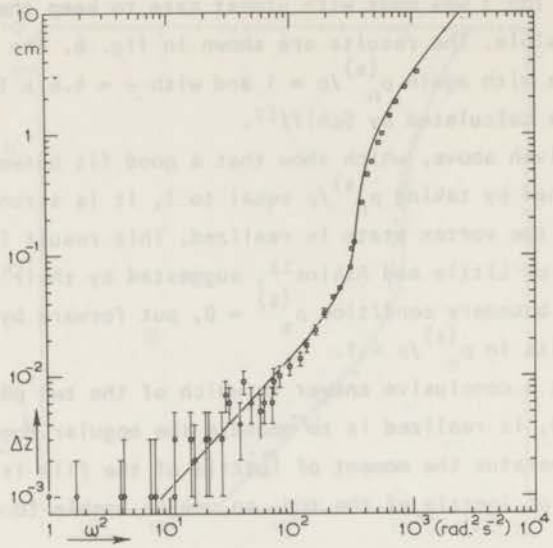

Fig. 6 *Experimental and calculated results of top 3* ($\kappa = 4.6 \times 10^{-6}$ *cm*$^{4/3}$, $\rho_n^{(s)}/\rho = 1$). (o) $z_0 = 1.40$ *cm*, *T = 1.71 K (21-12-1970);* (□) $z_0 = 1.40$ *cm*, *T = 1.71 K (22-12-1970).*

temperature (1.10 K), *i.e.* a small increase of the bath temperature results in a large Δz in the standpipe. When one regulates the bath back to the correct temperature, the evaporated liquid does not condense back.

When rotating the top, no Δz was observed. Even at high angular velocities, about 30 rad/s, only a small Δz appeared, probably due to a warming up of the bath. The conclusion is, therefore, that the relaxation time to reach equilibrium in an ordinary rotating liquid (with a film) is very large, and that the effects in He II are due to the greater mobility of the film.

3. A rotating He II film in a multiply connected geometry

To extend the investigations on the meniscus of a rotating film and at the same time studying the possibility of creating persistent film flow by rotation, two new pieces of apparatus were constructed, which will be called the torus and the spiral, both having a multiply connected geometry.

3.1 The rotating torus

The torus is shown in fig. 7 and is made of glass glued together with epoxy (E). The inner side of the cylindrical shell (T), with height h, is connected to the standpipe (C), with radius r_s, by a channel drilled through the glass. The open volume V is connected to the bath by a few holes (H) in order to ensure a constant temperature also at the inner wall of the shell T. As is the case with the top, a fixed amount of helium gas is sealed off at liquid-nitrogen temperature, in such a way that at a desired temperature region below T_λ, bulk liquid is condensed into the standpipe. Since a moving film is thinner

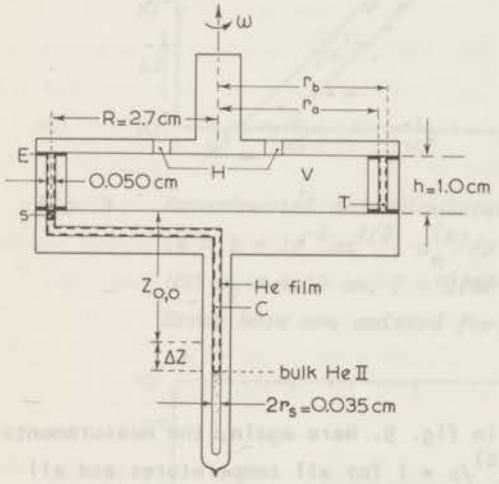

Fig. 7 *Schematic drawing of the torus.*

than a static one, the persistent flow created by rotation should result in an amount of excess liquid in the standpipe C after the rotation is stopped. In the same run, the meniscus, *i.e.* the thickness, of the film during rotation of the apparatus is studied by measuring the decrease in height of the bulk level (Δz) as a function of the angular velocity (ω).

Let us first consider the film thickness in the rotating apparatus. The derivation of Δz as a function of ω goes along the same lines as followed in section 2.2.2 for the top. In this geometry, however, the changes in film thickness on the horizontal edges are neglected and the inner- and outer side of the shell are considered as equivalent with $r_a \approx r_b \approx R$ (see fig. 8). All other simplifications are the same as those with the top. The complete calculations will not be given again, as they are straighforward, but only the approximations for small and high angular velocities.

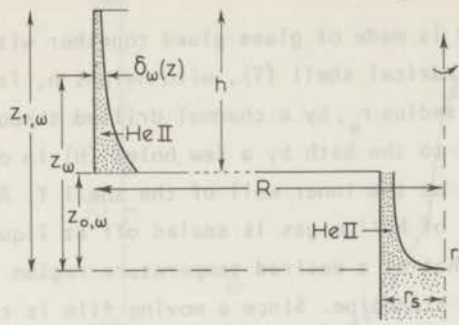

Fig. 8 *The schematic geometry used in the calculations for the torus.*

For small ω^2 one finds

$$\Delta z = \frac{4}{3} \frac{\rho_n^{(s)}}{\rho} \frac{Rh}{r_s^2} \frac{\kappa}{z_{0,0}^{4/3}} \frac{\omega^2 R^2}{2g}$$

and for high values of ω^2 one finds again

$$\Delta z = \frac{\omega^2 R^2}{2g} - z_{0,0} \quad .$$

Some experimental results are shown in fig. 9. Here again, the measurements can be fitted with one value of κ and $\rho_n^{(s)}/\rho = 1$ for all temperatures and all angular velocities, suggesting that the superfluid fully participates in the rotation. The full curves are calculated with $\rho_n^{(s)}/\rho = 1$ and $\kappa = 2 \times 10^{-5} \text{cm}^{4/3}$. Note that this large value of κ is probably due to the same mechanisms described in chapter I as now pores or cracks, especially due to the epoxy, can be filled with liquid as the angular velocity is increased.

The rotation is stopped after reaching an angular velocity of about 35 rad/s. One now expects a persistent current to be maintained in the torus. A decrease of thickness would show up as a negative Δz, indicating more liquid in the capillary after the rotation than before. The dimensions of the torus are such that a $\Delta z = 10^{-3}$cm corresponds to a $\Delta\delta \simeq 5$ Å. However such an effect was never observed.

In order to make sure that the vapour does not influence the results, an identical apparatus was constructed, except for a superleak (S) placed between the toroïd and the standpipe (see fig. 7). The superleak is full of liquid due to the capillary rise. In this way there is no connection between the vapour in

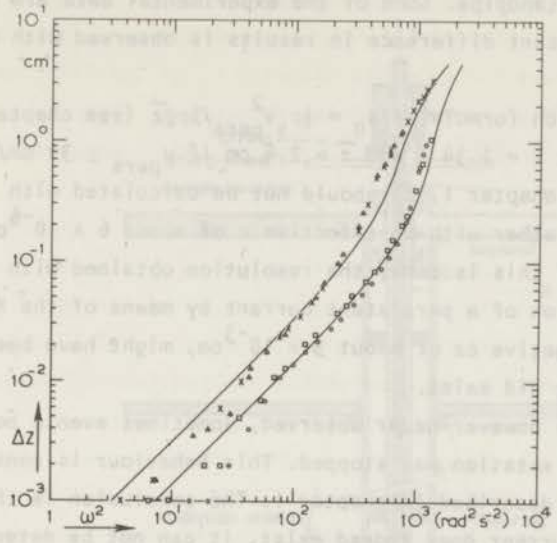

Fig. 9 *Experimental and calculated results for the torus* ($\kappa = 2 \times 10^{-5}$ cm$^{4/3}$, $\rho_n^{(s)}/\rho = 1$). (Δ,×) $z_0 = 1.89$ cm, $T = 1.09$ K; (□) $z_0 = 4.10$ cm, $T = 1.09$ K; (○) $z_0 = 3.94$ cm, $T = 1.69$ K. *Error bars are omitted for clarity.*

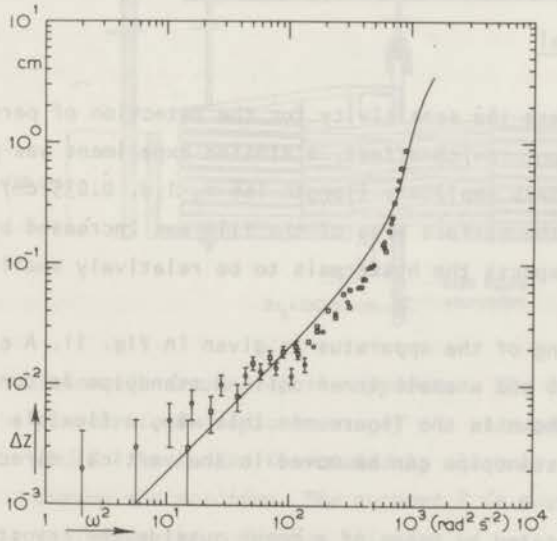

Fig. 10 *Experimental and calculated results for the torus with superleak* ($\kappa = 24 \times 10^{-6}$ cm$^{4/3}$, $\rho_n^{(s)}/\rho = 1$). (○) $z_0 = 3.40$ cm, $T = 1.32$ K (10-3-1971); (□) $z_0 = 3.40$ cm, $T = 1.32$ K (11-3-1971).

the toroïd and in the standpipe. Some of the experimental data are shown in fig. 10, but no significant difference in results is observed with or without the superleak.

From the Kontorovich formula $\Delta\delta/\delta_0 = \frac{1}{2}\rho_s v_{pers}^2/3\rho g\bar{z}$ (see chapter II) one obtains a $\Delta\delta/\delta_0 \simeq 6\%$ at T = 1.34 K and $\bar{z}$ = 2.4 cm if $v_{pers} \simeq 30$ cm/s. In view of the remarks made in chapter I, δ_0 should not be calculated with $\kappa = 2 \times 10^{-5} cm^{4/3}$ but rather with an effective κ of about $6 \times 10^{-6} cm^{4/3}$, as was found for top 2. If this is done, the resolution obtained with the torus is marginal for detection of a persistent current by means of the Kontorovich effect, but a small negative Δz of about 5×10^{-3}cm, might have been observed if a persistent current did exist.

Such an effect was however never observed, sometimes even a positive Δz was measured after the rotation was stopped. This behaviour is consistent with the hysteretic effects described in chapter I. The conclusion is therefore, that if a persistent current does indeed exist, it can not be detected in this experimental arrangement. The expectation that a persistent flow is present after stopping the rotation seems reasonable as the linear velocity at the outer perimeter before slowing down should be high enough to slip the necessary amount of circulation into the multiply connected system.

3.2 The rotating spiral

In order to increase the sensitivity for the detection of persistent film flow by means of the Kontorovich effect, a similar experiment was performed, but now using a long glass capillary (length 166 m, i.d. 0.035 cm) wound into a spiral. In this way the surface area of the film was increased by a factor of about 40, and one expects the hysteresis to be relatively small (see chapter I).

A schematic drawing of the apparatus is given in fig. 11. A closed circuit is formed by the spiral and a small inner coil. A standpipe is connected to the highest point, as is shown in the figure. In this way, a flexible connection is obtained, so that the standpipe can be moved in the vertical direction with respect to the circuit.

The circuit is rotated by means of a motor outside the cryostat, which drives the supporting bucket surrounding the coils. The system is filled in the usual way. The whole system is immersed in a helium bath, of which the temperature is kept constant to within 10^{-4} - 10^{-5} K.

The measuring procedure is the same as with the torus, although complicated

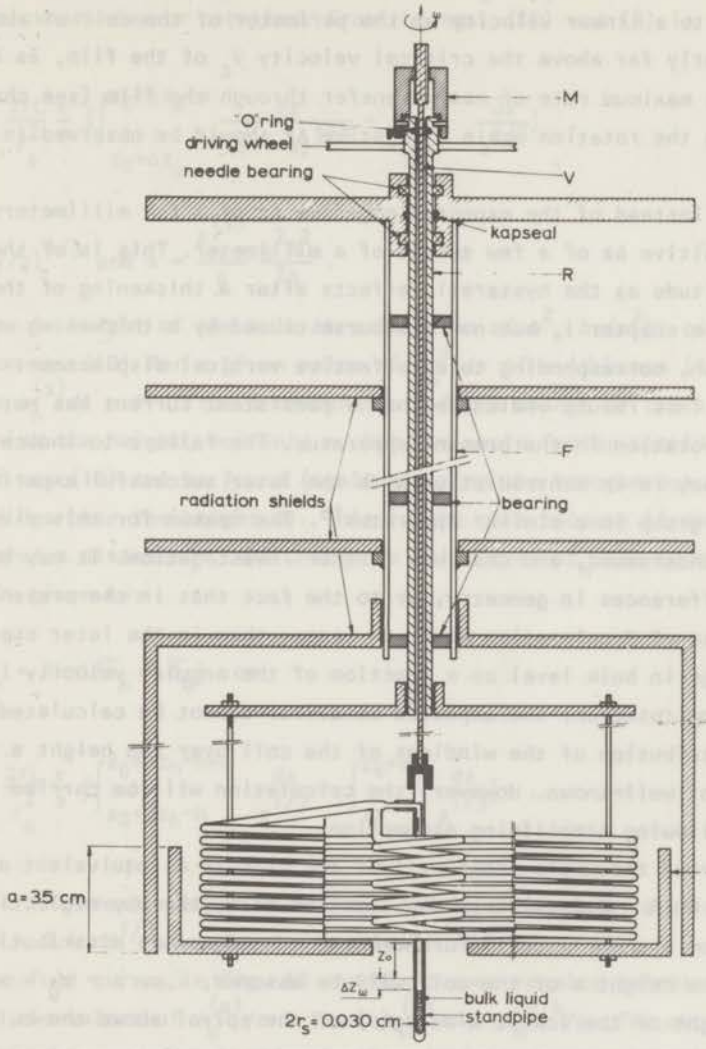

Fig. 11 *Schematic drawing of the apparatus. The micrometer M is used for vertical displacements of the standpipe connected to the rod V. The bucket is rotated by the tube R to which M is fixed during the rotation. The support F is mounted to guide R and to fasten the radiation shields.*

by the occurrence of standing third-sound waves, as described in chapter II. The influence of these third-sound waves, which are practically undamped, is largely eliminated by averaging over at least two periods.

The apparatus is accelerated up to angular velocities of about 18 rad/s, corresponding to a linear velocity at the perimeter of the coil of about 110 cm/s, clearly far above the critical velocity v_c of the film, as determined from the maximum rate of mass transfer through the film (see chapter II). After stopping the rotation again a negative Δz should be observed in the standpipe.

However, instead of the expected negative Δz of a few millimeters one observes a positive Δz of a few tenths of a millimeter. This is of the same order of magnitude as the hysteretic effects after a thickening of the film, as described in chapter I, but now of course caused by a thickening of the film due to rotation, corresponding to an effective vertical displacement $h_{eff} = \frac{\omega^2 R^2}{2g}$. This result indicates that a persistent current has not been generated by rotation in the present apparatus. The failure to induce persistent flow in this way is in contradiction with the later successful experiments done by the Leiden group in a similar apparatus[18]. The reason for this discrepancy is still not understood, and deserves further investigation. It may be connected with minor differences in geometry, or to the fact that in the present experiments, the rate of deceleration was much larger than in the later ones.

The change in bulk level as a function of the angular velocity is also measured during rotation. The expected behaviour cannot be calculated exactly, since the distribution of the windings of the coil over the height a (see fig. 11) is not well-known. However, the calculation will be carried out by making the following simplifying assumptions.

Let us treat the whole inner wall of the circuit as equivalent and at the same distance R (R = 6.0 cm) from the rotation axis, thereby neglecting contributions from the small coil. Furthermore, a homogeneous distribution of the length over the height a of the coil will be assumed, *i.e.* $z - z_0 \propto x$, where z_0 is the height of the lowest winding(s) of the spiral above the bulk level in the standpipe before starting the rotation, and x the distance along the capillary. Note that in order to keep the height a small, the windings are packed as closely as possible, with the result that the assumptions made above are not very well obeyed in the actual experimental arrangement.

From the conservation of the amount of liquid at constant temperature, the following equation can be written down:

$$\pi r_s^2 \Delta z_\omega = 2\pi r L(\overline{\delta}_\omega - \overline{\delta}_0) \quad , \tag{11}$$

where r_s is the inner radius of the standpipe, r the inner radius of the long

capillary, L the length of this capillary, and $\overline{\delta}_\omega - \overline{\delta}_0$ the change in the averaged thickness due to rotation. From the eqs. (11) and (4) it follows:

$$\Delta z_\omega = \frac{2rL}{r_s^2}\frac{\kappa}{a}\left[\int_{z_0+\Delta z_\omega}^{z_0+\Delta z_\omega+a}\frac{dz}{(z-\alpha)^{1/3}} - \int_{z_0}^{z_0+a}\frac{dz}{z^{1/3}}\right] , \qquad (12)$$

with $\kappa = (\gamma/g)^{1/3}$ and $\alpha = \frac{\rho_n^{(s)}}{\rho}\frac{\omega^2R^2}{2g}$.

The decrease in height of the bulk as a function of ω^2, $\Delta z(\omega^2)$, can be calculated from eq. (12) for a given value of $\rho_n^{(s)}/\rho$ if κ is known (for large ω^2 one expects $\rho_n^{(s)}/\rho = 1$). From a measurement of the change of the static film thickness with the height, not only κ, but the whole factor outside the brackets of eq. (12) can be found (again assuming the homogeneous distribution of the windings over the height a). This is the case because if the standpipe is raised over a distance h, the change in bulk level Δz_h due to the change in thickness is given by:

$$\pi r_s^2 \Delta z_h = 2\pi rL(\overline{\delta}_h - \overline{\delta}_0) \quad \text{or}$$

$$\Delta z_h = \frac{2rL}{r_s^2}\frac{\kappa}{a}\left[\int_{z_0+\Delta z_h-h}^{z_0+\Delta z_h-h+a}\frac{dz}{z^{1/3}} - \int_{z_0}^{z_0+a}\frac{dz}{z^{1/3}}\right] . \qquad (13)$$

A few static film measurements were done, and in this way a value of the factor $\frac{2rL}{r_s^2}\frac{\kappa}{a} = 2.1 \pm 0.4$ cm$^{1/3}$ was found and substituted in eq. (12).

The two full curves in fig. 12 represent some results calculated in this way for the two values of $\rho_n^{(s)}/\rho = 1$ and $\rho_n^{(s)}/\rho = \rho_n^{bulk}/\rho$. The experimental data for this low temperature show that the numerical agreement with the calculations is rather poor for small ω^2. At higher temperatures, the experimental points are even found to be above the $\rho_n^{(s)}/\rho = 1$ curve at the low angular velocities. At high angular velocities, all the results obey the expected relation $\Delta z_\omega = \omega^2R^2/2g - z_0$ rather well, in view of the simplifications (see fig. 13). Although an explanation of the rather strange discrepancies has not been found, we would like to mention the apparent temperature dependence of the observed $\Delta z(\omega^2)$. This is shown in fig. 14, where up to $\omega \approx 5$ rad/s it seems as if $\Delta z(\omega^2)$ is proportional to ρ_n/ρ. This result is itself in accordance with eq. (12) if at low angular velocities no vortex formation occurs in the

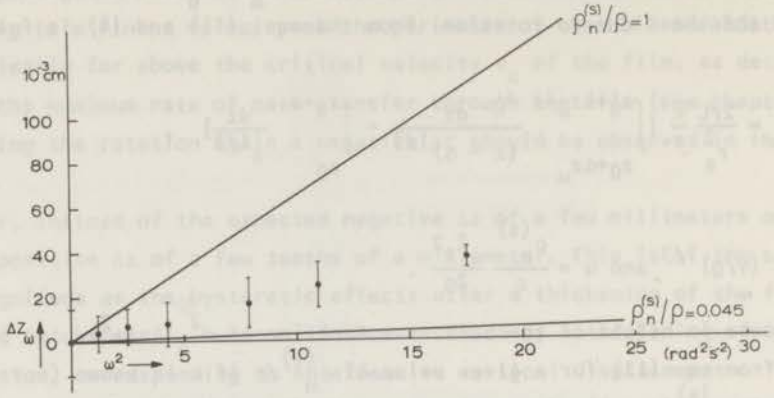

Fig. 12 *Results from one measuring run at T = 1.288 K and for z_0 = 1.08 cm obtained with the rotating spiral. The full curves are calculated from eq. (12) for the relevant values of $\rho_n^{(s)}/\rho$. The error bars account for the uncertainty caused by the effectiveness with which the third-sound waves are eliminated.*

superfluid. Hence it can be speculated that, if the unknown effect responsible for the bad numerical agreement does not affect the temperature dependence, the superfluid in the spiral does not participate in the rotation for $\omega \lesssim 5$ rad/s. This result is in sharp contrast with the results obtained with the torus, where no temperature dependence was found.

A possible explanation for this difference might be that the angular velocity at which vortex formation occurs in a rotating system, in order to minimize the free energy, is much larger in a narrow annular region of radius R than in a bucket of the same radius. According to Fetter[19], for bulk liquid this critical angular velocity is given by:

$$\Omega_{c1} = \frac{h}{\pi m d^2} \ln \frac{2d}{\pi a} \quad ,$$

with d the width of the annular region and a $\simeq$ 1 Å. Since the entire film on the surface perpendicular to the rotation axis is involved in this kind of vortex formation, the relevant quantity for the spiral is the inner diameter of the capillary d = 0.035 cm and for the torus the distance between the vertical walls d = 0.050 cm. This yields $\Omega_{c1}^{torus} \simeq 2$ rad/s and $\Omega_{c1}^{spiral} \simeq 4$ rad/s, both within the measuring range, but Ω_{c1}^{torus} is too small to detect a possible temperature dependence of $\Delta z(\omega^2)$, for $\omega < \Omega_{c1}^{torus}$, due to lack of measuring accuracy in

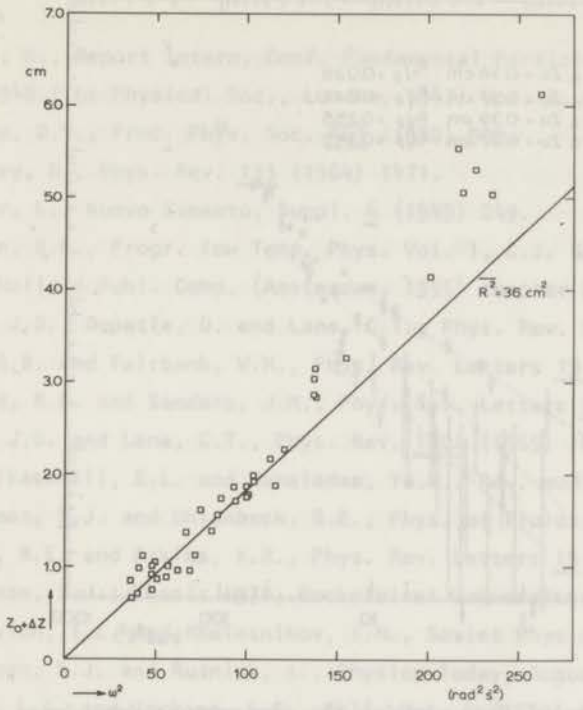

Fig. 13 *The high angular-velocity data of the rotating spiral compared with the relation* $\Delta z + z_0 = \omega^2 R^2/2g$ *for various temperatures* ($1.252\ K \leq T \leq 1.828\ K$) *and various* z_0 ($0.33\ cm \leq z_0 \leq 4.46\ cm$). *The full curve is calculated using* $\overline{R^2} = 36\ cm^2$. *For clarity the error bars are omitted.*

this velocity region.

It should be emphasized that this critical phenomenon is quite different and independent from the critical phenomenon described by Langer and Fisher[20], by which the linear critical velocity v_c is determined. The occurrence of this critical velocity, which can be deduced from the critical mass transport, allows for the creation of persistent film flow by rotation[18]. From the critical mass transfer, it can be deduced that the corresponding $\omega_c^{torus} \approx 8$ rad/s and $\omega_c^{spiral} \approx 4$ rad/s. Therefore, in the velocity region where the temperature dependence is observed in the spiral, the latter critical velocity is also not exceeded and the superfluid remains at rest†. We would like to remark that in a device in which $\Omega_{c1} > \omega_c$ one can expect the Kontorovich effect to occur for

† For note see page 90.

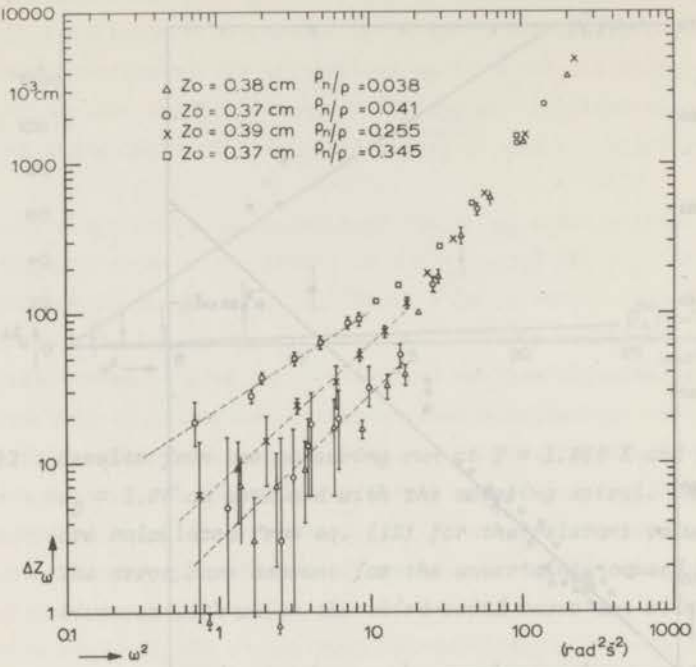

Fig. 14 *Experimental data showing the temperature dependence of* Δz_ω *at low angular velocities. For the error bars see the caption of fig. 12.*

$\omega_c < \omega < \Omega_{c1}$, which would show up as a negative slope of the curve Δz against ω^2 in this velocity region.

Measurements are in preparation by the Leiden group to investigate the ideas mentioned above, which up to this moment are rather speculative. Also the experiments on the temperature dependence will be further extended.

---

† Note that, even at the lowest angular velocities, the superfluid cannot be completely at rest in the rotating spiral, as there is no cylindrical symmetry, especially because of the small coil which is wound in the same sense as the large one. Therefore the condition $\oint_c \vec{v}_s \cdot \vec{dl} = 0$ in the lab - frame of reference implies $v_s \neq 0$ in this rotating apparatus.

References

1. London, H., Report Intern. Conf. Fundamental Particles and low Temp., July 1946 (The Physical Soc., London, 1947) Vol. 2, p. 48.
2. Osborne, D.V., Proc. Phys. Soc. A63 (1950) 909.
3. Mersevey, R., Phys. Rev. 133 (1964) 1471.
4. Onsager, L., Nuovo Cimento, Suppl. 6 (1949) 249.
5. Feynman, R.P., Progr. low Temp. Phys. Vol. I, C.J. Gorter, ed., North-Holland Publ. Comp. (Amsterdam, 1955) chapter 2.
6. Reppy, J.D., Depatie, D. and Lane, C.T., Phys. Rev. Letters 5 (1960) 541.
7. Hess, G.B. and Fairbank, W.M., Phys. Rev. Letters 19 (1967) 216.
8. Packard, R.E. and Sanders, J.M., Phys. Rev. Letters 22 (1969) 823.
9. Reppy, J.D. and Lane, C.T., Phys. Rev. 140A (1965) 106.
10. Andronikashvili, E.L. and Mamaladze, Yu.G., Rev. mod. Phys. 38 (1966) 567.
11. Putterman, S.J. and Uhlenbeck, G.E., Phys. of Fluids 12 (1969) 2229.
12. Little, R.E. and Atkins, K.R., Phys. Rev. Letters 19 (1967) 1224.
13. Putterman, S.J., Thesis 1970, Rockefeller University, New York.
14. Bekarevich, I.L. and Khalatnikov, I.M., Soviet Physics-JETP. 13 (1961) 643.
15. Putterman, S.J. and Rudnick, I., Physics Today, August 1971.
16. Grimes, L.G. and Jackson, L.C., Phil. Mag. 4 (1959) 1346.
17. Schiff, L., Phys. Rev. 59 (1941) 839.
18. Verbeek, H.J., Van Spronsen, E., Van Beelen, H., De Bruyn Ouboter, R. and Taconis, K.W., Physica 77 (1974) 131.
19. Fetter, A.L., Phys. Rev. 153 (1967) 285.
20. Langer, J.S. and Fisher, M.E., Phys. Rev. Letters 19 (1969) 560.

SUMMARY

The experiments on the moving He II film described in this thesis were carried out as an attempt to solve the elsewhere reported discrepancies between the behaviour of bulk helium and the helium film. This was done by using a new method of measuring changes in film thickness. This technique is based on the fact that in a closed volume, containing liquid and vapour in equilibrium, the amount of liquid, *i.e.* film- and bulk liquid together, is constant at constant temperature. By taking a large surface area covered with film one can study changes in film volume, *i.e.* film thickness, by monitoring the changes in the amount of bulk liquid.

In chapter I, this new technique is illustrated on measurements of the static film thickness as a function of the height above the bulk liquid. The results prove that changes in film thickness of the order of 1 Å can indeed be measured accurately. Therefore the same technique was used in the main experiments.

In chapter II, the thickness of a moving film is compared with that of a static one. The result of the experiments is that for the first time, a thinning of the moving He II film has been measured, and moreover that this thinning was found to be in agreement with the Landau equations and the vapour-liquid equilibrium conditions as valid for bulk helium. The thinning of a moving film, the so-called Kontorovich effect, was measured both for stationary- and non-stationary flow in long, narrow capillaries (lengths up to 200 m). Together with a discussion of the thinning, an analysis is given of acceleration effects on the film thickness, and the influence of third-sound waves on the measurements. The deviations of the measured values of the thinning and the theoretical values for the longest capillary can probably be attributed to retardation effects due to the finite speed of third sound.

In chapter III, the behaviour of a rotating He II film is studied. The purpose of this experiment was to find the conditions for a shrunken temperature-dependent meniscus. The results obtained with the first pieces of apparatus, the top and the torus, are consistent with the idea that vortex formation in the film leads to a classical temperature-independent meniscus, as it does for bulk helium. The results with the rotating spiral however, might indicate the occurrence of the shrunken meniscus. This is probably due to the fact that in such a narrow capillary, the angular velocity at which vortex lines appear is much larger than for instance in the top. The numerical agreement however, between the expected values and the measured ones, is rather poor,

so further investigations should be carried out.

In the last chapter, attempts to generate persistent flow in a saturated helium film by rotation are also described. For the detection of this flow, the Kontorovich effect was used. The accuracy obtained with the torus did not permit any conclusion about the possibility of generating a persistent current in this way. The conclusion from the results of the spiral is that at the moment of detection, no persistent current existed. A definite explanation for the latter case has not been found, since recent successful experiments performed by the Leiden group in a similar apparatus show very clearly that persistent flow can be generated by rotation.

SAMENVATTING

In dit proefschrift worden metingen beschreven van de dikte van een bewegende heliumfilm beneden de lambda temperatuur, 2,17 K. De resultaten van experimenten die destijds door anderen zijn gedaan met de bewegende film waren in tegenspraak met de gangbare theorie van Landau en leidden tot theoretische speculaties. De hier beschreven proeven zijn opgezet teneinde zo mogelijk het probleem van de discrepantie tussen de theorie en het experiment tot een oplossing te brengen. Hierbij is gebruik gemaakt van een nieuwe techniek om veranderingen in de filmdikte te meten.

Het uitgangspunt van de nieuwe meetmethode is dat voor een afgesloten volume, gevuld met vloeibaar helium in evenwicht met zijn damp, bij konstante temperatuur geldt dat het vloeistofvolume, d.w.z. vrije vloeistof en filmvloeistof tezamen, konstant is. Door een groot oppervlak bedekt met filmvloeistof te nemen, kan men de verandering van de filmdikte bestuderen door de verandering van de hoeveelheid vrije vloeistof te meten.

In het eerste hoofdstuk wordt de nieuwe meettechniek geïllustreerd aan de hand van een experiment, opgezet om de dikte van een stilstaande film te bepalen als funktie van de hoogte boven de vrije vloeistof. De resultaten tonen aan dat met behulp van deze methode inderdaad dikteveranderingen, in de orde van 1 Å, gemeten kunnen worden. In de hieropvolgende experimenten worden de dikteveranderingen dan ook met behulp van deze techniek gemeten maar nu als funktie van andere variabelen.

In het tweede hoofdstuk wordt de dikte van een stromende film vergeleken met die van een stilstaande. In een zodanig dunne film is alleen de superfluïde component beweeglijk. Uit de bewegingsvergelijkingen van Landau volgt, dat tengevolge van de snelheid van het superfluïde een Bernoulli-effect zal optreden. Tezamen met de damp-vloeistof evenwichtsvoorwaarden moet dit resulteren in een diktevermindering van de film. Dit wordt het Kontorovich-effect genoemd. In tegenstelling tot vroegere experimenten is deze diktevermindering nu inderdaad waargenomen, zowel bij stationaire als niet-stationaire stromingen in zeer lange, nauwe capillairen (lengte tot 200 m). De experimentele resultaten duiden op een goede overeenstemming tussen de theorie en het experiment. Tegelijk met het Kontorovich-effect wordt een analyse gegeven van de invloed van versnellingseffecten op de filmdikte en van de invloed van een oppervlaktegolf, het z.g. derde geluid, op de waarnemingen. De afwijking tussen de experimentele resultaten en de theorie kunnen waarschijnlijk worden toegeschreven aan retardatie-effecten

tengevolge van de eindige voortplantingssnelheid van het derde geluid.

In het laatste hoofdstuk wordt het gedrag van de roterende heliumfilm bestudeerd. Het onderzoek is opgezet om de voorwaarden op te sporen waaronder een geslonken, temperatuurafhankelijke meniscus optreedt. Deze meniscus zou moeten ontstaan als de superfluïde component, in tegenstelling tot de normale component van helium, niet deelneemt aan de rotatie. De resultaten, verkregen met de eerste toestellen, de tol en de torus, zijn consistent met de opvatting dat wervelvorming ook in de film een klassieke meniscus doet ontstaan op dezelfde wijze als in het vrije helium. De resultaten met de ronddraaiende spiraal daarentegen doen vermoeden dat we in het nauwe capillair te maken hebben met een geslonken meniscus. Dit is mogelijk toe te schrijven aan het feit dat in een dergelijk nauw capillair de wervelvorming pas bij veel grotere hoeksnelheden zal optreden dan bijvoorbeeld bij de tol. De numerieke overeenstemming is evenwel, vergeleken met de vorige experimenten, zo matig dat het probleem zeker een nadere bestudering waard is.

In het laatste hoofdstuk worden ook de pogingen beschreven om een persisterende stroom door middel van rotatie op te wekken. Het waarnemen van deze persistentie gebeurt met behulp van het Kontorovich-effect. Bij de proeven met de torus laten de resultaten echter geen conclusies toe, bij de spiraal daarentegen duiden de resultaten erop dat op het moment van detectie de persisterende stroom niet aanwezig was. Recente, succesvolle proeven met een sterk erop gelijkend toestel van de werkgroep in Leiden tonen aan dat een persisterende stroom wel degelijk door rotatie kan worden opgewekt. Een verklaring voor het verschil in resultaten van beide toestellen is nog niet met zekerheid gevonden.

Teneinde te voldoen aan het verzoek van de Faculteit der Wiskunde en Natuurwetenschappen volgt hier een kort overzicht van mijn studie.

Na in 1963 het diploma h.b.s.-B te Deventer behaald te hebben, begon ik mijn studie wis- en natuurkunde te Leiden. In 1966 legde ik het kandidaatsexamen a' af. Vervolgens was ik werkzaam op het Kamerlingh Onnes Laboratorium in de groep die onder leiding staat van Prof. Dr. K.W. Taconis, Prof. Dr. R. de Bruyn Ouboter en Dr. H. van Beelen. Bij het onderzoek van superfluïde stromingsverschijnselen assisteerde ik Dr. W.M. van Alphen en Dr. J.F. Olijhoek. Mijn eerste zelfstandig onderzoek betrof persisterende stromen in een circuit bestaande uit samengestampte poeders, z.g. superlekken. Het doctoraal examen natuurkunde behaalde ik in 1969 na de daartoe vereiste tentamens te hebben afgelegd.

Van juni 1968 tot augustus 1972 was ik praktikumassistent voor pré-kandidaten. Sinds augustus 1972 ben ik als docent verbonden aan de Pedagogische Academie, Rijksopleiding voor Onderwijzer te 's-Gravenhage. Daarnaast bleef ik als wetenschappelijk medewerker verbonden aan de Rijksuniversiteit te Leiden.

Na mijn doctoraal examen heb ik tezamen met drs. R.G. Jurriëns onderzoeken verricht aan onder andere de warmtegeleiding van He II in superlekken en capillairen. Het onderzoek van verzadigde heliumfilms, beschreven in dit proefschrift, is eind 1970 gestart. Gedurende dit hele onderzoek profiteerde ik van de stimulerende samenwerking met drs. H.J. Verbeek.

Velen van de technische- en administratieve staf van het Kamerlingh Onnes Laboratorium ben ik dank verschuldigd bij de totstandkoming van dit proefschrift. In het bizonder de heer P.J.M. Vreeburg voor het vakkundig vervaardigen van de glazen onderdelen van de toestellen. Het metaal-technische gedeelte van de opstelling en de toestellen werd grotendeels vervaardigd door de heren G. Vis en A.J.J. Kuyt. De heer J.D. Sprong dank ik voor het voorzien van vloeibaar helium. De tekeningen in dit proefschrift zijn vervaardigd door de heer W.F. Tegelaar, die tevens voor de foto's zorg droeg, en de heren J. Bij en J.J. Ober. Veel steun kreeg ik van het Rijkszuivelstation, vooral van de heer M. Karruppannan, bij het vervaardigen van de glazen spiralen. Ik ben zeer erkentelijk voor het typewerk dat mevr. E. de Haas-Walraven verzorgd heeft en de correctie van de Engelse tekst door Dr. R.C. Thiel.